Utah State University

DigitalCommons@USU

Jun 17th, 12:00 AM - Jun 20th, 12:00 AM

Conference Proceedings

Blake Tullis

Robert Jansson

UtahState University
MERRILL-CAZIER LIBRARY

Conference Proceedings

4th International Junior Researcher and Engineer Workshop on Hydraulic Structures

Photos courtesy Sigurdur M. Gardarsson, University of Iceland (left) and Donna Barr, USU (center, right).

June 17-20, 2012

Utah State University

Logan, UT USA

Editors: Blake P. Tullis and Robert Jansson

Conference Proceedings:
4th International Junior Researcher and Engineer Workshop
on Hydraulic Structures

This report is published by Utah State University. Online copies of this report can be found at http://digitalcommons.usu.edu/ewhs/. The interpretation and opinions expressed herein are solely those of the author(s). Considerable care has been taken to ensure accuracy of the material presented. Nevertheless, responsibility for the use of this material rests with the user.

Yahoola Creek Dam labyrinth weir spillway, Dahlonega, Georgia (USA). Photograph courtesy of Schnabel Engineering

TABLE OF CONTENTS

FOREWARD

This International Junior Researcher and Engineer Workshops on Hydraulic Structures (IJREWHS) or Junior Workshop followed three previous successful workshops organized by the IAHR Hydraulic Structures Technical Committee. The first Junior Workshop was held in Montemor-o-Novo (Portugal) in 2006 and was organized jointly with the Instituto Superior Técnico (IST) and the Portuguese Water Resources Association (APRH). The second Junior Workshop was held at the University of Pisa (Italy) in 2008. The third Junior Workshop was held at Heriot-Watt University (Edinburgh, Scotland) in 2010. The growing success of this workshop series led to the organization of the Fourth International Junior Researcher and Engineer Workshop on Hydraulic Structures (IJREWHS'12). The IJREWHS'12 (Fig. 1 and 2) was held at Utah State University (Logan, Utah, USA), June 17-20, 2012. A half-day technical tour included the visit to Campbell Scientific world headquarters, and two dams (Hyrum Dam and Porcupine Dam) (Fig. 3). The IJREWHS'12 workshop addressed both conventional and innovative aspects of hydraulic structures, their design, operation, rehabilitation and interactions with the environment. The workshop provided an opportunity for young researchers and engineers, both graduate and young researchers and engineers in both public and private sectors, to present ideas, applications, and preliminary results of their own research in an inspiring, friendly, co-operative, and non-competitive environment. The event was attended by 13 junior participants and by 11 national and international experts from the hydraulic research community (Fig. 3 and 4). In total 15 lectures were presented, including 2 keynotes, representing a total of 5 countries: Belgium, Chile, Columbia, Portugal, and the United States of America.

K. Warren FRIZELL (US Bureau of Reclamation) presented a keynote lecture on the cavitation. He provided an historical overview of hydraulic structure cavitation events with the spillways at Hoover and Glen Canyon Dams. He discussed the basic behavior of cavitation near baffle blocks in hydraulic jump basins and a new baffle block design with ventilation that may reduce the potential for cavitation damage. He also addressed research on cavitation on stair-stepped spillways. Both studies were conducted in a Low Ambient Pressure Chamber facility.

The second keynote lecture, given by Prof. Rollin HOTCHKISS (Brigham Young University, USA), provided guidance for writing good peer-reviewed journal papers.

During the workshop, the junior participants chaired sessions, played the role of "advocatus diaboli" (devil's advocate), and prepared the reports for all sessions to identify key scientific elements and pending questions (Fig. 4). The active involvement of junior participants in managing workshop activities is considered a main feature of the International Junior Researcher and Engineer Workshops on Hydraulic Structures series. In order to help junior participants in

these tasks, specific guidelines were provided. Another interesting feature of the workshop was the presence of engineering consultants and research experts, with the aim to stimulate the debate during the presentations between junior and senior participants, as well as during the subsequent round table discussion (Fig. 4D). The publication of the workshop papers marked the successful conclusion of this event. Two active members of the Hydraulic Structures Technical Committee, including the Committee Chair, edited the proceedings. They contain 12 papers including a keynote lecture paper, involving 28 authors from 5 countries and 3 continents, plus 6 session reports, and photographs of the workshop and of the technical visit (Fig. 3 to 5). Each paper was peer-reviewed by a minimum of two experts. The discussion reports were included for the benefit of the readers.

The proceedings include a keynote lecture paper on hydraulic structure cavitation, five technical papers dealing with physical or numerical modeling of free-surface flow hydraulic structures, two technical papers dealing with the interactions between sediment processes and hydraulic structures, three papers dealing with pipe system modeling, and one technical paper on water level measurement instrumentation. These are followed by six discussions reports. Innovative designs for overflow weirs are presented in two papers. An improved understanding of performance of existing hydraulic structures is discussed in several papers on flow characteristics and hydrodynamics along and downstream of spillways. The requirement for water in industrial applications is addressed by papers on optimization of applied designs for navigation, hydropower, and cooling water intakes. The interaction between hydraulic structures and nature, including minimization of the potential impacts of structures on natural river processes as human development encroaches further on the natural water systems, is presented in the papers on bridge pier scour. Finally, the use of computer programs to assist in studying, understanding and designing of water related infrastructure is addressed in three papers on numerical modeling techniques. The full bibliographic reference of the workshop proceedings is: TULLIS, B., and JANSSEN, R. (2012). Proceedings of the Fourth International Junior Researcher and Engineer Workshop on Hydraulic Structures (IJREWHS'12), 17-20 June 2012, Logan, Utah, USA. (DOI:10.15142/T3F59H).

Each paper of the proceedings book should be referenced as, for example: MURZYN, F. (2010). "Assessment of Different Experimental Techniques to Investigate the Hydraulic Jump: Do They Lead to the Same Results?" in Proceedings of the Fourth International Junior Researcher and Engineer Workshop on Hydraulic Structures (IJREWHS'12), 17-20 June 2012, Logan, Utah, USA.

(a)

(b)

Figure 1 – Group photos of (a) junior and senior workshop participants and (b) senior researchers (Warren Frizell and Rollin Hotchkiss not present).

(a)

(b)

(c)

(d)

(e)

Figure 2 – Technical field trip: (a) Campbell Scientific, (b) Porcupine dam duck bill spillway, (c) Hyrum dam irrigation diversion, (d) collateral damage from field trip, (3) Porcupine dam hooded cone valve.

(a)

(b)

(c)

(d)

Figure 3 – Photos of Junior Workshop presentations: (a-c) student presentations, (d) Rollin Hotchkiss keynote on how to write quality journal papers.

(a)

(b)

Figure 4 – Roundtable discussions of presentations (a) led by junior researcher session chair with (b) senior researcher participation.

ORGANIZING COMMITTEE

Blake Tullis	USA	Chair
Brian Crookston	USA	Vice-Chair
Robert Janssen	Australia	Vice-Chair IAHR Hydraulic Structures Technical Committee, Chair of 3rd IJREWHS, Edinburgh, Scotland, 2010
Stefano Pagliara	Italy	Chair IAHR Hydraulic Structures Technical Committee, Chair 2nd IJREWHS, Pisa Italy, 2008
Jorge Matos	Portugal	Past Chair IAHR Hydraulic Structures Technical Committee, Chair 1st IJREWHS, Montemor-o-Novo, Portugal, 2006

ACKNOWLEDGEMENTS

ORGANIZING INSTITUTIONS AND SPONSORS

Organizing Institutions
- IAHR-International Association for Hydro-Environment Engineering and Research
- Utah State University

Sponsors
- Schnabel Engineering

STATISTICAL SUMMARY

- 24 Participants from seven countries and four continents (including: students, engineers, senior researchers).
- 15 Presentations, including two keynote addresses seven countries and four continents.

PROCEEDINGS

- 12 Peer-reviewed papers.
- 28 Authors and co-authors from five countries and 3 continents.
- 11 Expert reviews from 6 countries

LIST OF WORKSHOP PARTICIPANTS

Nathan Christensen	USA	MS Student
Mitch Dabling	USA	MS Student
Gonzalo Duró	Argentina	MS Student
Bryan Heiner	USA	Project Engineering
Mohonad Khodier	USA	PhD Student
Josh Mortensen	USA	Project Engineering
Iordanis V. Moustakidis	USA	
Riley Olsen	USA	MS Student
Boris Rodriquez	Chile	Project Engineering
François Rulot	Belgium	PhD Student
Maria Ximena Trujillo	Columbia	MS Student
Fadi Antoine Wakim	USA	Project Engineering
Adam Witt	USA	PhD Student

LIST OF EXPERT REVIEWERS

Fabian Bombardelli	USA
Daniel Bung	Germany
Hubert Chanson	Australia
Brian Crookston	USA
Sébastien Erpicum	Belgium
K. Warren Frizell	USA
Rollin Hotchkiss	USA
Robert Janssen	Australia
Jorge Matos	Portugal
Stefano Pagliara	Italy
Blake Tullis	USA

LIST OF SENIOR RESEARCHER PARTICIPANTS

Fabian Bombardelli	University of California Davis	USA
Dave Campbell	Schnabel Engineering	USA
Brian Crookston	Schanbel Engineering	USA
Sébastien Erpicum	University of Liege	Belgium
K. Warren Frizell	US Bureau of Reclamation	USA
Rollin Hotchkiss	Brigham Young University	USA
Robert Janssen	Bechtel Corporation	Australia
Jorge Matos	Instituto Superior Técnico	Portugal
Greg Paxson	Schnabel Engineering	USA
Bruce Savage	Idaho State University	USA
Blake Tullis	Utah State University	USA

CAVITATION IN HYDRAULIC STRUCTURES – BRIDGING THE GAP BETWEEN THE LABORATORY AND THE REAL WORLD

K. Warren FRIZELL

Technical Service Center, Bureau of Reclamation, USA, kfrizell@usbr.gov

ABSTRACT: Recollections of a thirty-five-year career at the hydraulic laboratory of the Bureau of Reclamation are presented within the context of using all the tools at your disposal to reach the best possible answer to your research questions. Cavitation in hydraulic structures will be the main topic used to illustrate this premise, using historic examples and current research to demonstrate study approaches, testing techniques, and applied solutions to real world problems.

Keywords: cavitation, hydraulic structures, tunnel spillways, baffle blocks, stepped spillways.

INTRODUCTORY REMARKS

On the occasion of the opening of the 4th International Junior Researcher and Engineer Workshop on Hydraulic Structures, I'd like to thank the IAHR Hydraulic Structures Committee and the workshop organizers for inviting me to speak here today. I would also like to welcome all of you that are participating and hope that these next few days will be a valuable and enriching experience and that you'll have some fun as well. As with the three previous International workshops, the goal of this meeting is to provide young researchers and engineers the opportunity to present and discuss their research in a friendly environment and to receive constructive criticism and suggestions from their peers and a committee of senior researchers on both their written and oral presentations. Hopefully it will help to generate some new ideas, not necessarily directly related to the technical parts of your work but to help you to better convey your ideas and results—a worthy topic in these days of increased competition for research dollars and clients. This is the first workshop to be held outside of Europe and it's nice to see a good group of participants.

I began my engineering career as a student trainee in the hydraulic laboratory of the Bureau of Reclamation in 1976 while working on my undergraduate degree in Mechanical Engineering. After graduation and working for a few years, I returned to the University of Minnesota and the

St. Anthony Falls Laboratory to work on a graduate degree in Civil Engineering. Throughout my early career in Reclamation and at St. Anthony Falls, I had the good fortune to have some great mentors and colleagues. It feels a bit like "old home" week here as the other invited keynote speaker, Professor Rollin HOTCHKISS, was at University of Minnesota at the same time I was, back in the 1980s. I've continued to work at the lab in Denver and can say that I could not have imagined anything much better from the standpoint of working on a huge variety of "real world" problems in the area of hydraulics and, in particular, hydraulic structures. I'm thinking about retirement now after more than 35 years at the lab and I certainly have many fond memories of engineering and research with Reclamation.

This phrase, "the real world"—it isn't a fictional place. I don't want to give the impression that academia isn't the real world, but generally it's rare at the university to get the chance to work on solving problems specific to a facility and then get to see if your recommendations really worked! We usually think of the university as a place where more "basic" or general research is performed. Perhaps research can best be defined as seeing what everyone has seen, and then doing what no one else has done. Begin with the end in mind! This is one of the things that I was fortunate to observe during my graduate studies. In general an incredible amount of work went into formulating and writing proposals for research dollars. When I first arrived I thought, they already knew the answer—what's the point? I soon learned that taking this approach led to success in the lab, and while the strides forward were not always monumental, they seldom were backwards.

Much of the work that we do at Reclamation's lab is a direct result of some type of problem. Our agency has a relatively short history—just over 110 years—but no lack of issues and problems to address. Damage and/or failures are often the most common study drivers; however, it may also be a new application of existing technology or a search of how to renew an aging structure using state-of-the-art practices. Results from this type of "applied" research are often site-specific but can still be valuable to the engineering community. We are less involved in generalized studies these days due to changes in funding and a shift in our mission; however, depending on how clever you are in planning and performing a study, the final product may provide a wealth of data, a new understanding of the problem, and spur on new studies in the future.

Since most of my career has been involved with testing and applied research, I'm going to discuss how those paths can occasionally grow to allow generalization and advance the state-of-the-art on a particular topic. I will present some "real world" problems that involve cavitation in hydraulic structures and show the importance of how those observations, along with the specific laboratory studies and studies of the phenomena, can all be pulled together to enrich the final

solution. The first topic will be cavitation in tunnel spillways, followed by a quick overview of cavitation on baffle blocks in stilling basins, and finally some recent laboratory work on cavitation potential in stepped spillways.

CAVITATION

Cavitation is generally defined as the formation of the vapor phase of a liquid. The word can be used to describe everything from the initial formation of small bubbles (inception) to large attached cavities (supercavitation). Unlike boiling which is induced by raising the vapor pressure of the liquid through heating, cavitation is induced by lowering the local hydrodynamic pressure to the liquid's vapor pressure. Cavitation can affect performance in turbomachinery, thrust in propulsion systems, accuracy of fluid meters, and cause extreme noise and vibration. Perhaps the issue we are most concerned about with hydraulic structures is the possibility of cavitation erosion (or damage). Damage is generally thought to be the result of the implosion or collapse of cavitation bubbles or cavities of vapor as they travel to areas of increasing pressure. If the implosions are near solid boundaries, the sudden collapse can generate shock waves with pressures rises of many orders of magnitude—large enough to cause material bonds to be destroyed, resulting in a process usually called "pitting." Increased time and intensity of this pitting can result in complete failure of structural components.

Tunnel Spillways

As I began my career, Henry FALVEY was at the lab and was our "cavitation expert." He was beginning to write a monograph on cavitation in chutes and spillways (FALVEY 1990) and introduced me to the subject of cavitation in tunnel spillways by predicting that when Glen Canyon Dam filled and they used the spillways, there was going to be significant damage. Reclamation's first tunnel spillways constructed were for Hoover Dam. During the first extended operation (4 months in 1941 at a mean discharge of 383 m^3/s), a post release inspection revealed a large eroded hole (9 m x 35 m x 14 m deep) near the end of the vertical bend, Figure 1. Engineers deduced that a hump in the tunnel profile just upstream from the hole was responsible for initiating the cavitation and resulting damage. They recommended that the hole be filled and the surface made smooth as possible. In addition a suggestion was made to study some method to inject air into the flow near the area that had been damaged. BRADLEY (1945) documented a 1:60 scale Froude-based model to study a variety of methods to cause enhanced air entrainment in the Hoover spillways in 1945. The ability to provide enough air near the boundary of the vertical curve, even for the best performing arrangements, was less than

acceptable. He realized that while the model measurements were accurate, scale effects were present due to the inability to scale viscosity and surface tension, and that prototype entrainment rates would likely be much higher. Uncertainties in what the actual aeration rates might be, resulted in abandoning this plan as unfeasible. The hole was filled and the surrounding concrete was "polished" using grinding (terrazzo machine).

Figure 1 – Hoover Dam tunnel spillway following first substantial flows, 1941.

These guys had definitely been on the right track. They believed that air would "cushion" the surface being attacked and lessen the damage. They had also realized that their scale model had issues due to the inability to properly scale the two-phase flow properties. While their reasoning was not entirely correct about the true physics of the problem, it led to continued investigations. Just a few years after this, in 1953, PETERKA (1953) published the first true laboratory evidence that air mixed in with the water had an influence on the damage that results from cavitation. He showed that in a qualitative way, entrained air reduced the severity of the pitting

on a test sample within an oscillator vibrating at 7800 Hz. In addition he used a venturi-type device with concrete test blocks and flow velocities of over 30 m/s to conclusively show that air content reduced the amount of cavitation pitting (loss of material) and reduced the noise associated with cavitation. Entrained air of 7.4% resulted in no measurable loss of material. He showed in his test rig, by measuring appropriate pressures, that the cavitation index varied linearly with increasing air entrainment, ranging from 0.109 with no air to 0.288 for 7.1% air, without any other changes to the flow conditions (see Figure 2).
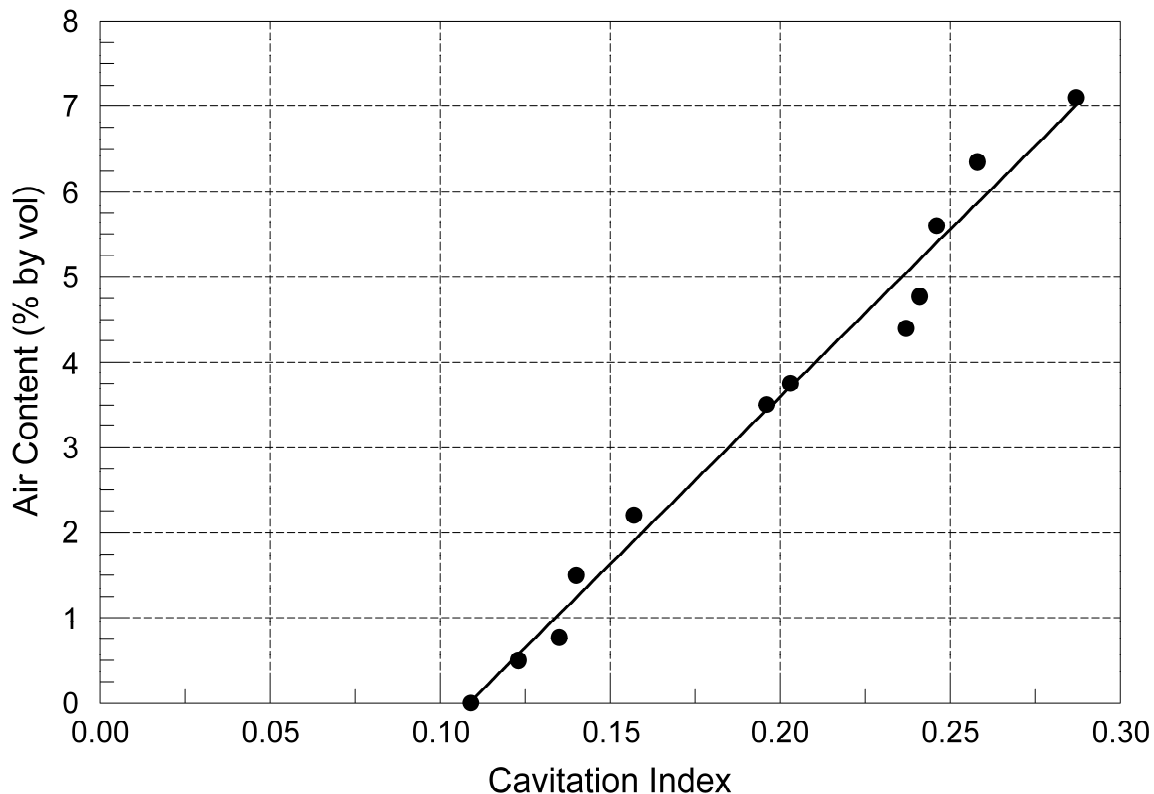
Figure 2 – Air content effects on the cavitation index.

Subsequent damage, model studies, and prototype testing at Yellowtail Dam and Glen Canyon Dam solidified the use of aeration slots in the control of cavitation damage in large tunnel spillways. During this same time frame in the 1980s, other researchers were also working on aerator designs for a variety of high-head chute type spillways, especially in South America. There had been several occasions of significant damage (Tarbela, Karun) to tunnels and spillways around the world, and it became an important design challenge for the times.

Cavitation in the laboratory

Specific cavitation studies in the laboratory to this point had rarely directly addressed cavitation in hydraulic structures. Although EULER first postulated about the possibility of cavitation in 1754, it was near the turn of the 20th century before actual studies of the phenomenon began. REYNOLDS observed cavitation in tubular constrictions, and PARSONS was the first to use a water tunnel and reduced pressures to study the loss of thrust to a ship whose propeller was "cavitating." Many institutions around the world used water tunnels and specialized chambers that allowed the study of cavitation. From the 1940's thru the 1960's, there was extensive work on cavitation inception, bubble dynamics, collapse dynamics, and damage due to all sorts of hydrodynamic cavitation applied to all different fields of interest.

Researchers quickly found that cavitation was not a simple process. Multitudes of scale effects have been discovered; including Reynolds number (velocity), vaporous versus gaseous cavitation, correctly modeling transition to turbulence and turbulent pressure fields, nuclei size and distribution, and dissolved gas content. With these scale effects present, we could question, what can we learn from laboratory experiments that will help us predict full-scale prototype performance? We may still be in the clouds a bit but with proper care, we trudge on. The next topic will be a look at model testing of cavitation on stilling basin baffle blocks.

Stilling basin baffle blocks

The use of baffled stilling basins in high-head, high velocity flows has often lead to problems with cavitation damage to the blocks and surrounding floor areas. Some of the first evidence was the stilling basin at Bonneville Dam. This COE dam is on the Columbia River and features an overflow spillway with a short stilling basin that features a couple of rows of baffle blocks. The structure was completed in the late 1930's and shortly after it was put into service, considerable damage to the blocks and surrounding invert was observed. A lab study at Carnegie Institute of Technology in a "vacuum tank" was one of the first documented studies of cavitation in hydraulic structures. Much of the previous and ongoing work had been concerning cavitation of propellers, and cavitation on bodies of revolution – or just basics such as offsets into/away from the flow, gate slots, and singular irregularities. These tests showed evidence of the type and location of the cavitation on this particular geometry, which correlated nicely with damage observed in the field, Figure 3. Attempts to "streamline" the blocks to reduce the damage were somewhat successful, but not entirely.

Reclamation's standard baffle block design (used in the type III basin) was based on creating the most energy dissipation possible. So the use of these blocks in a high velocity flow might pose some cavitation issues. They were not recommended for velocities >15 m/s and in order to

keep dissipation at a maximum, the front face should be vertical and rounding corners or other streamlining was discouraged. In the late 1970's Reclamation constructed a "vacuum chamber" geared at studying cavitation in hydraulic structures. This chamber was called the Low Ambient Pressure Chamber or LAPC. It provided the ability to model a structure (or part of a structure) using typical "Froude-based" techniques but also could provide equal cavitation indices in the model and prototype. This was accomplished by lowering the "ambient" pressure within the chamber – such that lower velocities could generate the hydrodynamic pressures capable of causing cavitation.
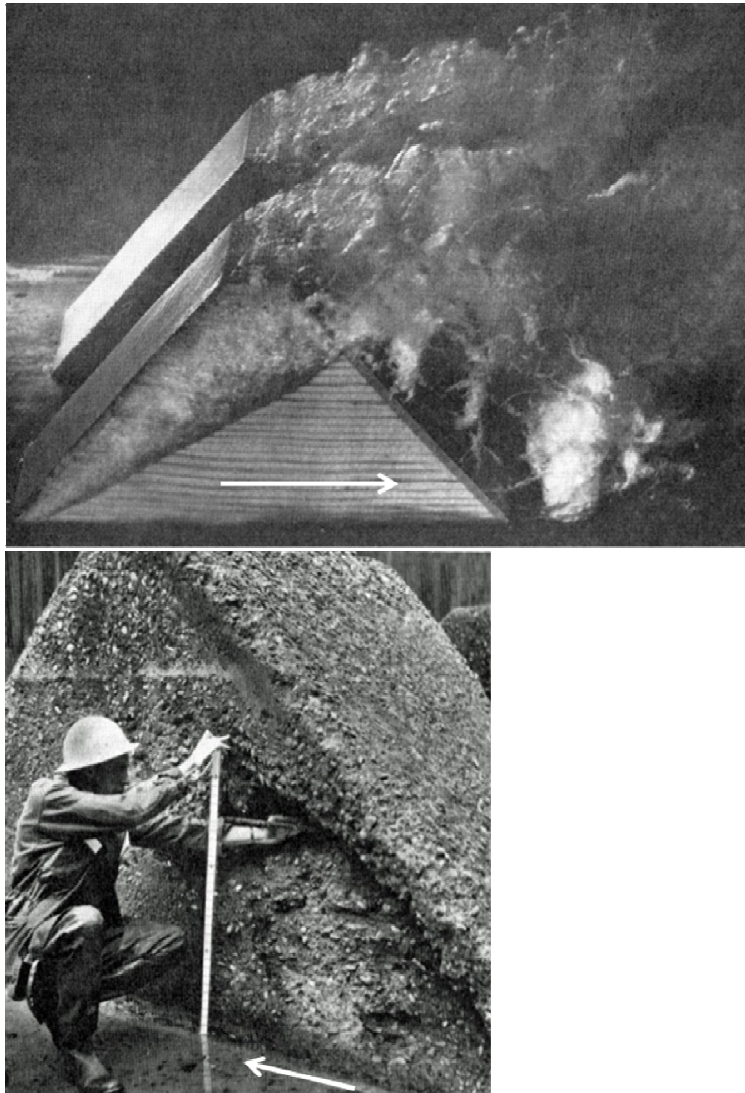
Figure 3 – Laboratory tests (Carnegie) and resulting damage pattern in the Bonneville Dam prototype structure, early 1940's.

A recent study (FRIZELL, 2010) looked at a modified type III stilling basin for the Folsom Auxiliary spillway. The cavitation potential of the standard block shape was studied with the goal of modifying the shape to be free from cavitation damage. Incoming velocities to this basin are in the 25–37 m/s range, so the presence of cavitation is highly likely, realizing that if damage is to occur we would prefer that it be downstream from the blocks and not on or around the blocks themselves. Initial tests in a sectional model of the LAPC showed the locations for cavitation formation and actually cleared up a couple of misconceptions about the type of forms of cavitation that have resulted in previous damage to similar block shapes out in the field. Real time visualization can be problematic, as often cavitation is not a steady process. However, details can be revealed when taken at high-speeds and slowed down for viewing. We initially see a horseshoe vortex form near the invert. This vortex contains a vapor core and is very stable, but following the vortex downstream reveals that it does not impact any of the solid boundaries within the basin. Bubble cavitation and attached sheets of bubbles are present on the blocks, and damage has been observed in these areas. But perhaps the most interesting find was the vortices that form in the shear layers downstream from the blocks and actually attach to the floor, move downstream and implode. The floor damage that had been observed (as in the Bonneville basin) was once thought to be the result of the horseshoe vortex interacting with flow coming around the blocks—not really the case.

These insights gave us some ideas about keeping energy dissipation at a maximum while trying to remove cavitation damage from the immediate vicinity. Due to the extreme velocities, we thought that formation of a ventilated cavity or supercavitation may be possible with the right shape. Ideally the cavity would envelope the entire block downstream from the rectangular vertical face, yielding no possible damage to the blocks themselves. We did manage to find a shape that kept traveling cavitation away from solid flow boundaries throughout the flow ranges and transitioned to supercavitation near the maximum flow rate, Figure 4. Through the use of the lab model, we were able to verify the incipient cavitation index for both the standard and new block shapes and at what flow index a ventilated cavity would form.

Figure 4 – Ventilated cavity forming around new baffle block design.

The Folsom auxiliary spillway studies provided yet another opportunity to study something that really has only been picked around previously—cavitation potential in stepped spillways. This proposed structure has some rather unique design features: an inlet structure of top-seal radial gates with 30 m head, design specific discharge of 74 m^2/s, maximum specific discharge of 172 m^2/s, and a combination smooth and stepped chute terminating in a modified type III stilling basin. Velocities in excess of 30 m/s on the spillway and depths over 6 m have the designers concerned about possible cavitation damage.

Cavitation on stepped spillways

Cavitation damage has not been reported in previously constructed stepped channels. Reasons are probably two-fold: (1) design recommendations have been conservative based on lab studies, and the measurement of pressures on the steps (limiting unit discharge to 30 m^2/s) and (2) steps are known for substantial self-aeration—triggered much more quickly than on a smooth chute (studies and experience with aeration preventing cavitation damage). If cavitation can form, then where would the cavitation initiate and what possible damage may occur.

Our studies began with a plan to evaluate the flow field present and then observe and measure creation of cavitation by testing the channel in the LAPC. Measurements at atmospheric pressures were completed to characterize the channel (measure pressure gradient, pressures on steps, complete PIV measurements). Once these tests were completed for slopes of 21.8 degrees and 68.2 degrees for two step heights (relative roughnesses), the channel was moved into the LAPC.

Each of the four cases was tested in the LAPC (2 slopes, 2 roughness heights). The chamber was initially filled with city water and then circulated while under vacuum for a period of about 8 hours. By doing this "degassing" process, the water was slightly under saturated at the reduced operating pressure—a condition where cavitation inception has been shown to be less dependent on total dissolved gas content. The flow rate (velocity) was then incrementally increased, and acoustic data and high-speed video were recorded. We used an acoustic emissions sensor to indicate critical conditions within the model, such as inception, in much the same manner as hydrophones or dynamic pressure transducers have been used in the past. We discovered that cavitation could indeed form on stepped channels. The initial formation was within the high intensity shear layer that is associated with the step tips (the pseudo-bottom). There was some formation of bubbles on the step tips themselves, but the bubbles were quickly carried into the shear layer and either appeared as a swarm of bubbles or organized into stream wise vertex-like structures, Figure 5.

Our goal was to see if the critical cavitation data from a stepped spillway would follow the model proposed by ARNDT and IPPEN (1968) for cavitation on uniformly rough surfaces. This required us to interpret our data in a manner to extract the friction factor so that we could compute the coefficient of friction. We ended up using the velocity profiles that were extracted from the PIV measurements and applying a method suggested by NIKURADSE and later applied by CHAMANI (1997) to calculate the friction factor. Then plotting the C_f versus our critical cavitation indices from the experiments, we found they fit reasonably well with the model of ARNDT and IPPEN. From a designers standpoint this was great news! Although the implication of a friction factor to the macro-roughness elements of a stepped spillway is still just an "approximate" way to handle the complex flow, we can now predict the critical cavitation index based on this friction factor.

Figure 5 – Photo of cavitation formation within the shear layer of the 21.8-deg stepped channel.

The site-specific studies concerning cavitation potential on the new Folsom auxiliary spillway, along with some additional research funds, ended up expanding the state of knowledge concerning cavitation on uniformly rough surfaces. From the small triangular grooves tested by Arndt and Ippen to these large macro-roughness elements tested at Reclamation's laboratory, in the end, it is the design engineer that is the "winner." Careful consideration in the design of the model and test program yielded a result that was not entirely unexpected. Reclamation and others had assumed that cavitation in stepped spillways might be described by the same "theory" as the uniformly rough boundary layer work revealed 40 years earlier, but the experiments are the key to actually show that the theory is supported by data.

CLOSING

In closing, I have presented several topics related to cavitation in hydraulic structures and hope that I have illustrated the value in looking not only to specific examples previously studied but also delving into related testing and research of the general phenomena. Using all that is available just might help explain and enhance your present work. Research doesn't always go as planned; sometimes your best attempts to prove out a hypothesis come crashing down, but then there can also be that serendipitous moment of discovering something totally unexpected!   I

remember being told once that it was better to be clever than smart; however, achieving meaningful results in your research can be enhanced by cleverly applying your (and others') knowledge to the topic.

ACKNOWLEDGMENTS

Special thanks to Perry L. JOHNSON, Henry T. FALVEY and Roger E.A. ARNDT, the mentors who most greatly influenced my career.

REFERENCES

ARNDT, R.E.A. and IPPEN, A. (1968). "Rough Surface Effects on Cavitation Inception." *J.Basic Eng.*, June 1968, pp. 249-261.

BRADLEY, J.N. (1945). "Study of Air Injection Into the Flow in the Boulder Dam Spillway Tunnels – Boulder Canyon Project." *Bureau of Reclamation* Report No. HYD-186, 15 pages.

CHAMANI, M.R. (1997). "Skimming flow in a large model of a stepped spillway." Ph.D. thesis, University of Alberta, Canada.

FALVEY, H.T. (1990). "Cavitation in Chutes and Spillways," Engineering Monograph No. 42, *United States Department of the Interior, Bureau of Reclamation*, USA, 146 pages.

FRIZELL, K.W. (2009). "Cavitation Potential of the Folsom Auxiliary Spillway Stilling Basin Baffle Blocks." *Bureau of Reclamation* Report HL-2009-06, 28 pages.

PETERKA, A.J. (1953). "The Effect of Entrained Air on Cavitation Pitting." *Proceedings of the Joint Meeting of the IAHR, ASCE*, Minneapolis, MN, August, 1953.

TECHNICAL PAPERS

ARCED LABYRINTH WEIR FLOW CHARACTERISTICS

Nathan A. CHRISTENSEN

Utah Water Research Laboratory, Dept. of Civil and Environmental Engineering,

Utah State University, USA, nate.chris10sen@gmail.com

Blake P. TULLIS, Ph.D.

Utah Water Research Laboratory, Dept. of Civil and Environmental Engineering,

Utah State University, USA, blake.tullis@usu.edu

ABSTRACT: The increase in predicted extreme flood event magnitudes has required the modification of many existing reservoir spillway flow control structures with more hydraulically efficient designs. The arced labyrinth is a relatively new, highly efficient, nonlinear weir design specifically applicable to reservoir applications. Flow characteristics of eleven laboratory-scale arced labyrinth weir geometries were studied at the Utah Water Research Laboratory with sidewall angles $\alpha = 12°$ and $20°$. Rating curves, flow conditions, and discharge efficiencies were documented for each configuration to increase the hydraulic database of arced labyrinth weirs.

Arced labyrinth weirs with $\alpha = 20°$ were found to have discharge efficiencies 5 to 10% higher than $\alpha = 12°$ weirs. They also generated more flow anomalies (i.e. unstable nappe aeration) due to approach flow interaction with cycle orientation and weir position. The hydraulic efficiency of projecting, traditional labyrinth weirs, as a function of abutment wall geometry, was also evaluated. No standardized design method currently exists for arced labyrinth weirs, and relatively little is known about their hydraulic characteristics; this discussion increases the hydraulic information available for the arced labyrinth weir design.

Keywords: Arced labyrinth weirs, approach flow, labyrinth spillways, discharge efficiency.

INTRODUCTION

Weirs are hydraulic structures used for measuring discharge, controlling flood water, providing water storage, facilitating water flow diversions, and altering flow regime in a channel or river. Weirs are also commonly used as head-discharge control structures in reservoir (spillways) and channel applications. Predicted probable maximum flood (PMF) magnitude increases caused by

improved datasets, land-use changes, and/or climate change have resulted in a growing need to increase existing dam discharge capacities. This might be done by replacing an existing linear weir with a more hydraulically efficient nonlinear weir or by adding an additional spillway.

Weir head-discharge relationships can be described empirically using a standard form of the weir equation [Eq. (1)] (HENDERSON 1966). In this equation, Q is the weir discharge, H_T is the total upstream head measured relative to the crest elevation, L is the weir length, C_d is the discharge coefficient, and g is the acceleration of gravity.

$$Q = C_d \frac{2}{3} L H_T^{3/2} \sqrt{2g} \tag{1}$$

Per Eq. (1), the weir discharge is directly proportional to L. Since the width of the spillway channel is often restricted, one way to increase discharge capacity is to increase L by folding the weir (in plan view) into trapezoidal segments, or cycles, creating a nonlinear, labyrinth, or 3-D weir (FALVEY 2003). Figure 1 shows a photograph of a prototype labyrinth weir (Yahoola Dam, Georgia, USA.)

Figure 1 – Photograph of prototype labyrinth weir (photo courtesy of Schnabel Engineering)

KOCAHAN and TAYLOR (2000) suggested that the labyrinth shape allows more discharge than a linear ogee weir at the beginning of a flood. Labyrinth weirs also represent constructible alternatives to widening the spillway channel (TULLIS et al. 1995). Due to their increased discharge efficiency, labyrinth weirs require less upstream driving head for a given discharge. Replacing a linear weir with a labyrinth weir could result in more reservoir volume being utilized for water storage due to a reduction in required reservoir volume set aside for flood routing. For reservoir applications, the labyrinth weir cycles can be arranged in an arced configuration, taking better advantage of converging approach flow patterns. A labyrinth weir layout where the downstream apexes of each cycle follow the arc of a circle is termed an arced labyrinth weir.

Previous model studies have shown arced labyrinth weirs to be viable options for reservoir weir applications where approach flow conditions are non-channelized. For Maria Cristina Dam (Spain), the approach flow conditions and discharge capacity were improved by arcing 6 of the 7 labyrinth weir cycles within the limited footprint area of the spillway (CORDERO-PAGE et al. 2007).

Based on laboratory experiments of labyrinth weirs in reservoir applications, CROOKSTON (2010) concluded that "the arced configurations were found to be the most efficient labyrinth weirs tested" and that "an arced cycle configuration can increase discharge efficiency as it improves the orientation of the cycle to the approaching flow (~90° to the weir centerline is desirable)." CROOKSTON and TULLIS (2012 a, b, & c) further introduced arced labyrinth weir-specific geometric parameters (Figure 2) and tested several physical weir models. These tests and nomenclature are referred to and adopted in this study.
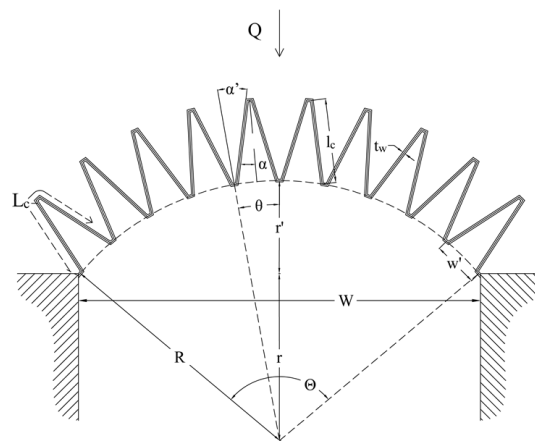
Figure 2 – Schematic of 10-cycle arced labyrinth weir including CROOKSTON and TULLIS (2012a) nomenclature.

Due to their infinite variability in possible geometric configurations, arced labyrinth weirs can provide unique challenges to designers. The objective of this report is to help expand the hydraulic database for arced labyrinth weirs and provide additional insight for their implementation in reservoirs. Since limited information is currently available in the literature, including a limited number of physical model tests, a thorough study of arced labyrinth weir hydraulics is needed. The information presented herein is intended to increase that knowledge base. Additional information and insights can also be found in CHRISTENSEN (2012).

EXPERIMENTAL SETUP

All arced labyrinth weir testing was performed in an elevated head box (7.3m x 6.7m x 1.5m) located at the Utah Water Research Laboratory (UWRL), at Utah State University. Eleven laboratory-scale models were built with geometries intended to expand the work of CROOKSTON and TULLIS (2012a, 2012b). These physical models were selected for detailed analysis of flow anomalies and characteristics not easily observable with numerical or analytical simulations.

The configurations tested included: sidewall angles (α) of 12 and 20 degrees; cycle arc angles (θ) of 0º, 10º, 20º, and 30º; and cycle numbers (N) equal to 5, 7, and 10. All weirs were fabricated using high-density polyethylene (HDPE) sheeting with wall thicknesses (T_w) of 254 mm, wall heights of 0.305 m, and half-round crest shapes. Each weir was installed on a level HDPE apron in the model reservoir. All arced labyrinth weirs were installed projecting into the reservoir, as shown in Figure 2. Piezometric head (±0.15mm) was measured upstream of each weir at a location where the velocity head was negligible (i.e., total head equals piezometric head). The weir discharge was measured using a calibrated flow meter (±0.25%) in the upstream supply piping. C_d values were calculated using total head, measured discharge, and Eq. (1).

Discharge efficiency was determined based on head-discharge relationships. Because the weir length was not maintained constant for all arced labyrinth weir configurations tested, the discharge efficiency, as quantified by the relative value of C_d, represents the weir unit discharge (discharge divided by the weir length) at a given upstream head condition. 2-D flow velocities were measured upstream using a Sontec® flow-tracker device. Velocity vector fields were then digitized to characterize the nature of the approach flow field. These relationships were compared to previous data presented by CROOKSTON and TULLIS (2012 a, b, & c).

RESULTS & DISUSSION

CROOKSTON (2010) tested six arced labyrinth weir models ($\theta = 10°, 20°, 30°, \alpha = 6°, 12°$). In this study, $\alpha = 12°$ data were repeated, and $\alpha = 20°$ data were added to extend CROOKSTON's (2010) findings. These variations are categorized into geometrically similar and geometrically comparable weirs. Geometric similarity refers to a condition where all geometric parameters for one labyrinth weir are uniformly scaled in producing the geometry of a second labyrinth weir. Arced labyrinth weirs with geometrically similar cycles, but arranged with different arc angles (θ), are referred to as geometrically comparable.

C_d data were collected from $0.1 \leq H_T/P \leq 0.9$ for $N=5$ configurations and $0.1 \leq H_T/P \leq 0.5$ for $N > 5$. C_d vs. H_T/P trend lines were developed using data-fitting software. Figure 3 shows the experimental C_d vs. H_T/P data for $\alpha = 12°$ and 20° sidewall angled weirs.

Cycle Arcing Effects

Based on the data presented in Figure 3, several observations were made. For both the $\alpha = 12°$ and 20° sidewall angled weirs, the discharge efficiency, as characterized by C_d, increased with increasing θ, particularly for relatively lower heads. Increasing the cycle arc angle, which subsequently reduces the arc radius, splays out the labyrinth weir cycles to better accommodate 180° converging approach flow conditions. At relatively high heads ($H_T/P > 0.4$ to 0.6),

however, the discharge efficiency gains from the larger θ values tended to be lost. As local submergence formed in the outlet cycles at higher heads, the approach flow streamlines in the reservoir began to orient themselves more with the downstream channel centerline and less with the inlet cycle centerlines. The distal cycles were also exposed to greater flow separation and turbulence at the weir/training wall boundary. The combined effects resulted in increased head loss and decreased hydraulic efficiency.
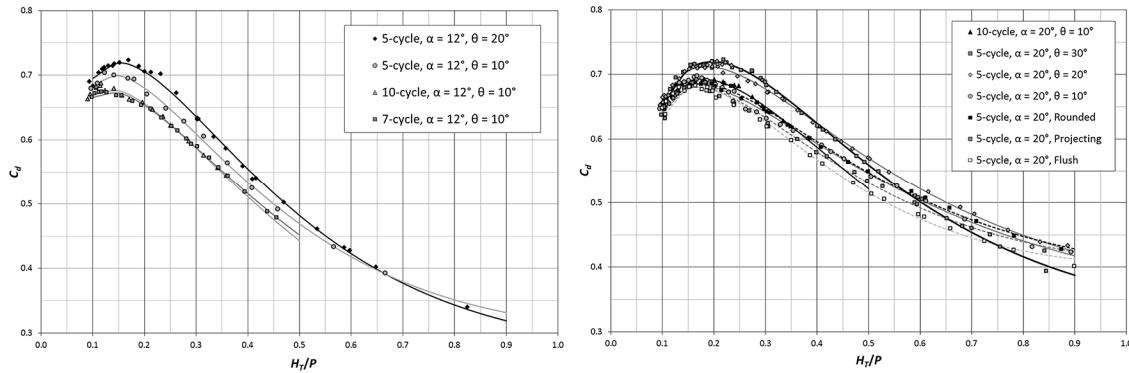
Figure 3 – Sidewall angle $\alpha = 12°$ (left) & 20° (right) discharge data with trend lines

As local submergence increased in the arced labyrinth weir and the approach flow streamline orientations adjusted, the head-discharge control point began to transition from the weir crest to the points farther downstream. At very high heads, the weir was fully submerged and the control point shifted to the discharge channel inlet (contracting sidewalls downstream of the labyrinth weir). Velocity data were collected in the reservoir upstream of each arced weir configuration, and velocity vector fields were digitized to show the changes in flow alignment (caused by a control point shift). The velocity vectors in Figure 4 illustrate changes in approach flow alignment with increasing upstream head.
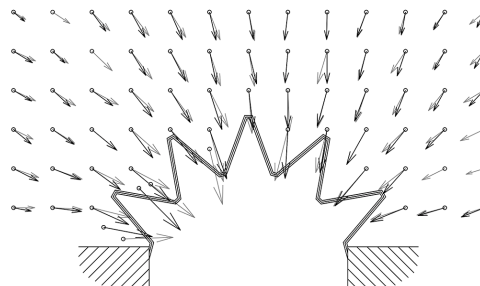
Figure 4 – Change in approach flow velocity vector alignment with as a function of upstream head (5-cycle, $\alpha = 20°$, $\theta = 30°$): $H_T/P = 0.3$ (grey), $H_T/P = 0.6$ (black).

Abutment Influences for Traditional Labyrinth Weirs in Reservoir Applications

CROOKSTON (2010) investigated the influence of abutment wall geometries on the discharge efficiency of traditional labyrinth weirs in reservoir applications. The same reservoir-specific labyrinth weir/abutment wall geometries were also evaluated in this study for $\alpha = 20°$ labyrinth weirs. The placement of the weir, either projecting into the reservoir or flush with the outlet, was also investigated. Three traditional labyrinth weir configurations were tested: projecting, flush (square-edged abutments), and rounded abutments (Figure 5).
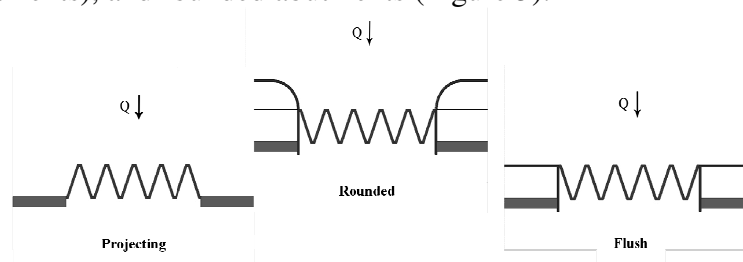
Figure 5 – Weir Placement & Abutment Types

For $\alpha = 20°$ weirs, the rounded inlet was approximately 3% more efficient than the projecting and flush configurations for $H_T/P > 0.2$. Compared to the projecting weir (at similar heads, $H_T/P = 0.3$), the rounded inlet prevented unstable nappe formation on inner sidewalls and caused the nappe to remain in a clinging/non-aerated state for more time (Figure 6). For $\alpha = 20°$ weirs, the rounded inlet also eliminated flow separation and turbulent flow over the crest, allowing for nappe stabilization and improved discharge efficiency. The flush setup was consistently less efficient for all sidewall angles. Applying these results to arced labyrinth weirs may indicate that rounded inlets would help alleviate instability and flow separation concerns on some arced labyrinth weirs, especially for distal cycles on $\alpha \geq 20°$ weirs, further improving overall weir efficiency. Note that as the overall labyrinth weir length increases, the influence of abutment-induced flow separation on hydraulic efficiency diminishes.
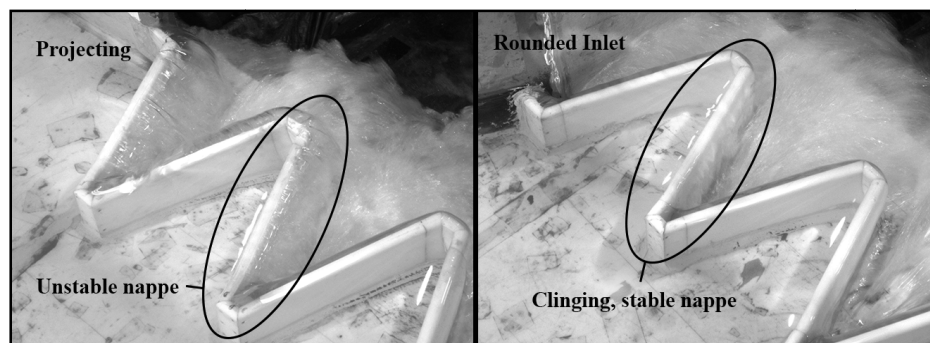
Figure 6 – Projecting weir (Left) vs. rounded inlet weir (Right) at $H_T/P = 0.3$

Sidewall Angle Effects

The investigation of the effect of the sidewall angle on flow can be seen in C_d data for $\alpha = 12°$ and $\alpha = 20°$ arced labyrinth weirs normalized to C_d data for non-arced projecting weirs. These data indicate that for the $\alpha = 12°$ and $20°$ configurations, arcing a labyrinth weir in a reservoir increases discharge efficiency by approximately 10 to 20% (Figure 7). The relative increase in discharge efficiency, compared to the projecting configuration with the same α, is more significant for $\alpha = 12°$ than $\alpha = 20°$.
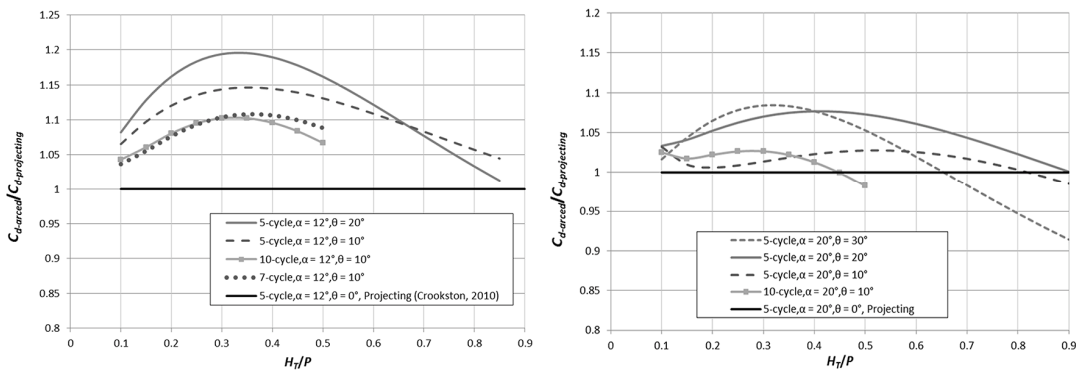
Figure 7 – Arced weir compared to non-arced weir in reservoir for $\alpha = 12°$ (Right) & $20°$ (Left)

CONCLUSIONS

The flow characteristics observed in this study provide additional insights into understanding arced labyrinth weir behavior. All data were compared to CROOKSTON (2010) data and highlight the importance of selecting effective configurations. Larger sidewall angles and cycle arc angles present various problems for efficiency, such as flow turbulence at weir/wall boundaries, local submergence, and nappe instability. Rounded inlet modifications may help alleviate some of these concerns, particularly for projecting, traditional labyrinth weirs (non-arced). Selection of appropriate α and θ geometries should be accomplished on a case-by-case basis.

   This study will benefit future designers because it explains some of the flow characteristics that directly impact implementation of arced labyrinth weirs. Although no design method exists for this type of weir, this project takes multiple steps forward toward creating one.

NOMENCLATURE

   α =   Sidewall angle (used for linear or arced configurations)

   α' =   Upstream sidewall angle, $\alpha' = \alpha + \theta/2$

H_T = Total measured head relative to the crest

l_c = Centerline length of the sidewall

$L_c \ or \ L$ = Centerline crest length of entire weir

$L_{c\text{-}cycle}$ = Centerline crest length of one cycle

N = Number of cycles

P = Weir crest height

Q = Flow

R = Arced radius, $R = (W^2/4 + r'^2)^{1/2}$

r' = Segment height from channel opening to perpendicular downstream apex

r = Segment height from channel opening to center of imaginary arc circle

θ = Cycle arc angle, $\theta = \Theta/N$

Θ = Central arc angle, $\Theta = W'/R$

t_w = Wall thickness at crest

W = Downstream channel width

W' = Labyrinth weir arc length (through downstream apexes), $W' = R\Theta$

w' = Cycle arc width, $w' = W'/N$

REFERENCES

CHRISTENSEN, N.A. (2012). "Flow characteristics of arced labyrinth weirs." *M.S. Thesis*. Utah State University Library, Logan, UT, USA, pp. 22-51

CORDERO PAGE, D., GARCIA, V.E., GRANELL NINOT, C. (2007). "Aliviaderos en Laberinto. Presa de Maria Cristina." *Ingenieria Civil*, CEDEX, Madrid, Spain, Vol. 146, pp. 15-18. (Spanish)

CROOKSTON, B.M. (2010). "Labyrinth Weirs." *Dissertation*. Utah State University Library, Logan, UT, USA, pp. 44-66, 95-122

CROOKSTON, B.M., and TULLIS, B. (2012 a). "Arced labyrinth weirs." *J. Hydraul. Eng.,* Vol. 138, No. 6. pp. 555-562

CROOKSTON, B.M., and TULLIS, B. (2012 b). "Discharge efficiency of reservoir-application-specific labyrinth weirs" *J. Irrig. and Drain. Eng.,* Technical Note, ASCE, 138(6): 564-568

CROOKSTON, B.M., and TULLIS, B. (2012 c). "Labyrinth weirs: nappe interference and local submergence" *J. Irrig. and Drain. Eng.,* ASCE, 138(8): 757-765

FALVEY, H. (2003). "Hydraulic Design of Labyrinth Weirs." *ASCE Press*, Reston, VA, USA, pp. 32.

HENDERSON, F. (1966). "Open Channel Flow." *Channel controls*, MacMillan, New York, pp. 174-176

KOCAHAN, H., and TAYLOR, G. (2002). "Rehabilitation of Black Rock Dam. Seepage and Inadequate Spillway." *Hydroplus Inc.*, Arlington, VA, USA. pp. 12.

TULLIS, J.P., NOSRATOLLAH, H., WALDRON, D. (1995). "Design of Labyrinth Spillways." *J. of*

Hydraul. Eng., Vol. 121, No. 3, pp. 247-255.

STAGED AND NOTCHED LABYRINTH WEIR HYDRAULICS

Mitchell R. DABLING

Utah Water Research Laboratory, Dept. of Civil and Environmental Engineering,

Utah State University, U.S.A., mrdabling@gmail.com

Brian M. CROOKSTON, Ph.D.

Schnabel Engineering and Utah State University, U.S.A., bcrookston@gmail.com

ABSTRACT: Replacement spillways are frequently required to pass revised and larger design storm events. Generally matching the outflow hydrograph of the existing spillway is also a common design requirement. Labyrinth spillways can increase spillway discharge capacity. Staged and notched sections of crest have been used in design to satisfy discharge hydrograph requirements. However, inadequate hydraulic design information is available specific to staged and notched labyrinth weirs. In this study, the flow characteristics of multiple staged and notched labyrinth weir configurations (laboratory-scale) were tested. Head-discharge relationships were evaluated experimentally and compared with computed results using superposition (predicting the discharge over the upper and lower stages separately and summing). The results of this comparison show that, for all configurations tested, the superposition technique estimated actual discharges by approximately ±10%.

Keywords: labyrinth spillways, staged weir, head-discharge relationship, flood impacts

INTRODUCTION

Labyrinth Weirs

Dams are a critical infrastructure component throughout the world. They provide water supply (municipal, agricultural, industrial), flood control, hydropower, navigation, and recreation. The benefits provided by many existing dams are still needed today, with new dams regularly under construction to meet growing needs. However, aging infrastructure, new spillway design flood criteria, and increasing water supply demands often require spillway rehabilitation.

As shown in Figure 1, the geometry of a labyrinth weir can significantly increase the crest length within a given channel width. The additional crest length will generally increase discharge capacity for a given upstream water elevation. As a result of their hydraulic performance, labyrinth weirs have been of interest to practitioners and researchers for many years. A selection of labyrinth weir design publications focused on discharge performance are: HAY and TAYLOR (1970), DARVAS (1971), HINCHLIFF and HOUSTON (1984), LUX and

HINCHLIFF (1985), MAGALHÃES and LORENA (1989), TULLIS et al. (1995), MELO et al. (2002), FALVEY (2003), TULLIS et al. (2007), CROOKSTON (2010), CROOKSTON et al. (2012), and CROOKSTON and TULLIS (2012a,b,c). Labyrinth weirs have been used with great success to increase spillway capacity and manage upstream flooding.
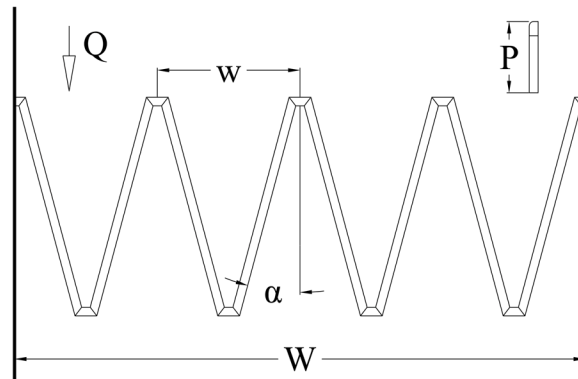
Figure 1 – Labyrinth weir geometric and hydraulic variables

Replacement spillways are frequently required to pass revised and larger design storm events; they are also often required to generally match the outflow hydrograph of the existing spillway. For example, peak outflows from a new spillway may be required to be less than or equal to the existing spillway peak outflows for the more frequent (e.g., 2-, 10-, and 100-year) flood events. The increased hydraulic capacity of a labyrinth spillway can decrease reservoir attenuation and increase peak outflows, which could potentially increase downstream flooding for moderate floods that occur with greater frequency (PAXSON et al. 2011).

Staged Labyrinth Spillways

In order to meet spillway peak outflow requirements, a variety of spillway types (e.g., broad-crested weirs, ogee spillways, labyrinth spillways) have been designed and built that feature multiple crest elevations. Such spillways are termed staged or notched spillways. Although the terms 'notch' and stage' have been used interchangeably in conversation and published literature, this paper defines a stage as any portion of the spillway crest set at a different elevation. A notch refers to a low stage with a crest length that is less than the labyrinth sidewall length. A notch or lower stage(s) may be set at the normal pool elevation and convey base flows and runoff from smaller storms (e.g., up to the 100-year event). The higher stage would provide the additional discharge capacity required for the more extreme event (e.g., probable maximum flood). In addition to 'tuning' the head-discharge rating curve, notched or multi-staged crests confine base-flows and smaller storm events to a portion of the spillway and, at very low heads,

can thicken the nappe in the lower stage(s) to prevent nappe vibration, and limit algal growth. The recently constructed Lake Townsend Dam (presented in Figure 2) features a 7-cycle staged labyrinth spillway; 2 cycles have a lower stage elevation by approximately 0.3 m.

Figure 2 – Staged labyrinth spillway at Lake Townsend, Greensboro, NC, USA

Although numerous design methods have been published for labyrinth weirs, there is insufficient design information available regarding labyrinth weirs with staged or notched crests. Practicing engineers would benefit from this information, as it would facilitate more accurate stage-discharge relationship estimations. The objective of this study is to investigate the hydraulic performance of notched and staged labyrinth weirs.

EXPERIMENTAL SETUP

Physical modelling was conducted at the Utah Water Research Laboratory (UWRL) in a gravity-fed rectangular laboratory flume (1.2-m x 14.6-m x 1.0-m deep). A 4-cycle 15° sidewall angle (α = 15°) labyrinth weir with a quarter-round crest shape was tested with the following crest stage/notch configurations (see Figure 3): apex notches, one-half sidewall length notch (centered on upstream apex), one staged cycle, and an unmodified labyrinth (constant crest elevation). Staged and notched section depths were 20% of the weir height and featured a quarter-round crest shape. However, due to the size of the apex notches, the crest within those notches was flat-topped. The test matrix is summarized in Table 1.
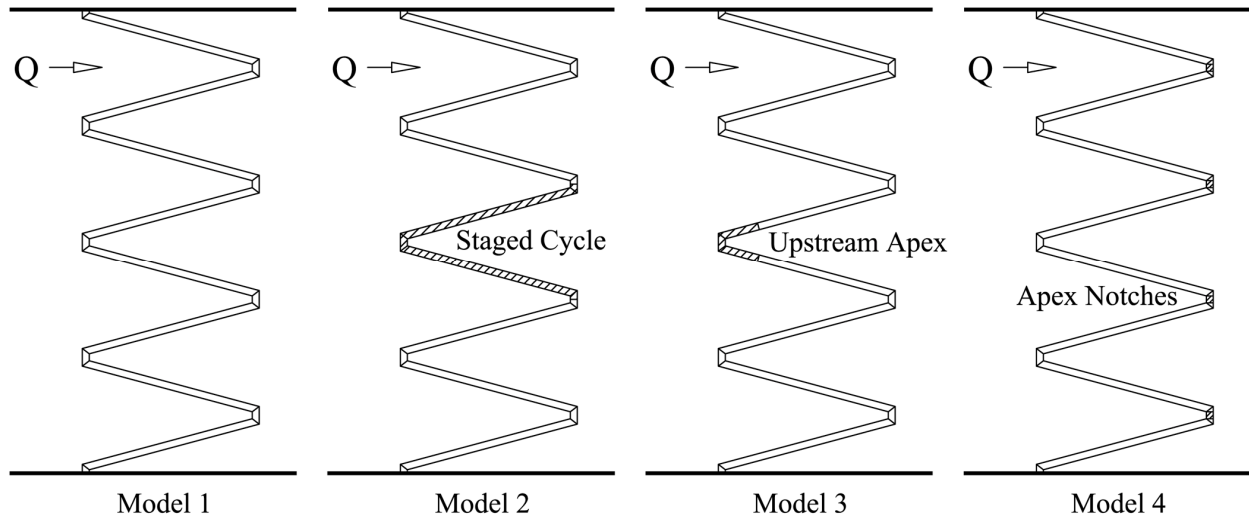
Figure 3 – Schematic of tested weir configurations

Table 1 – Physical model test matrix

Labyrinth Geometry	Model		Stage/Notch Geometry	
	(#)	Description	l_{stage}	Crest Shape[†]
$\alpha = 15°$, $N = 4$	1	No Stage	0.0 mm	QR
$L_{c\text{-}cycle} = 995.7$ mm	2	Staged Cycle	995.7 mm	QR
$P = 152.4$ mm	3	Notched Upstream Apex	232.6 mm	QR
$w = 305.9$ mm	4	Apex Notches	18.4 mm x 4	Flat

† QR = Quarter Round where $R_{crest} = 1/2\ t_w$

EXPERIMENTAL RESULTS

Head-discharge Performance

Eq. 1 was selected to quantify the head-discharge relationship of the tested physical models. It is a common form of the weir equation (HENDERSON 1966) and was used to calculate discharge coefficients for varying flow conditions.

$$Q = \frac{2}{3} C_d L \sqrt{2g} H_t^{3/2}$$ (1)

In Eq. (1), Q is flow rate; Cd is a dimensionless discharge coefficient that varies with weir type, geometry, crest shape, and flow conditions; L is the weir crest length; g is the gravitational acceleration constant; and Ht is the free-flow (non-submerged) upstream total head measured relative to the weir crest elevation. Ht was used rather than the piezometric head (h) to account for approach flow velocities. A stilling well equipped with a point gauge readable to ±0.15mm

located 6.5P (P is the weir height) upstream of the weir, was used to measure h. Ht was then calculated as h+V2/2g. Approximately 15 to 30 flow measurements were taken for each weir configuration. Cd values were computed for each measured flow condition and are presented in Figure 5. An empirical curve-fit equation based upon the headwater ratio, Ht/P, was fit to experimentally determined Cd values (R2 > 0.995) and is presented as Eq. (2). Corresponding curvefit coefficients are presented in Table 2.

$$C_d = a \left(b^{\frac{H_t}{P}} \right) \left(\frac{H_t}{P} \right)^c + d \qquad (2)$$
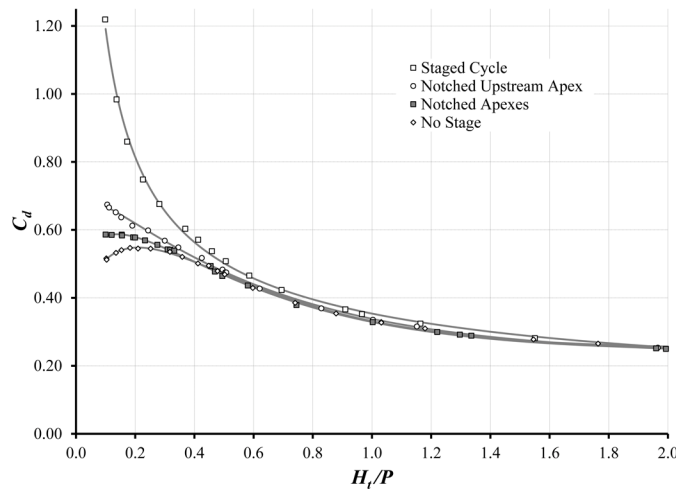
Figure 4 – Head-discharge relationships of tested weirs

Table 2 – Physical model test matrix

Model		Coefficients for Eq. 2			
(#)	Description	a	b	c	d
1	No Stage	1.3400	0.0616	0.5860	0.2489
2	Staged Cycle	0.2617	0.7997	-0.6117	0.1445
3	Notched Upstream Apex	0.6312	0.1701	0.0819	0.2309
4	Notched Apexes	0.9058	0.0976	0.3232	0.2407

Figure 4 presents the head-discharge relationships for each labyrinth model; the experimental setup did not allow flow measurement specific to the staged section. Note in Figure 4 that the experimentally determined C_d values are greater than C_d values of the unmodified labyrinth weir for a given H_t/P. This is partly due to flows concentrated over the low stage, which impacted the discharge performance of the entire spillway model. Because of the additional flow over these notches, C_d value estimations are higher than those typical of a labyrinth weir with similar cycle geometry and a single crest elevation. This can result in C_d values being greater than 1.0.

The applicability of the principle of superposition was investigated (total Q is a function of the sum of Q over each stage) using the experimental results for comparison. Flow was calculated over the high stage of the labyrinth weir using Eq. 1 with the weir length adjusted to $L = L_c - l_{stage}$. To calculate the flow over the notch/stage, $L = l_{stage}$. H_t data and single-stage C_d were used to calculate flow over each stage. The flow over each stage was calculated independently and then summed to estimate discharge for the models. The percent error was then calculated between the predicted flow rate and the observed experimental results [$100*(Q_{predicted} - Q_{laboratory})/Q_{laboratory}$]. These data are presented in Figure 5.
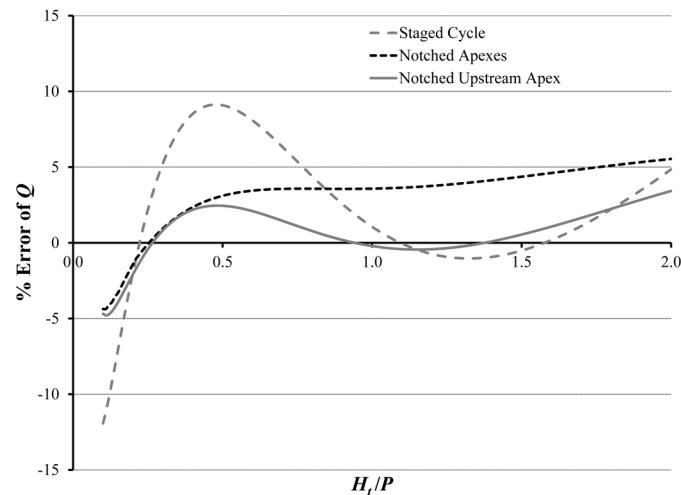
Figure 5 – % Error of Q at varying levels of H_t/P

Because the apex notches were essentially channelized and flat topped, the C_d values used were from JOHNSON's (2000) study of flat-topped broad crested weirs. For other weir configurations, calculating flow using a contracted weir equation was evaluated (HAESTAD 2002), but this data set produced larger % error values than using labyrinth C_d values, therefore the experimental results from the non-staged labyrinth weir from this study were used.

For low levels of upstream head ($H_t/P < 0.25$) the superposition method underestimates the weir flow by up to 15%. At higher levels of head, the accuracy of the superposition method varied from 2% underestimation to 9% overestimation depending on weir configuration and the value of H_t/P. Flow imbalance over the model resulted in head-discharge relationships and weir coefficients that are not typical of non-staged labyrinth weirs.

CONCLUSIONS

The results of this study provide design guidance for staged and notched labyrinth weirs and identify the accuracy of using superposition to estimate staged labyrinth weir discharges. This study was performed to increase the understanding of the design and flow characteristics of staged and notched labyrinth weirs. It is anticipated that additional data analysis will result in a more accurate technique to estimate discharge over staged and notched linear weirs and will help practicing engineers design replacement spillways more accurately and efficiently. Recommendations for future research include varying the notch location, length, and depth. Multiple stages at two or more elevations would also be of interest.

NOMENCLATURE

A = labyrinth weir sidewall angle;

C_d = dimensionless discharge coefficient;

g = gravitational constant;

h = piezometric head;

H_t = total upstream head of a weir relative to the crest elevation;

L = weir centerline crest length;

$l_{c\text{-}cycle}$ = weir centerline crest length of one cycle;

l_{stage} = centerline crest length of notch/stage;

N = number of cycles in labyrinth weir;

P = weir height;

Q = flow;

REFERENCES

CROOKSTON, B.M. (2010). "Labyrinth weirs." Ph.D. dissertation, Utah State Univ., Logan, UT.

CROOKSTON, B.M. and TULLIS, B.P. (2012a). "Arced labyrinth weirs." *J. of Hydr. Engrg., ASCE,* 138(6). Posted ahead of print 5 January 2012.

CROOKSTON, B.M. and TULLIS, B.P. (2012b). "Discharge efficiency of reservoir-application-specific labyrinth weirs." *J. Irrig. Drain. Engr., ASCE,* 138(6). Posted ahead of print 19 December 2011.

CROOKSTON,B.M. and TULLIS, B.P. (2012c). "Hydraulic design and analysis of labyrinth weirs. Part 1: Discharge relationships." *J. Irrig. Drain. Engr., ASCE,* (under final review).

CROOKSTON, B.M. and TULLIS, B.P. (2012d). "Hydraulic design and analysis of labyrinth weirs. Part 2: Nappe aeration, instability, and vibration." *J. Irrig. Drain. Engr., ASCE,* (under final review).

DARVAS, L. (1971). "Discussion of performance and design of labyrinth weirs," by Hay and Taylor. *J. of Hydr. Engrg., ASCE,* 97(80): 1246-1251.

FALVEY, H. (2003). "Hydraulic design of labyrinth weirs." ASCE, Reston, VA.

HAY, N., and TAYLOR, G. (1970). "Performance and design of labyrinth weirs." *J. of Hydr. Engrg., ASCE,*, 96(11), 2337-2357.

HINCHLIFF, D., and HOUSTON, K. (1984). "Hydraulic design and application of labyrinth spillways." *Proc. of 4th Annual USCOLD Lecture.*

LUX III, F. and HINCHLIFF, D. (1985). "Design and construction of labyrinth spillways." *15th Congress ICOLD, Vol. IV, Q59-R15,* 249-274.

MAGALHÃES, A., and LORENA, M. (1989). "Hydraulic design of labyrinth weirs." *Report No. 736*, National Laboratory of Civil Engineering, Lisbon, Portugal.

MELO, J., RAMOS, C., and MAGALHÃES, A. (2002). "Descarregadores com soleira em labirinto de um ciclo em canais convergentes. Determinação da capacidad de vazão." *Proc. 6° Congresso da Água,* CD-ROM, Porto, Portugal. (in Portuguese).

PAXSON, G., CAMPBELL, D., and MONROE, J. (2011). "Evolving design approaches and considerations for labyrinth spillways." *Proc. 31st Annual USSD Conf.,* San Diego, CA, USA. CD-ROM.

TULLIS, B.P., YOUNG, J., and CHANDLER, M. (2007). "Head-discharge relationships for submerged labyrinth weirs." *J. of Hydr. Engrg., ASCE,* 133(3), 248-254.

TULLIS, P., AMANIAN, N., and WALDRON, D. (1995). "Design of labyrinth weir spillways." *J. of Hydr. Engrg. ASCE,* 121(3), 247-255.

PHYSICAL MODELING AND CFD COMPARISON: CASE STUDY OF A HYDRO-COMBINED POWER STATION IN SPILLWAY MODE

Gonzalo DURÓ

Hydromechanics Laboratory, National University of La Plata, Argentina, gzduro@gmail.com

Mariano DE DIOS and Alfredo LÓPEZ

Hydromechanics Laboratory, Argentina, dediosmariano@gmail.com, lopito.82@gmail.com

Hydromechanics Laboratory Director: Sergio O. LISCIA

ABSTRACT: This study presents comparisons between the results of a commercial CFD code and physical model measurements. The case study is a hydro-combined power station operating in spillway mode for a given scenario. Two turbulence models and two scales are implemented to identify the capabilities and limitations of each approach and to determine the selection criteria for CFD modeling for this kind of structure. The main flow characteristics are considered for analysis, but the focus is on a fluctuating frequency phenomenon for accurate quantitative comparisons. Acceptable representations of the general hydraulic functioning are found in all approaches, according to physical modeling. The k-ε RNG, and LES models give good representation of the discharge flow, mean water depths, and mean pressures for engineering purposes. The k-ε RNG is not able to characterize fluctuating phenomena at a model scale but does at a prototype scale. The LES is capable of identifying the dominant frequency at both prototype and model scales. A prototype-scale approach is recommended for the numerical modeling to obtain a better representation of fluctuating pressures for both turbulence models, with the complement of physical modeling for the ultimate design of the hydraulic structures.

Keywords: CFD validation, hydro-combined, k-ε RNG, LES, pressure spectrum

INTRODUCTION

In the last decades, numerical simulation of three-dimensional flow patterns has become an appealing tool for the representation of the particular dynamics induced by different hydraulic structures, e.g., power station intakes (KHAN et al. 2004), pump intakes (LI et al. 2004), spillways (JOHNSON and SAVAGE 2006), and breach dam breaks (LAROCQUE et al. 2013). In addition, CFD (Computational Fluid Dynamics) has also been applied for fundamental physics research, e.g., ADRIAN (2007) summarized developments through direct numerical simulation and particle image velocimetry of hairpin vortex organization and packet formation. From an engineering perspective, CFD is especially attractive for hydraulic design due to its

flexibility in simulating alternative geometries and performing sensitivity analyses, visualization capabilities, modeling large structures or areas, and low costs (once validated) compared to undertaking physical modeling (DEWALS 2013).

On the other hand, physical modeling offers different characteristics to derive adequate hydraulic design and gain insight into the hydrodynamics (NOVAK 2010). The complexity of prototype flows is represented if scale factors are adequately chosen. However, design, building and operation of physical models may take long periods of time. Moreover, flow visualization can be difficult, while non-intrusive and accurate measurement of variables requires care, methodology and appropriate instrumentation.

Careful interpretation and critical analysis should be exercised in both numerical and physical approaches, combined with result validation, in order to use them with confidence when dealing with hydraulic design changes.

The present work aims at, first, introducing the flow characteristics of a hydro-combined power station in spillway mode with a remarkably high discharge capacity, and second, presenting numerical results in contrast with experimental data to provide insight into the capabilities of a commercial CFD code to represent the main hydraulic variables, i.e., discharge, mean pressures, water levels, and vortex shedding frequency. As a consequence, the study intends to contribute to the literature of CFD validations in the case of a complex hydraulic structure and the analysis of prototype-scale CFD modeling results for two turbulence models, and provide insights to identifying the most convenient approaches when facing hydraulic design.

The hydraulic structure in this study is part of a very challenging project that involves the modification of five existing bays in the Aña Cuá spillway, located in the Paraná River, to generate 273 MW rather than freely discharge as at present. Each unit of the powerhouse will be able to operate either as a turbine or as a spillway, thanks to the operation of a second tainter gate.

METHODOLOGY

The study had a hybrid approach, which considered the results of both numerical and physical modeling of the structure in question to characterize its main hydraulic functioning. This composite modeling allowed for further comparisons between these tools to identify respective advantages and drawbacks.

First, an analysis was made at model scale comparing the results of the k-ε RNG (Renormalization-Group) and the LES (Large Eddy Simulation) turbulence models with experimental measurements, taking into consideration the general hydraulic behavior, discharge

capacity, water levels in the middle longitudinal profile, mean pressures at fixed locations, and dominant pressure fluctuation frequency at the discharge canal. This last item can be easily identified, particularly at locations 2 and 4 (Figure 4), allowing either of them to be independently studied. Point 3 was not considered due to its more complex pressure spectrum, in which the dominant frequency was not as clearly identifiable as in the aforementioned points.

Second, prototype-scale simulations with both turbulence models were compared with up-scaled experimental data: the discharge and the dominant pressure fluctuation at the discharge canal nose.

The scenario under study comprised a combination of an extraordinary flood event and the minimum reservoir level, which is the worst condition regarding the potential formation of a hydraulic jump over the discharge canal, as identified in both the physical model and the numerical tests. A single unit was analyzed, functioning between two other operating units so that a symmetric approaching flow in the reservoir could be assumed. Finally, one preliminary hydraulic design was studied through both physical and numerical modeling.

Physical modeling

The experimental study was conducted at the National University of La Plata. The physical model (Figure 1) had a 1:40 scale. The power station model had a length of 2.63 meters from the spillway piers to the end of the discharge canal above the turbine (Figure 4), and it was connected downstream and upstream to 0.475 meters wide flumes.

Figure 1 – Physical scale model (left). Upstream flume and point gauge (right)

The water levels were regulated by means of a bell-mouth spillway situated in a cylindrical basin (Figure 1) and a sluice gate, at the upstream and downstream flume extremes, respectively. The discharge was measured from a V-shaped sharp-crested weir with an accuracy estimated to

be 4%. The water levels were measured with a point gauge with a vertical accuracy of 0.1 millimeters. The pressure was sampled with a pressure transducer during 200 seconds at 100 Hz.

CFD modeling

The CFD code applied to this study was FLOW-3D™ v9.4.5, developed by FlowScience Inc., which numerically solves the Navier-Stokes equations using the k-ε RNG model or the LES technique and a Smagorinsky subgrid-scale model. The free surface is represented through the Volume-Of-Fluid method (HIRT and NICHOLS 1981). Solid boundaries are defined by the FAVOR® method, the accuracy of which depends on the cell size chosen. A third-order advection method is used to approximate the solutions. Four simulations were carried out to compare results between the two different turbulence models at model and prototype scales.

The CFD modeled geometry (Figure 2) was analogous to the physical model structure and flumes. It had uniform roughness coefficients of 0.0001 meters at model scale and 0.001 meters at prototype scale, assuming for the latter a smooth concrete surface. The domain was divided into three blocks for meshing purposes to optimize the simulation run time: the upstream flume representing the reservoir, the power station, and the downstream flume representing the tail water. The mesh blocks had uniform cubic cells, with sides at model scale that were 0.0125 meters for the flumes and 0.00625 meters for the power station, equaling 1/27 and 1/54 of the total energy head over the spillway crest, respectively. The inlet and outlet boundary conditions were set up as stagnation pressures so that the total energy head at the reservoir and the river could be properly represented.
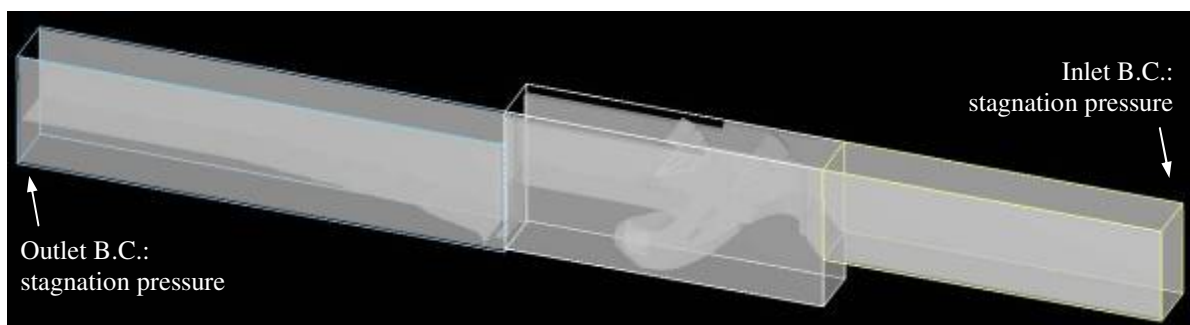
Figure 2 – Mesh blocks for the modeled domain with the boundary conditions

Preliminary simulations with coarse meshes were conducted to reach the steady flow condition. At a later stage, finer meshes were used, which were more demanding in terms of computing time and data storage, to finally arrive at the previously described (Table 1). It is worth mentioning that, in this process, grid independence was achieved in terms of discharge capacity with both turbulence models, i.e., the same volume flow rate, reported in Table 1, was

recorded between the final mesh (0.00625 m high cells) and the previous one (0.0125 m high cells). In addition, mass conservation was verified between mesh blocks, showing a maximum discharge difference of 0.2% for all the final simulations. The turbulent mixing length equals 7% of the water depth at the spillway crest for k-ε RNG.

RESULTS

The general behavior predicted by CFD simulations was in agreement with the one observed in the physical model. According to the visual inspection, the flow along the power station was straight until the tailwater, even over the turbine intake and the discharge canal. The flow regime remained supercritical after the spillway crest and no major perturbations were observed along the power station.

Free surface, discharge, and mean pressures
The free surface simulated by the k-ε RNG model appeared smoother than the one obtained by the LES model (Figure 3), and both were able to predict two cross waves arising over the turbine intake. However, only the LES model predicted an oscillating free surface over the discharge canal and small fluctuating diagonal waves against the walls that moved downstream, a phenomenon also confirmed by observation in the physical model.

The discharges obtained by numerical simulations at the model scale were higher than the physical model measured discharge, namely, 13% for the k-ε RNG model and 10% for LES. Down-scaling the discharges from the prototype-scale simulations through Froude's similarity law showed a discharge increase of 2.1% compared to the model-scale numerical results.

There was a fair general agreement between the water levels in the physical model and those obtained with the CFD simulations (Figure 4). However, both numerical models presented higher mean temporal values than the experimental, which can be clearly appreciated over the spillway crest. Over the discharge canal (points 4-10), temporal oscillations of the water level were observed, but as they could not be measured with the point gauge, the applied criterion to make quantification possible was to adopt the highest level during periods of 30 seconds at each point. As a result, the actual mean temporal values over the canal are slightly (approximately 1 cm) below the measured ones, plotted in Figure 4.

The analysis of mean pressures at different fixed locations in the physical model showed that CFD simulations overestimated the experimental data by approximately 13%, which is consistent with the results obtained for the discharges.

Fluctuating phenomenon: vortex shedding
A high shear layer was located between the stream flowing over the turbine intake and the

recirculating water near the turbine bulb (blue velocities in Figure 3). The difference in velocity magnitudes between these two regions was significant, and as a consequence, the arising instability led to the formation of vortices. The employed turbulence models yielded divergent results in this respect: the LES wass able to simulate an oscillating free surface and fluctuating pressure and velocity fields (Figure 5), while the k-ε RNG model failed to represent any of these phenomena.
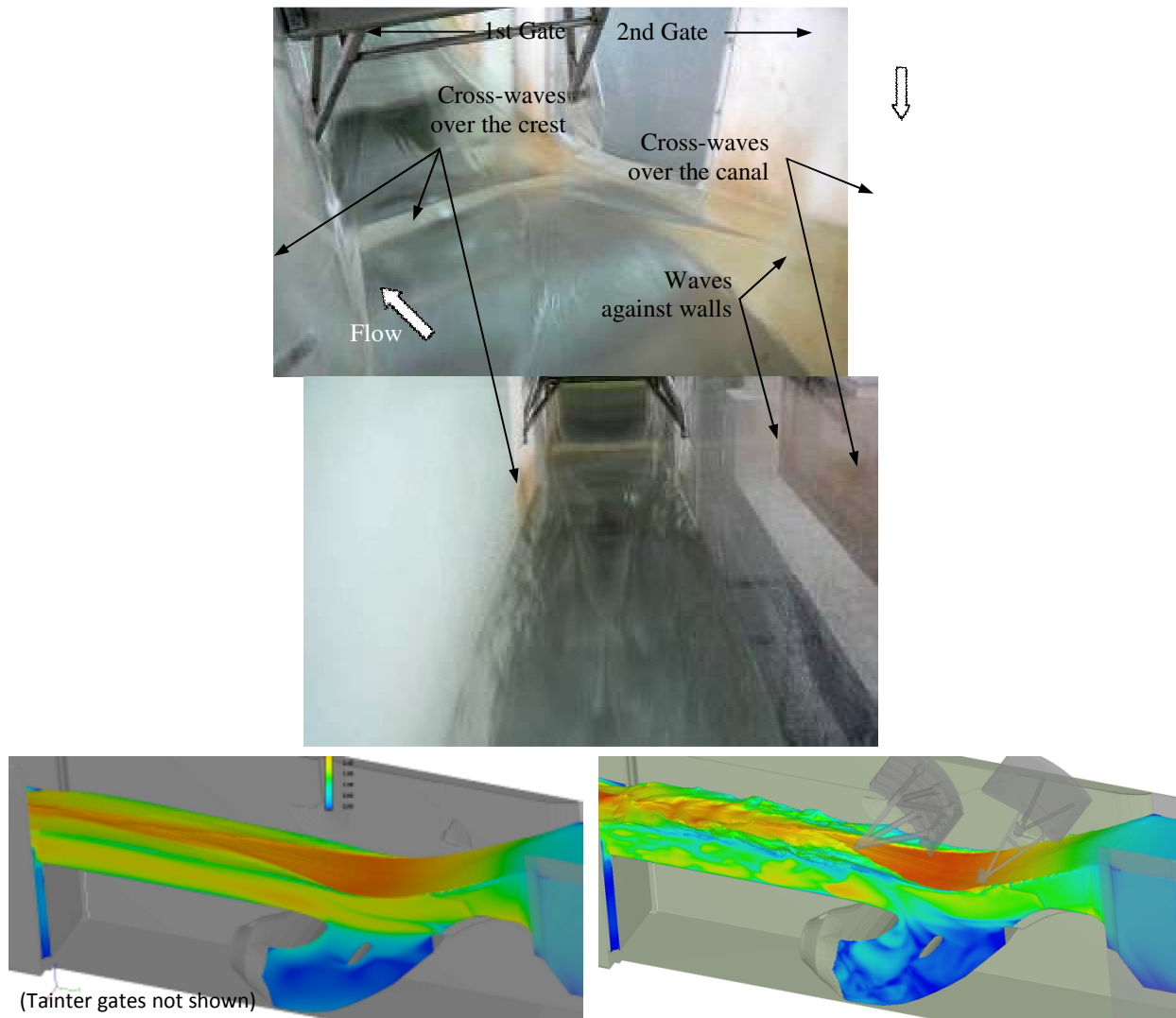
Figure 3 – Free surface views. Bottom left: k-ε RNG model. Bottom right: LES.

Only the frequency of the fluctuations was analyzed, neglecting the amplitude, since the magnitude of the latter was within the pressure transducer error, i.e., 0.02 meters, so no conclusions were drawn in that respect. The pressure acquisition frequency was 100 Hz, right above the Nyquist frequency (GRENANDER 1959), to avoid aliasing, even at the highest

considered frequency of analysis, which was 14 Hz (Figure 6).

Table 1 – Discharge flows, simulations characteristics, pressure sampling characteristics

	CFD - Model scale		Physical model	CFD - Prototype scale	
Turbulence model	k-ε RNG	LES	N/A	k-ε RNG	LES
Computing time for 30sec [hr]	142	94	N/A	13	12
Cell size (cube height) [m]	0.00625	0.00625	N/A	0.25	0.25
Discharge (Q_i) at model scale [m³/s]	0.159	0.155	0.141	0.162*	0.158*
Difference: (Q_i-Q_{PM})*100/Q_{PM}	12.8%	9.9%	0%	14.9%	12.1%
Discharge at prototype scale [m³/s]	1609*	1568*	1431*	1635	1598
Pressure sampling frequency [Hz]	100	100	100	100	100
Pressure sampling time [sec.]	30	15	200	20	20

*Calculated from Froude's similarity law
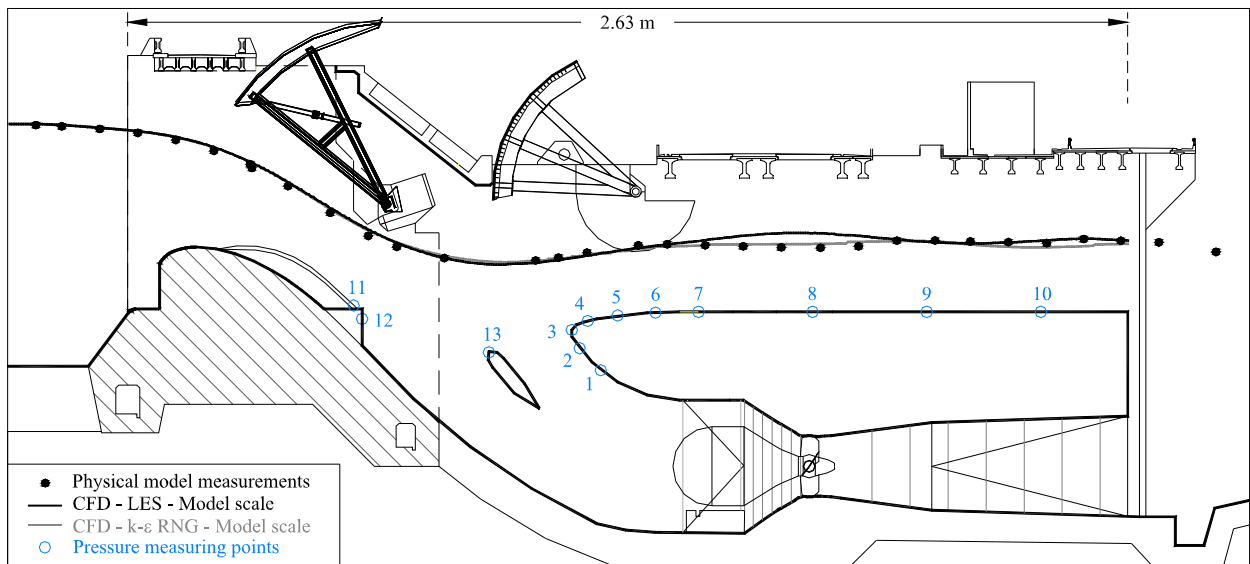
Figure 4 – Water levels: physical model (maximum values) and CFD results (mean values)

Table 2 – Pressure measurements and CFD results. Non-dimensional values: pressure relative to the total energy head over the spillway crest

Pressure point	1	2	3	4	5	6	7	8	9	10	11	12	13
Measured	1.03	0.89	0.92	0.47	0.29	0.37	0.41	0.48	0.47	0.44	0.88	0.78	0.90
k-ε Model scale	1.19	1.02	1.03	0.54	0.40	0.36	0.44	0.53	0.55	0.52	0.89	0.81	1.19
LES Model scale	1.21	1.09	1.05	0.49	0.39	0.39	0.47	0.56	0.58	0.54	0.81	0.84	1.21

A fast Fourier transform analysis of the pressures at point 2 (Figure 4), performed with the software Origin, revealed that there was a dominant frequency of 4.4 Hz in the physical model, which was higher than the 3.9 Hz predicted by the LES model (Figure 6). The mesh

discretization, which might not be sufficiently fine to represent this phenomenon more accurately, may have been the cause of this discrepancy, but further research is needed to prove this hypothesis. Another source of error may be the sampling time disparity: 15 s for the numerical tests and 200 s for the physical model.
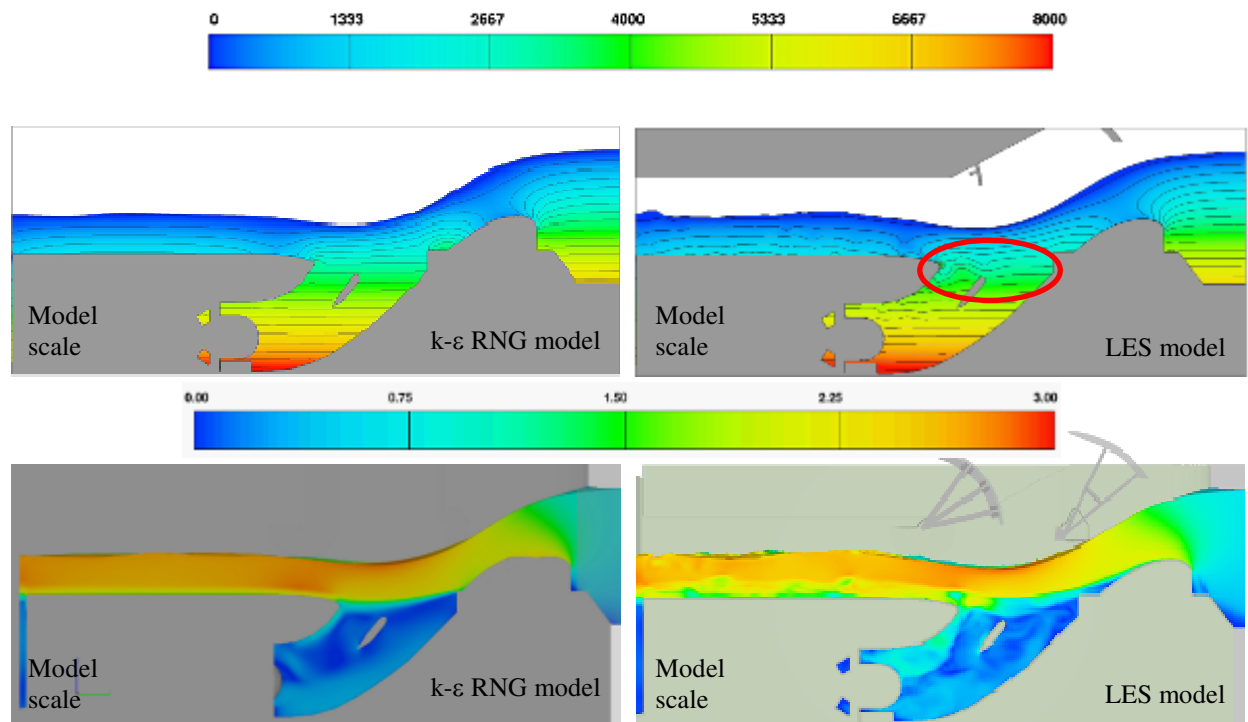
Figure 5 – Instantaneous pressures [Pa] and velocities [m/s] at model scale (bay center)
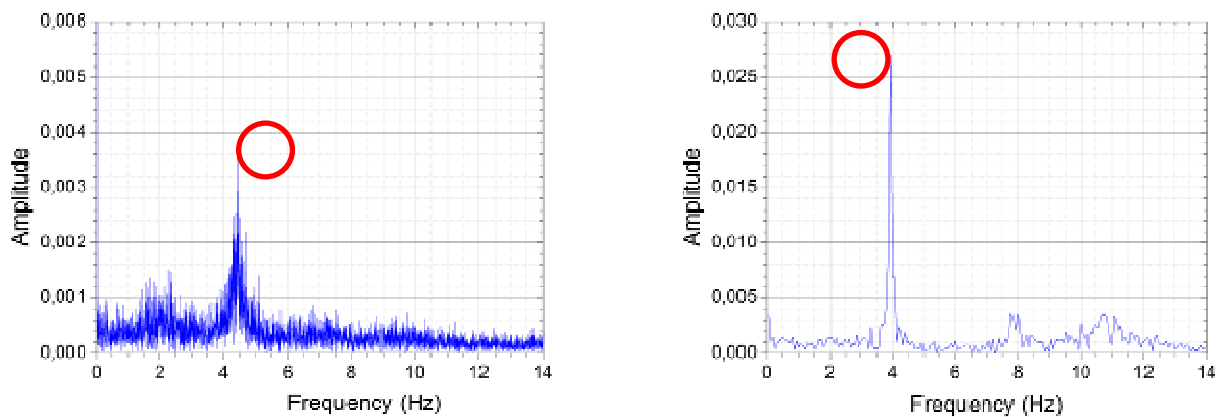
Figure 6 – Energy spectra of pressure at point 2. Left: physical model. Right: LES model

Prototype Scale Results

The simulations performed at prototype scale showed similar general hydraulic behaviors to the

model-scale numerical results (Figure 7). However, a 2.1% discharge increase was observed with both turbulence models. The K-ε RNG model and the LES predicted dominant frequencies of 0.70 Hz and 0.65 Hz, respectively (Figure 8). Corresponding Strouhal numbers of 0.22 and 0.21 did not differ substantially from the physical model value of 0.23. To compute the Strouhal numbers (St = f*L/V) the characteristic length and velocity were considered to be the water depth and the average velocity at the middle of the spillway step edge, respectively.

It is worth mentioning that the LES represented the dominant fluctuating phenomenon in spite of the high Reynolds numbers, which might impose limitations, e.g., to represent the boundary layer. These Reynolds numbers were $4.4*10^5$ and $1.1*10^8$ for the model and prototype scales respectively, considering the same location used for the Strouhal number computation.

In light of the fact that the k-ε RNG model with cell heights of 0.50 m in the powerhouse mesh block (preliminary coarser mesh used to accelerate flow stabilization) predicted a dominant frequency of 0.60 Hz, it is deemed likely that coarser meshes would give rise to lower dominant frequencies than the actual ones. This hypothesis would also explain the frequency difference shown in Figure 6 for the LES results at model scale.
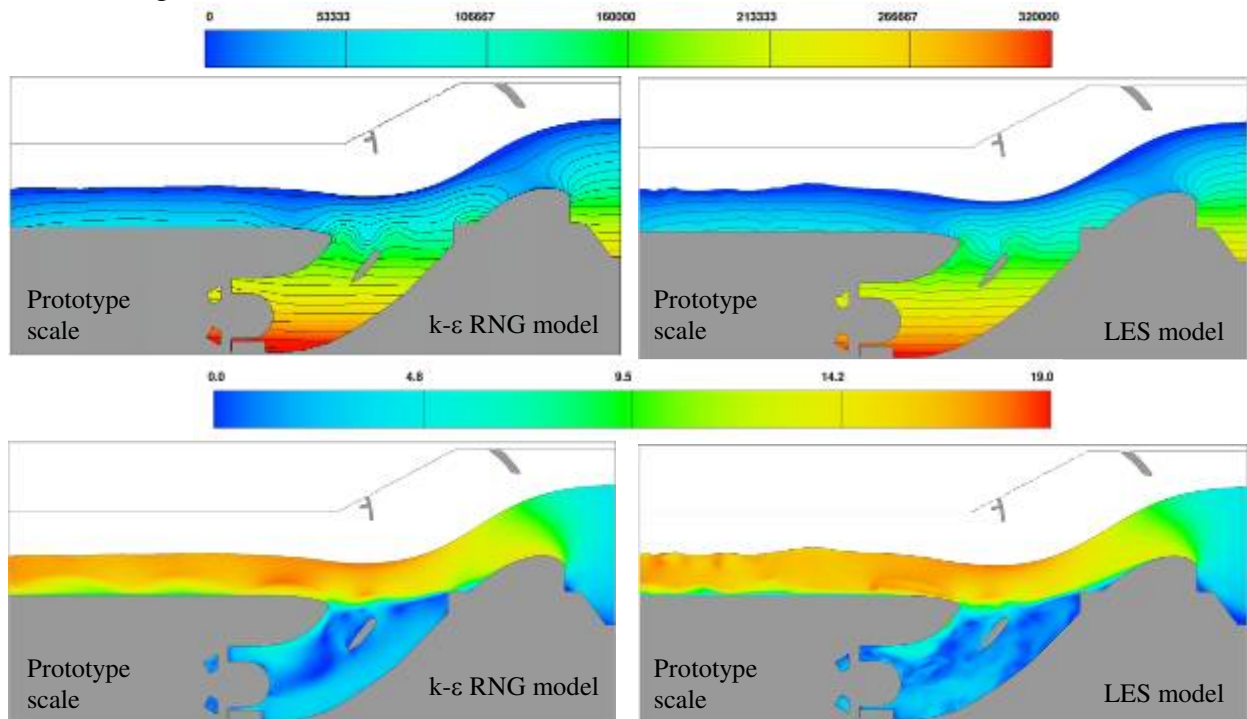
Figure 7 – Instantaneous pressures [Pa] and velocities [m/s] at prototype scale (bay center)
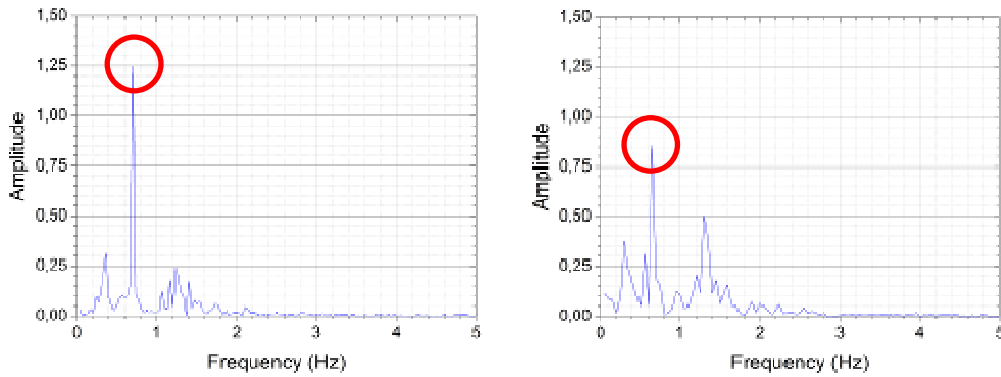
Figure 8 – Energy spectra of pressure in point 2 at prototype scale. Left: k-ε RNG. Right: LES

SUMMARY AND CONCLUSIONS

CFD simulations with both k-ε RNG and LES turbulence models at model and prototype scales provided acceptable representations of the general hydraulic behavior of the power station operating in spillway mode. Discharges predicted by CFD simulations were slightly higher than those measured with the physical model, namely, 13% for k-ε RNG model and 10% for the LES, a trend which holds even considering the estimated measurement error of 4% for the physical model. When numerically modeling at prototype scale, the discharge increased by 2.1% compared to the model scale, irrespective of the turbulence model applied. The analysis of mean pressures and water levels at model scale showed consistency with the aforementioned discharge increase, since higher values than the empirical ones were observed, especially the pressures with an average 13% rise. The presence of cross waves can be predicted in both turbulence models but the inability to empirically quantify mean water levels prevented the realization of more accurate comparisons.

The k-ε RNG model failed to predict fluctuating phenomena at the model scale, but did at the prototype scale regarding the dominant frequency. This discrepancy should be the subject of further research. Additionally, there is some evidence to consider that finer meshes lead to more accurate representation of fluctuating phenomena in terms of frequency, or from another perspective, that coarser meshes give rise to lower frequencies than the actual ones.

The LES closure model predicted the dominant fluctuating frequency fairly well at both model and prototype scales, in terms of pressure and water levels. However, this study cannot guarantee the accuracy of the phenomenon amplitude, so necessary precautions should be taken.

When dealing with design optimization processes in the engineering practice, the accuracy of both turbulence models seem fair enough for this case study, e.g., to suggest a freeboard from the free surface to the beams or to verify the ability of the structure to discharge without a flow regime change. In particular, the k-ε RNG model was good at representing mean flow

characteristics, whereas the LES also helped to understand with more detail the physics of the flow, even at small scales. A prototype scale approach was found to be a better representation of fluctuating pressures than the model-scale approach for both turbulence models, and thus it is recommended. Finally, for a complete cost-effective and precise hydraulic design, composite modeling is also recommended considering the aforementioned limitations of all the presented numerical approaches, which still need further development and higher degrees of accuracy to define the ultimate design of the structures.

ACKNOWLEDGMENTS

REFERENCES

ADRIAN R. J. (2007). "Hairpin vortex organization in wall turbulence." *Phys. Fluids* 19(4), 041301.

DEWALS B., ARCHAMBEAU P., RULOT F., PIROTTON M. and ERPICUM S. (2013). "Physical and Numerical Modelling in Low-Head Structures Design." *Proc. International Workshop on Hydraulic Design of Low-Head Structures, Aachen, Germany, Bundesanstalt für Wasserbau Publ., D.B. BUNG and S. PAGLIARA Editors, pp.11-30.*

GRENANDER, U. (1959). Probability and Statistics: The Harald Cramér Volume. Wiley.

HIRT, C. W. and NICHOLS B. D. (1981). "Volume of fluid (VOF) method for the dynamics of free boundaries." *Journal of Computational Physics* 39(1): 201-225.

JOHNSON M. C. and SAVAGE B. M. (2006). "Physical and numerical comparison of flow over ogee spillway in the presence of tailwater." *J. Hydraulic Eng*. 132(12): 1353–1357.

KHAN L.A., WICKLEIN E.A., RASHID M., EBNER L.L. and RICHARDS N.A. (2004). "Computational fluid dynamics modeling of turbine intake hydraulics at a hydropower plant." *Journal of Hydraulic Research*, 42:1, 61-69

LAROCQUE L.A., IMRAN J. and CHAUDHRY M. (2013). "3D numerical simulation of partial breach dam-break flow using the LES and k–□ turbulence models." *Jl of Hydraulic Research*, 51:2, 145-157

LI S., LAI Y., WEBER L., MATOS SILVA J. and PATEL V.C. (2004). "Validation of a three-dimensional numerical model for water-pump intakes." *Journal of Hydraulic Research*, 42:3, 282-292

NOVAK P., GUINOT V., JEFFREY A. and REEVE D.E. (2010). "Hydraulic modelling - An introduction." Spon Press, London and New York, ISBN 978-0-419-25010-4, 616 pp.

WATER LEVEL SENSORS, WHAT WORKS?

Bryan J. HEINER

U.S. Bureau of Reclamation, Hydraulic Investigations & Laboratory Services, USA,

bheiner@usbr.gov

Thomas W. GILL

U.S. Bureau of Reclamation, Hydraulic Investigations & Laboratory Services, USA,

tgill@usbr.gov

ABSTRACT: Water level sensors come in all shapes, sizes, and types and can range in price from a couple hundred to several thousand US dollars. This project utilizes real world examples from around the western United States to determine what level sensors work well and to document what characteristics may prevent them from providing accurate water level measurements in differing climates. Researchers have developed a calibration procedure that can be used in field or laboratory situations to obtain accurate calibrations of multiple types of water level sensors. Sensors that have been calibrated and installed are being monitored to determine their accuracy and reliability over several irrigation seasons.

Keywords: water level sensors, pressure transducers, ultrasonic, bubbler

INTRODUCTION

As water delivery entities are incorporating increasing levels of remote monitoring and automated control into their operations, there is increasing need for water level sensors that function reliably. In today's age, a wide variety of sensors are available to measure and monitor water levels. These sensors can range in price from a couple hundred to several thousand US dollars, depending on the type and configuration of sensors selected. This research discusses the need for water level sensors and answers a question that many hydraulic structure operators and managers pose to U.S. Bureau of Reclamation (Reclamation) engineers: What water level sensors provide accurate measurements over a sustained period of time and in a range of field

conditions?

RESEARCH METHODOLOGY

This on-going research is conducted in cooperation with irrigation districts and Area Offices throughout Reclamation. To better represent realistic water level sensor usage, actual projects requiring water level sensors were selected for this study. Researchers installed and monitored the field performance of several water level sensing technologies at Reclamation related field sites. The work done can be summarized with the following objectives:

1. Identify the water level sensors that will be tested. Equipment representing a full range of level sensing technologies commonly employed on canal systems and in conjunction with hydraulic structures will be included in the study.
2. Develop a protocol for periodic water level sensor equipment calibrations and checks. Configure portable calibration equipment that can provide accuracy on par with Reclamation's laboratory calibration equipment. This equipment will be used for regular on-site sensor calibrations.
3. Develop a standardized data collection process. Identify frequency of collection, variables (water level, temperature, elevation, time), and storage.
4. Identify sites within cooperating districts where existing water level monitoring stations can have additional (redundant and different) water level sensors added without extensive costs.
5. Implement calibrations and monitor each water level sensor's field performance over time using the protocols and standards identified in steps 2 & 3.
6. Document each water level sensor's performance and note constraints and/or ancillary capabilities offered by each type of instrument.

TYPES OF WATER LEVEL SENSORS TESTED

Submersible Pressure Transducer

   Submersible pressure transducers are installed in the water at the location where the level is to be measured. The transducers convert fluid pressure into a proportional electronic signal over a specified range of water levels. Sensor outputs can vary from 4–20 mA, 0–2.5 or 0–5 volt, SDI12 or Modbus.

Ultrasonic Downlooker

   Ultrasonic downlookers are installed suspended above the water at the location where the level is to be measured. Sensors are mounted normal to the water surface such that an acoustic

signal can be sent and the return signal off the surface of the water can be received. Sensor intelligence determines the distance to the reflective surface using the speed of the signal in the surrounding air. Sensor outputs can vary from 4–20 mA, 0–2.5 or 0–5 volt, SDI12 or Modbus.

Float, Pulley, and Potentiometer

These instruments are installed in stilling wells where a float attached to a cable is wrapped around a pulley. As the float raises and lowers, the pulley turns a potentiometer, which outputs an electronic signal based on its position. The float and pulley units that are being used in this study have been custom fabricated by Reclamation using an inexpensive potentiometer with a 0–5 volt output and other parts commonly found in a hardware store.

Bubbler

Submerged air-filled tubes are installed with the free end at the location where the water level measurement is desired. Water level is determined by measuring the required pressure to push a bubble out the end of the tube. Sensor outputs can vary from 4–20 mA, 0–2.5 or 0–5 volt, SDI12 or Modbus.

Table 1 contains a list of the level sensors that have been included in the study so far. Sensors were selected from literature review and from recommendations by end users and other interested parties. Often when sensors are selected for field deployment, price becomes a limiting factor either because of budget constraints or the number of sensors required to accomplish the desired operation. For this reason an approximate price has been included for each of the sensors. Please note that sensor prices can fluctuate, and the authors recommend requesting updated cost information from the manufacturers.

CALIBRATION PROCEDURE

Researchers developed a portable calibration stand and procedure that provides the ability to accurately calibrate sensors in the laboratory or field. The calibration stand consists of a 10-ft-long piece of heavy-duty structural steel (Unistrut) attached to a 5-ft piece of light-duty structural steel (Unistrut). The light-duty Unistrut attaches to a standard surveying tripod (Figures 1 and 2) and is staked to the ground at the base. Pressure transducers and bubblers are tested in a 2-inch clear PVC pipe that is oriented vertically and attached to the heavy duty Unistrut with hose clamps. The pipe is filled using a 12 volt pump and 5 gallon storage reservoir filled with water. Ultrasonic downlookers are tested using a control arm that attaches to the heavy duty Unistrut and can be adjusted up and down the calibration stand using a thumb nob set screw (Figure 3). Acoustic signals are reflected off a level surface mounted at the bottom of the test stand (Figure 4). Depth and distance measurements used to calibrate each sensor are taken using a tape

measure that is attached to the outside of the calibration stand and can be read in 0.005-ft or 0.0625-inch increments depending on the user's preference.

Table 1 – List of sensors and their approximate cost

	Manufacturer	Model	Approx. Cost ($/Unit)	Quantity
Pressure Transducer	AGP	PT-500	460	3
	AutoMata	Level-Watch	280	3
	Endress Hauser	FMX21	955	2
	Endress Hauser	FMX167	1045	1
	GE Druck	PTX 1730	525	2
	Global Water	WL400	590	2
	Instrumentation Northwest	98i	540	4
	Keller	Acculevel	480	2
	Keller	Levelgage	315	4
	Stevens	SDX	355	4
Ultrasonic Downlooker	Judd Communications	-	655	4
	AGP	IRU-2005	495	3
	AutoMata	Ultra-Ultra	720	2
	EMS	SR6	250	5
	Flowline	EchoPod DL10-00	255	2
	Flowline	EchoPod DX10-00	235	2
	Global Water (EMS)	WL700	665	2
	Nova Lynx (APG)	IRU 9423	475	2
	Siemens "The Probe"	7ML12011EF00	860	3
Other	Float, Pulley and Potentiometer	USBR Design	150	3
	Bubbler - Control Design	CD 103-1	595	4
	Bubbler - OTT	CBS – Std.	1690	1
	Dwyer Temperature & Humidity	RHP-2R11	200	3

To remain consistent throughout the research, calibrations are conducted the same for all level sensors and can be summarized in the following steps:

1. Setup and level the calibration stand.
2. Determine the range of the sensor/s that will be calibrated.
3. Setup the sensors with the same equipment that will be used to obtain the level measurements when installed in the field.
4. Collect 10 data points with the water surface or distance increasing.
5. Collect 10 different data points with the water surface or distance decreasing.
6. Determine the linear regression lines for each:

a. The rising water surface or distance calibration

b. The decreasing water surface or distance calibration

7. Compare the slopes and coefficient of determinations for both linear regressions.

8. Determine the average slope, print a tag with the sensors serial number, slope, and date of calibration, and attach it to the sensor cable.

Figure 1 – Calibration stand

Figure 2 – Calibration stand mount on tripod

Figure 3 – Ultrasonic mount

Figure 4 – Reflective surface for ultrasonics

SITE SELECTION

Geographic

Funding for this project was provided by Reclamation Science and Technology Research Program, with additional funds from Reclamation Area Offices and support from irrigation districts. To keep costs at a reasonable level and to ensure that the project would be useful to contributing partners, sites were selected where water level measurements were needed and existing infrastructure could support multiple measurement devices at one location.

Sites located near Yuma Arizona (extreme high temperature), Grand Junction Colorado (moderate temperatures), and Sterling Colorado (moderate temperatures) have already been identified and have instrumentation either installed and operational or in the process of being installed. Sites in Montana and North Dakota are both being investigated to represent a much colder environment.

Sensor location

Once a geographical location has been established, locating a site to install sensors that will provide stable water surface measurements is essential. This can be done by locating the instrument in a stilling well with a port of around 1/20–1/30 the size of the stilling well diameter connecting the well to the hydraulic structure (RECLAMATION 2001). Another method is to select a location free from drawdown influences, waves, or other disturbances that could influence water level readings. When installing a submerged sensor, it is important to make sure the sensor will not be damaged by debris or sediment in the flowing water.

SENSOR INSTALLATION PROCEDURE

The following procedure is followed when installing a new sensor at a site:

1. Determine the min and max water levels to be measured.
2. Determine the type of controller or base unit that will be used to record/transmit the data and what type of inputs it will accept.
3. Select multiple sensors that will accommodate the range and controller inputs.
4. Install a staff gauge and determine a reference to a readily identifiable datum or bench mark.
5. Install infrastructure that will allow multiple sensors to be installed in acceptable conditions (away from drawdown, waves, damage from debris, disturbances)
6. Install controller (base unit) in a secure location (preferably a lockable enclosure)
7. If applicable, install solar panel, ground-rod, antenna, and battery box.
8. Install sensors with the correct calibration slopes.
9. Trouble shoot sensors and base unit to ensure everything is working.
    a. Simulate different level measurements if possible to make sure sensor is working.
    b. Determine if the correct sign is used on the calibration slope by raising and lowering sensor ensuring that the output corresponds appropriately.
    c. Simulate radio communications (if necessary).
    d. Use controller menus to adjust offsets and shifts to check functionality.
10. Determine the sensor offset using a known datum, and program it into controller.

11. Record necessary information in the project book. Include: Installation date, sensor types and serial numbers, slopes, offsets, datum reference used and where it came from, controller ID and any other important information.

DATA COLLECTION

Data collected for each site becomes a unique challenge because each site will have unique sensors and datum. To help manage the data, water levels are recorded at least fifteen minutes apart. All data are arranged with a date and time stamp. In addition, all sites should log battery and charge voltage and internal base unit temperature, and one site in each geographical location should log the ambient air temperature. Where possible, manual data collection of the installed staff gauge will be taken periodically to compare to the logged data and determine what sensors, if any, are drifting or having any other issues. Data collection is in the beginning stages; any suggestions on how to improve the data management portion of the research are welcome.

KNOWN ISSUES

To date, there are several known issues that have arisen when it comes to installing and using water level sensors that may prevent accurate level measurements. Ultrasonic downlookers are sensitive to spider webs; most often the webs will concentrate near the sensor face and prevent accurate measurements. Although many of the manufacturers claim to be compensating for fluctuations in the temperature, the authors noticed that during rapid changes in temperature, some of the sensors that "compensate" for temperature fluctuations would not provide repeatable calibrations. Pressure transducers seem to be sensitive to calibration shifts if they are mishandled, dropped, or banged. To date, we have had one sensor stop working; we have not determined why, but we hope the manufacturer will replace the sensor as it malfunctioned after 2 months of use. Although many of the sensors claim to work with as little as 12 volts power, the authors have found that in most cases using a 12 to 24 volt converter to increase the supply voltage has provided more consistent measurements and calibrations. As more issues arise the authors will be documenting the problems and any solutions that are found.

CONCLUSIONS

To better understand water level sensors and to evaluate performance in a range of operating environments, the U.S. Bureau of Reclamation has been installing level sensors in varying climates and documenting any issues and successes that are observed. Sensors from multiple manufacturers and of multiple types have been purchased and installed in both hot and mild

climates including Yuma Arizona, Grand Junction Colorado, and near Sterling Colorado. Additional sites located in a colder environment are being investigated in Montana and North Dakota.

Once geographic locations are determined, sensor sites can be identified and equipment can be deployed in the field. Researchers developed a portable calibration procedure that allows all sensors to be calibrated before they are deployed. Sensors are calibrated in both a rising and decreasing water surface or distance, with 10 points in each direction. Calibrations are performed periodically when needed but at least once per year. Data is collected and compared against periodic manually recorded data to determine if sensors are drifting or calibrations have shifted. Data collection is just beginning and will be on-going for multiple years.

Several issues have already been documented that prevent accurate water level measurement, including by not limited to:

- Spider webs preventing ultrasonic downlookers from working
- Lagging temperature compensation in response to rapid temperature changes
- Sensors failing for no apparent reason
- 12-volt supply power inadequate for consistent measurements

As more issues and successes are found, the list will continue to grow.

ACKNOWLEDGMENTS

REFERENCES

RECLAMATION, U.S. BUREAU OF. (2001). "Water Measurement Manual" U.S. Government Printing office, Washing DC 20402. pp. 6-13.

USING PARTICLE IMAGE VELOCIMETRY (PIV) SYSTEM IN FISH PASSAGE THROUGH REHABILITATED CULVERTS

Mohanad KHODIER

Civil and Environmental Engineering, Utah State University, USA,

m.khodier@aggiemail.usu.edu

Blake P. TULLIS

Civil and Environmental Engineering, Utah Water Research Laboratory, USA,

blake.tullis@usu.edu

ABSTRACT: The Particle Image Velocimetry (PIV) system was used to investigate fish passage behaviour through a circular, 0.61-m diameter pipe with evenly spaced baffles along the invert. A section of the pipe wall between two adjacent baffles was replaced with a transparent window (Lexan) and a water box placed outside of the pipe to create a tested section. The test was conducted for different pipe slopes 0.5, 1.5, 2.5, and 3.5%. For each slope, the pipe was tested for different flow rates 28.3, 56.6, and 85 l/s. Also, the PIV was used to produce the velocity vector field by post-processing the particle images. Using the measured velocity field data, the velocity gradient (shear stress) was calculated for the entire field downstream of the baffle. The velocity gradients will be used to better understand the effect that installing baffles has on fish passage. Live fish were placed in the pipe under the same slope and discharge conditions and their behaviour observed, including favorite resting places. The flow characteristics near the fish resting places were also evaluated.

Keywords: PIV, fish passage, rehabilitated culverts, pipe baffles.

INTRODUCTION

Culverts are used to convey water flows from one side of a road to the other. One concern about using culverts is the ability for fish to move upstream through the culverts. One way to increase fish passage ability is to install baffles within the culverts along the invert. Baffles are elements built inside the culverts with regular spacing and specific height. Baffles decrease the flow velocity and increase the water depth for the fish passage by creating pools of slower water where the fish can rest (Rajaratnam and Katopodis, 1990). Rajaratnam tested multiple types of baffled culverts included slotted weir, offset, and weir baffles to compare their performance on fish passage. All baffles types had the same results for the fish passage.

Other studies were conducted on culvert slopes ranging from 1% to 5% (Rajaratnam and

Katopodis, 1990). Morris (1968) studied the effect of baffle height and the spacing length between baffles. Morris concluded that the baffle spacing to baffle height ratio should be between 8.5 and 10 for fish passage. Olsen and Tullis (2011) conducted multiple tests on baffled and non-baffled culverts at seven slopes (0–3.5%) and three flow rate for each slope. Olsen and Tullis (2011) concluded that the slope of the non-baffled culvert should be less than 0.5% with a flow rate of 28.3 l/s to have 50% of fish pass (specifically brown trout). The same percentage of the fish passing can be achieved with a slope of 3.5% and 28.3 l/s flow with a baffled culvert. In this study, the effect of shear stress and velocity gradient on fish passage in a baffled culvert was explored.

EXPERIMENTAL SETUP

Flow through a 18.3-m long, 0.61-m outer diameter baffled pipe was tested using the PIV system (Figure 1). The pipe was made from high-density polyethylene, HDPE. The wall thickness of the pipe was 19 mm, the baffle spacing was 0.9D, and the baffles height was 0.15D, where D is the inner diameter of the pipe (Figure 1).
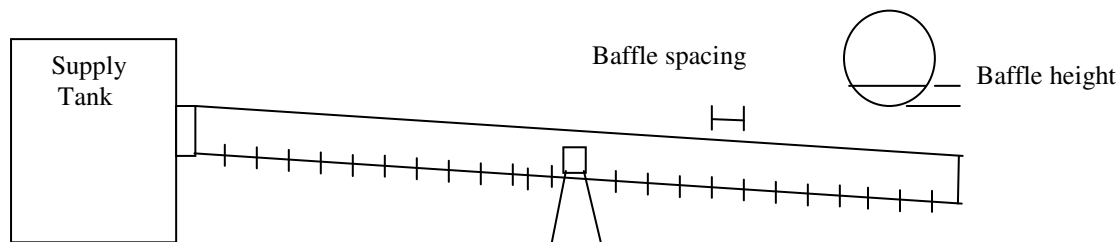
Figure 1 – Experimental setup

The upstream end of the pipe was connected to the supply tank, and the downstream end was opened to the atmosphere for discharging into a drainage system. A test section was placed at the middle of the pipe between two adjacent baffles. This test section consisted of a transparent 0.36-m wide by 0.4-m tall window made from a 3-mm thick flexible Lexan sheet that matched the pipe wall curvature (see Figure 2). In order to eliminate the distortion of the image through the curved window, a clear acrylic 0.58-m×0.69-m×0.64-m water box was placed on the outside of the pipe at the test section (see Figure 3). Laser light reflection off of the water free surface can also create imaging problems for the PIV system. To overcome this problem, a very thin black sheet (cloth) was placed at the top of the water surface to absorb the laser light. The sheet was buoyant and very lightweight so as not to significantly impact the flow geometry. The PIV system consisted of a CCD camera with 1280×1024 pixels resolution and a laser (Nd:YAG) with

light sheet optics to illuminate the desired area (see Figure 2). The PIV system was used to measure the velocity field and subsequently calculated the flow shear stresses.
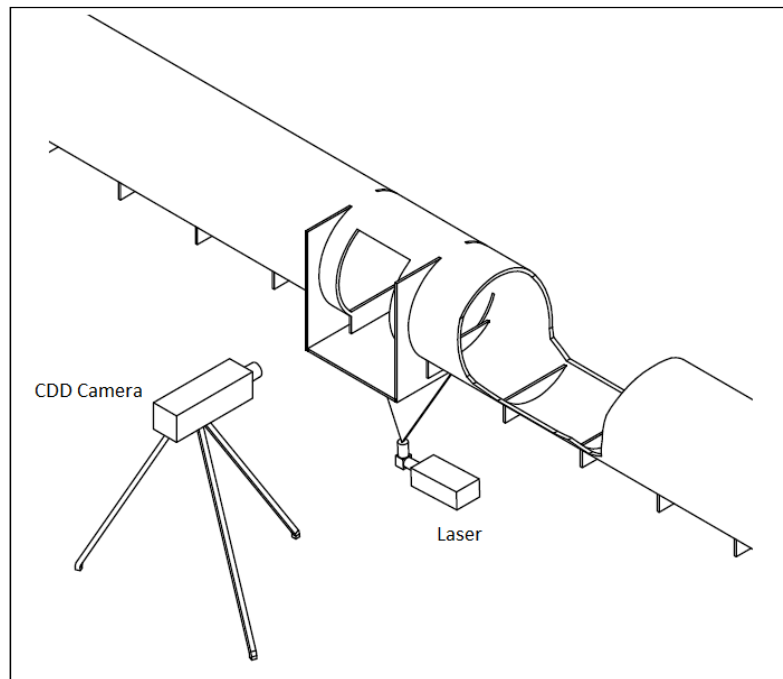
Figure 2 – PIV system and the test section
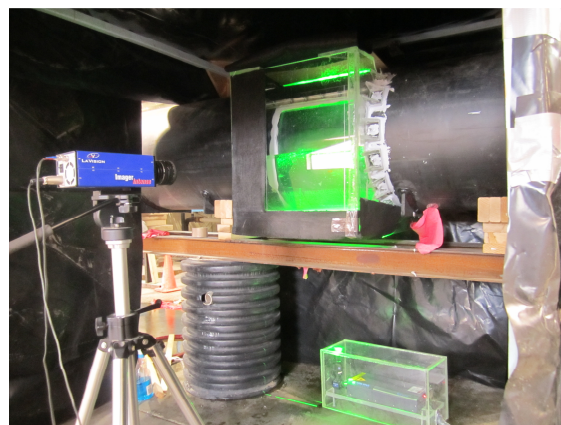
Figure 3 – PIV system and the attached box

RESULTS AND DISCUSSION

Multiple flow tests were conducted at the following pipe slopes: S= 0.5, 1.5, 2.5, and 3.5% at flow rates of Q= 28.3, 56.6, and 85.0 l/s. The PIV system was used to produce the velocity and the vector field by post-processing the 100 flow field images. The shear stress is given by the following equation:

$$\tau = \mu \frac{\partial U}{\partial y} \tag{1}$$

where τ is the shear stress (N/m^2) and μ is the dynamic viscosity (N·m/s^2). It can be noted from this equation that the shear stress is proportional to the velocity gradient. Figure 4 shows the velocity contour for the space between the baffles at S=0.5% and Q=85.0 l/s. The baffle height was at y = 85.75 mm from the pipe invert. The space between the baffles produced a low velocity field that allowed the fish to rest during the passage (see Figure 4).
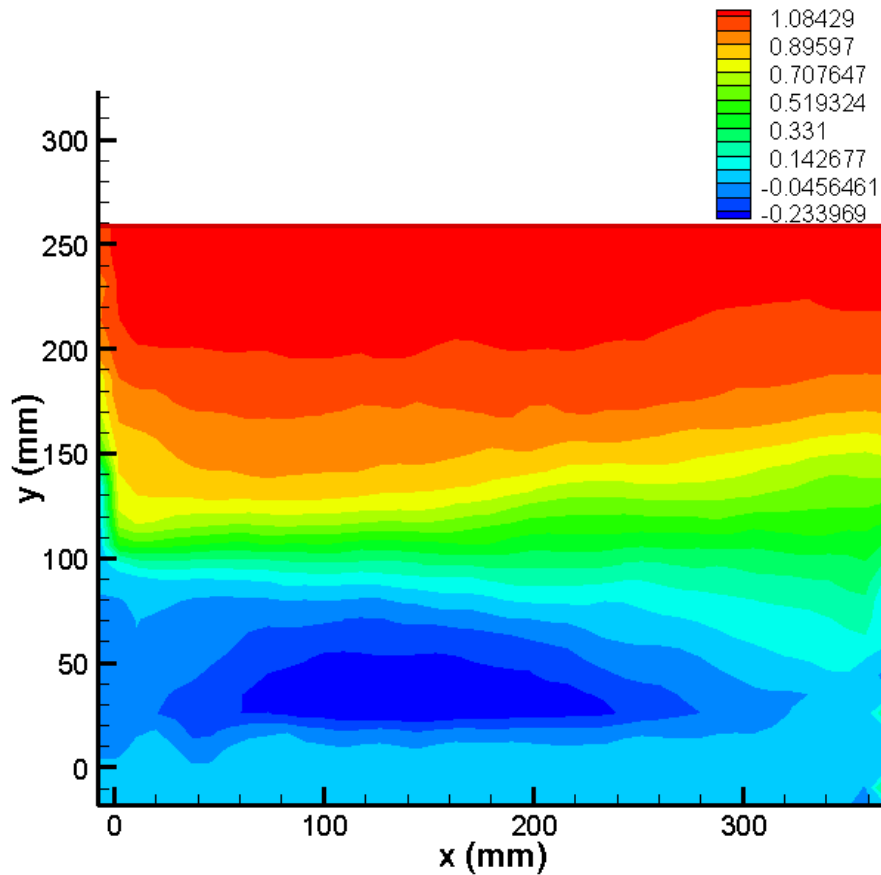
Figure 4 – Velocity contour for U (m/s) at S=0.5% and Q=85 l/s (T=6.4^{0}C)

It is noted that the space between the baffles reduced the velocity (kinetic energy) and creates an eddy with clock-wise oriented flow (see Figure 5). Figure 5 shows the velocity vector and the eddy direction for the space between the baffles only.
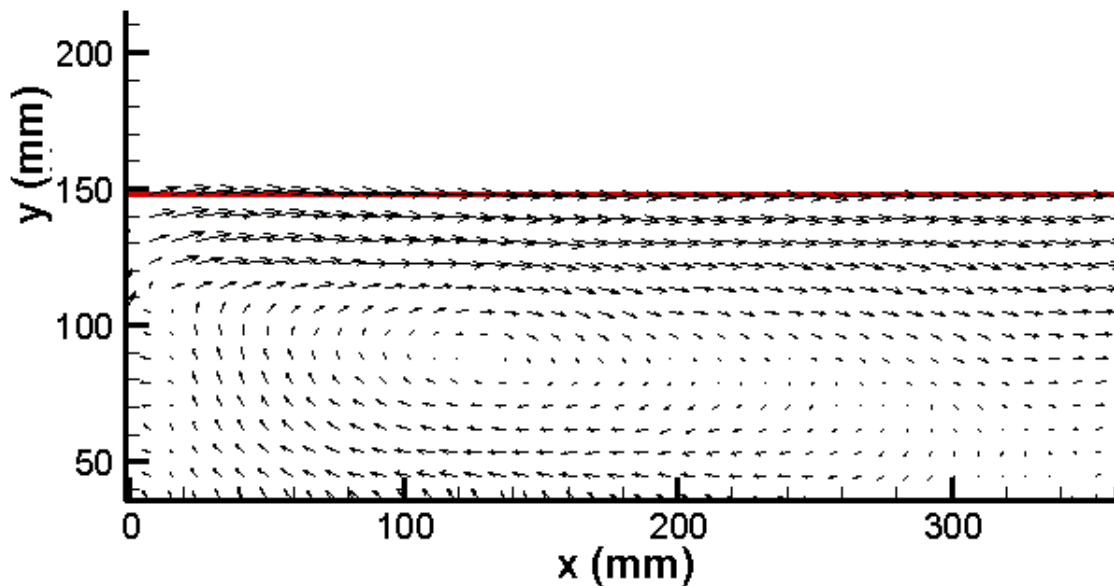
Figure 5 – Velocity vectors for S=1.5% and Q=85.0 l/s (T=5.5 ^{0}C)

In a typical flow through a pipe, the velocity gradient (shear stress) is maximum near the wall and reduced towards the center of the pipe. Installing baffles in the pipe will change this behaviour, as shown in Figure 6. The velocity gradient (shear stress) is minimum near the wall and increases toward the top of the baffles (at y=85.75 mm), where the velocity gradient is highest, and then decreases again with increased elevation in the water column. This behaviour is also true for different flow rates and slopes as shown in Figures 7, 8, and 9. It can be noted from these figures that the velocity gradient converges to a certain value (less than the maximum velocity gradient) as the flow goes downstream of the space between the baffles.

The downstream is the upstream for the next baffle space, so s fish jumping from one space to the next space will not suffer from the high velocity gradient. Figure 10 shows the location of the maximum velocity gradient for different for different flow rates. As the flow rate increases the maximum velocity gradient increases. It can be noted from this figures that the maximum velocity gradient is located near the top of the baffles (at y=85.75 mm).
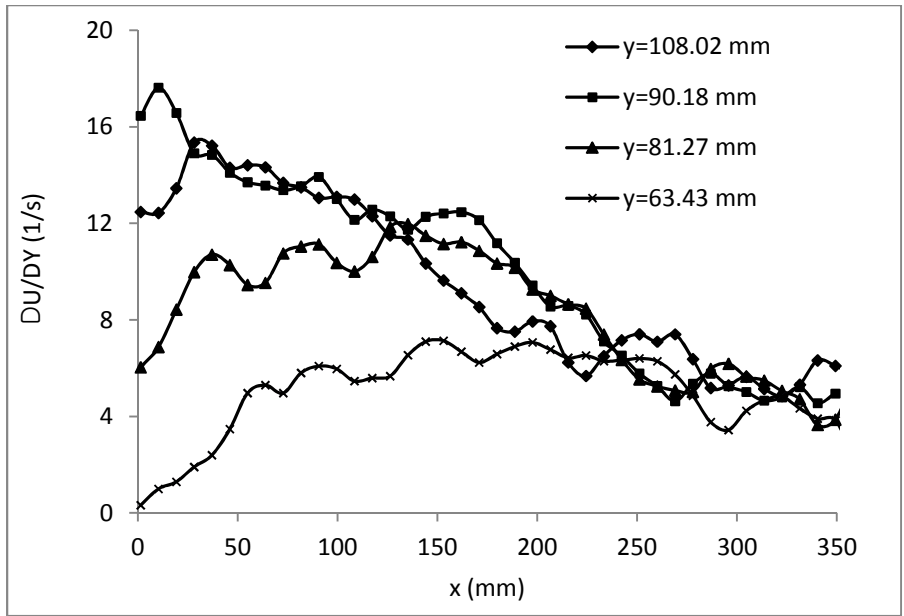
Figure 6 – Velocity gradient for S=0.5% and Q= 28.3 l/s (T=6.4 ^{0}C)
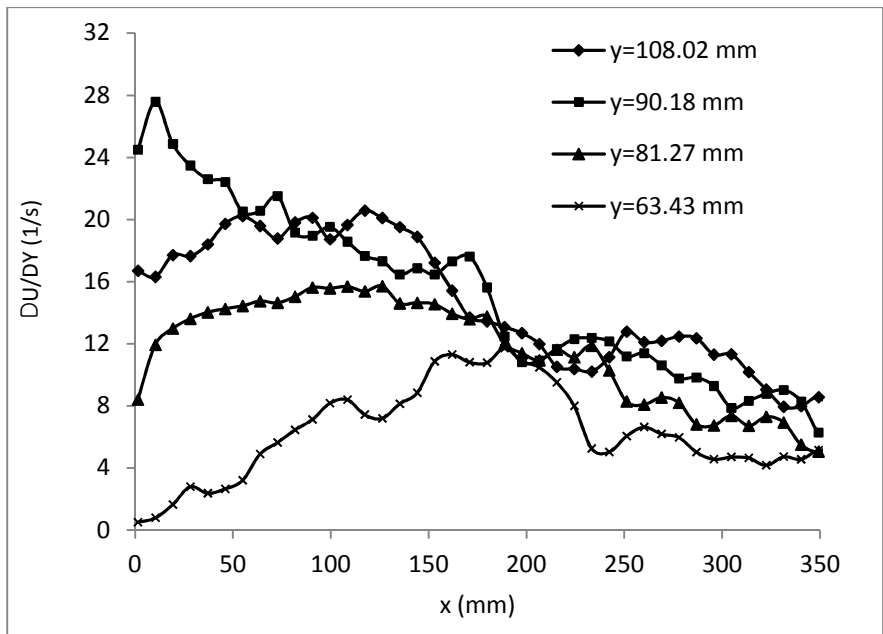
Figure 7 – Velocity gradient for S=0.5% and Q=85.0 l/s (T=6.4 ^{0}C)
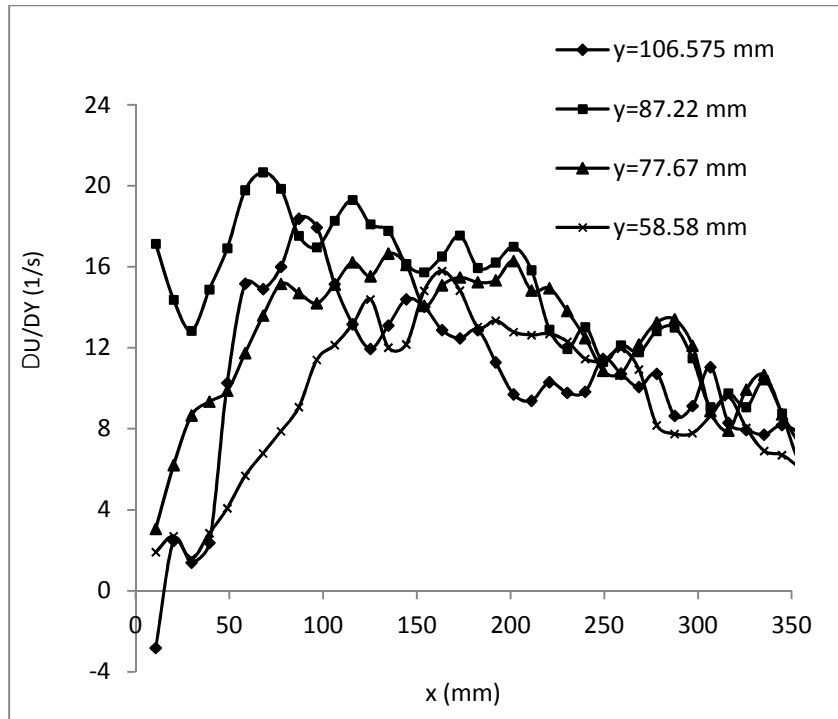
Figure 8 – Velocity gradient for S=3.5% and Q= 56.6 l/s (T=5.6 ^{0}C)
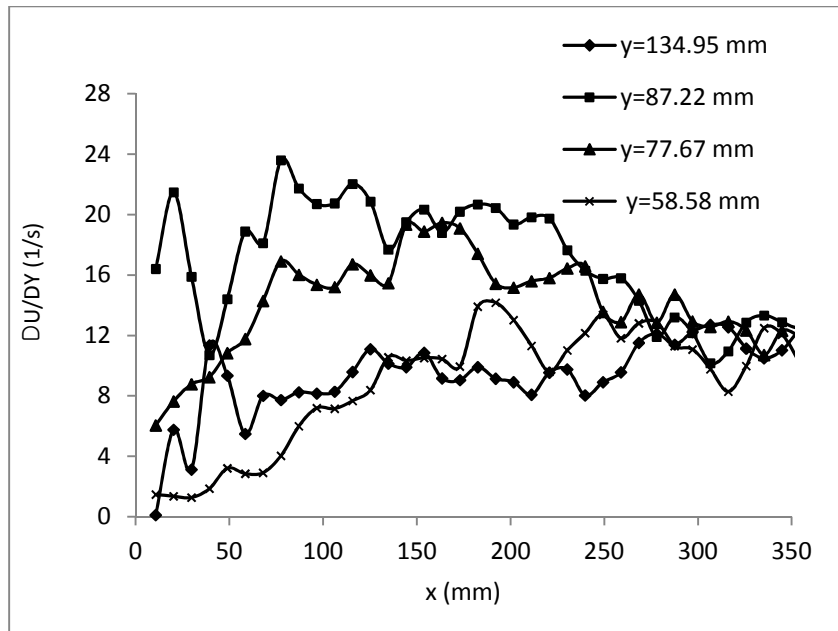
Figure 9 – Velocity gradient for S=3.5% and Q=85.0 l/s (T=5.6 ^{0}C)
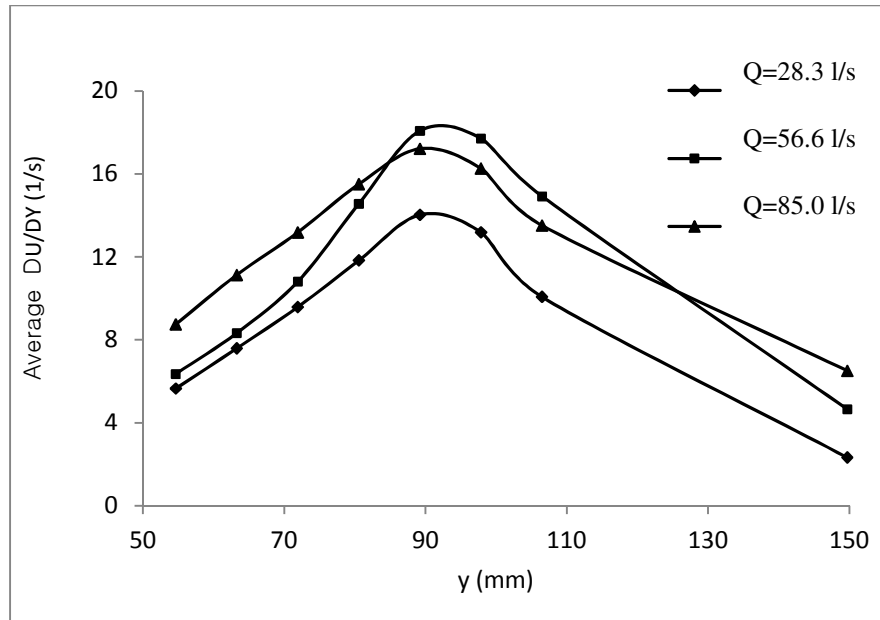
Figure 10 – Velocity gradient for S=1.5% (T=5.5 ^{0}C)

CONCLUSION

The PIV System was used to investigate the fish passage behaviour through a circular pipe. The 18.3-m long and 0.61-m outer diameter baffled pipe was tested at different geometrical slopes: 0.5, 1.5, 2.5, and 3.5%. For each pipe slope, the pipe was tested for different flow rates: 28.3, 56.6, and 85.0 l/s. The velocity and vector field were produced by post-processing the particle images. The velocity gradient (shear stress) is calculated for each flow and geometry condition. It can be concluded that installing baffles in the pipe will reduce the velocity and the velocity gradient in the space between the baffles, which makes a good environment for the fish to rest during passage in the pipe. The baffles will shift the maximum velocity gradient from the pipe wall to the top of the baffles. The velocity gradient increases as the slope increases. Also, the velocity gradient increases as the flow rate increases. Regardless of the slope and the flow rate, the velocity gradient converges downstream of the baffles spacing, where it has the approximately a small velocity gradient. In future studies, the fish will be monitored during passage through the baffled pipe to determine the place where fish most often rest.

REFERENCES

MORRIS, H. M. (1968).” Hydraulics of energy dissipation in steep, rough channels.” *Bulletin 19.* Research Division Virginia Polytech Institute. Blacksburg, Virginia.16-87 p.

OSLEN, A., and TULLIS, B. P., (2011). “Fish Passage Through Rehabilitated Culverts Laboratory Study”, *All Graduate Theses and Dissertations.* http://digitalcommons.usu.edu/etd/1082, Paper 1082.

RAJARATNAM , N. (1989).“Hydraulics of culvert fishways II: slotted-weir culvert fishways.” *Canadian Journal of Civil Engineering*, Vol. 16, No. 3, pp. 375-383.

RAJARATNAM , N., and KATOPODIS, C. (1990). “Hydraulics of culvert fishways III: Weir baffle culvert fishways.” *Canadian Journal of Civil Engineering*, Vol. 17, No. 4, pp. 558-568.

RAJARATNAM , N., KATOPODIS, C., and FAIRBAIRN, M., A. (1990). “Hydraulics of culvert fishways V: Alberta fish weirs and baffles.” *Canadian Journal of Civil Engineering*, Vol. 17, No. 6, pp. 1015-1021.

TULLIS, B. P., and HOLLINGSHEAD, T. (2009). “In-situ culvert rehabilitation: Synthesis study and field evaluation.” *Utah Water Research Laboratory*, Logan, Utah. 33 p.

MEASUREMENT OF TURBULENCE IN PRESSURIZED PIPE FLOW USING PARTICLE IMAGE VELOCIMETRY

Josh MORTENSEN

Hydraulic Investigations and Laboratory Services, US Bureau of Reclamation, USA,
jmortensen@usbr.gov

Abstract: Invasive mussel species can cause problems at a variety of water resource facilities by colonizing within piping systems, significantly reducing flow capacity. Exposing mussels to intense turbulence as they enter the system may be effective in reducing mussel settlement downstream. To quantify turbulence in a pressurized pipe, Particle Image Velocimetry (PIV) measurements were made downstream of a newly developed pipe fitting designed to generate intense turbulence for mussel control. Two-dimensional (2D) velocity data were collected throughout the pipe profile at various distances downstream of the fitting and were analyzed to quantify hydrodynamic properties of the turbulent flow including dissipation rate and Kolmogorov length scale. Results indicate that the fitting generated sufficient turbulent energy to drive the microscale length down to scales expected to influence invasive mussel species (near 200 μm). Spectral analysis of spatial data also revealed that near the Kolmogorov scale, energy was increased by more than one order of magnitude for a mean pipe velocity of 0.914 m/s and just less than one order of magnitude for 1.83 m/s.

Keywords: PIV, turbulence, energy spectrum, pipe flow.

INTRODUCTION

The main objective of this research was to quantify turbulence characteristics produced by a turbulence generation system designed to prevent invasive mussel colonization in pipes. Many water resource facilities such as dams, power plants, pumping plants, and irrigation systems have complex piping systems that are susceptible to mussel colonization (RECLAMATION 2009). Past research has indicated that turbulence in the flow field may reduce the impacts of mussel settlement on water conveyance and distribution systems (REHMANN et al. 2003). Their study showed that juvenile mussels (veligers) are more likely to be killed or injured when turbulent eddies are near the same size or smaller than the veliger, exposing them to damaging velocity

fluctuations and shear stresses. Another study reported that veligers were "fragile" and "highly susceptible to damage by physical forces…" (AMEC EARTH & ENVIRONMENTAL 2009). Similar results were found with other organisms such as plankton (PETERS and MARRASE 2000).

While most research of turbulence effects specific to quagga and zebra mussels has been performed in open channel situations, piping systems may also benefit by using turbulence as an effective mussel control. This study attempts to prevent mussel settlement in pipes by exposing them to intense turbulence as they flow through a specialized pipe fitting (turbulence generator). The turbulence generator is an active system that adds energy to the pipe flow without causing additional head losses. Details are not provided due to intellectual property concerns of the client. PIV was used to quantify hydrodynamic properties throughout the entire flow field downstream of the turbulence pipe fitting. PIV uses successive image pairs of illuminated particles in the flow field to create a 2D map of the velocity vectors and has been widely used to study turbulent flows (SAARENRINNE et al. 2001 and FOUCAUT et al. 2004) including turbulence effects on living organisms (PETERS and REDONDO 1997).

Turbulence parameters in a circular pipe were measured and quantified in Reclamation's Hydraulics Laboratory in Denver, CO. Turbulence parameters were measured within the downstream pipe profile to determine how they evolved with distance for two key pipe velocities (max. and min. of typical velocity range). Also, turbulence levels of common pipe flow were compared to turbulence generated by the specialized pipe fitting to quantify any gains in intensity. Results are valuable for future research efforts on pressurized pipe turbulence and its effects on invasive mussel species as well as using PIV methods for turbulence measurements in circular conduits.

TEST PROCEDURE AND MEASUREMENT

Measurements were made in a 0.203 m ID clear acrylic pipe test section directly downstream from the turbulence generator. The test section was level and was surrounded by a rectangular water jacket. A long straight section of pipe ($\approx$ 18 pipe diameters) allowed a uniform flow profile to develop upstream before arriving at the turbulence generator. Measurements were made at two mean flow velocities (U) shown in Table 1 with and without additional turbulence generation.

PIV images were taken of the pipe profile at 7.4 Hz and locations 1, 2, 5, and 10 pipe diameters downstream from the generator. Image size was 182.3 x 182.3 mm (2048 x 2048 pixels) of which only the top 105 mm portion of the image was analyzed (assumed symmetrical flow characteristics). Based on a sensitivity analysis (Fig. 1), 200 image pairs were required for testing as turbulence intensity and standard deviation stabilized.

Images were analyzed with the Flow Manager PIV software using cross correlation of 16-pixel x 16-pixel interrogation windows with a 50% horizontal and vertical overlap. Gaussian windowing and a No DC filter were used. A moving-average validation was applied to remove and substitute any vector that varied more than 10 percent from its neighbouring vectors (Table 1). Flow was seeded with clay particles with an average diameter of approximately 80 μm.
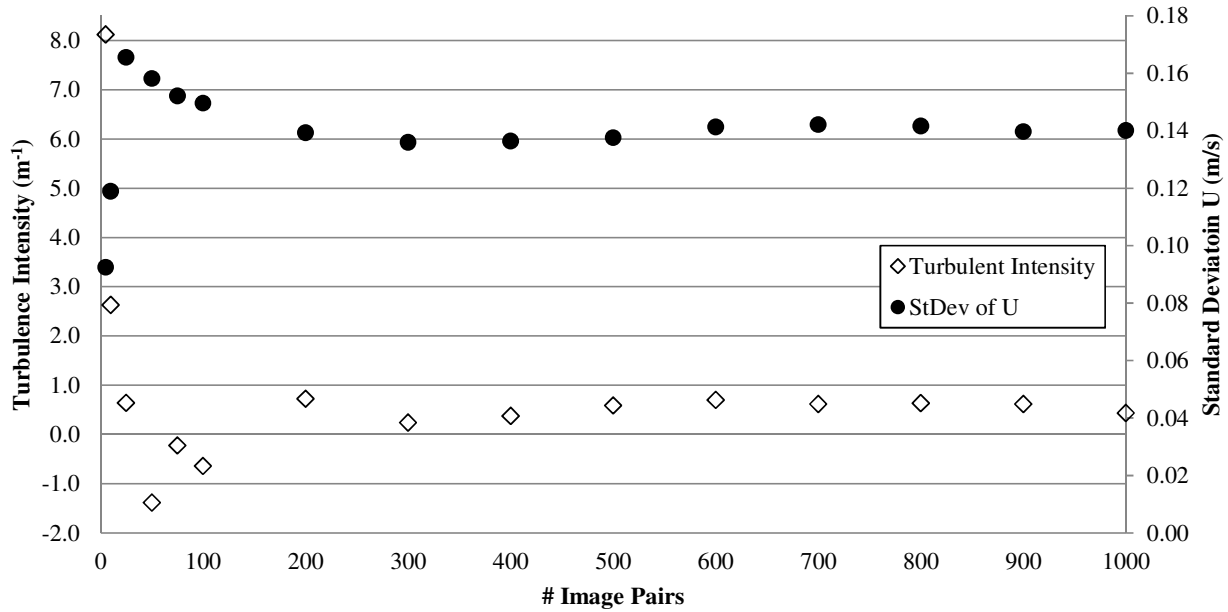
Figure 5 – Sensitivity analysis of number of image pairs.

The verified 2D vector data were imported into TecPlot where they were manipulated to find key turbulence parameters. As the eddy sizes neared the same scale as mussel veligers of particular interest to this study, the Kolmogorov length scale (TENNEKES and LUMLEY 1972) was the key parameter and was estimated using equations 1 and 2:

$$L_k = \left(\frac{\nu^3}{\epsilon_D}\right)^{\frac{1}{4}} \tag{1}$$

ν is the kinematic viscosity and ϵ_D is the energy dissipation rate, which was estimated directly from the 2D velocity vector data by equation 2 (GRUE et al. 2004).

$$\epsilon_D = 3\nu \left[\left(\frac{\partial u}{\partial x}\right)^2 + \left(\frac{\partial v}{\partial y}\right)^2 + \left(\frac{\partial u}{\partial y}\right)^2 + \left(\frac{\partial v}{\partial x}\right)^2 + 2\left(\frac{\partial u}{\partial y}\frac{\partial v}{\partial x}\right) + \frac{2}{3}\left(\frac{\partial u}{\partial x}\frac{\partial v}{\partial y}\right) \right] \tag{2}$$

Table 2 – Pipe flow characteristics and PIV vector validation.

U _m/s_	Re _no turbulence generator_	Avg % Substituted Vectors	Max % Substituted Vectors
0.914	189,000	2.77%	3.67%
1.83	378,000	8.29%	12.25%

Also, spectral analysis was used to compare the energy cascade of the various pipe flows. Spatial velocity data (stream wise velocity vector, u_1), taken through a vertical cross-section 1 diameter downstream of the generator, were used for the spectral analysis. This location was chosen because it was the location nearest the turbulence generator that could still be seen with the PIV, giving the closest representation of flow affected by the generator. Methods shown by DORON et al. (2000) were used to develop the energy spectrum from spatial data.

RESULTS

Turbulence measurements were made directly downstream of the generator section to show any additional turbulence a mussel may experience after passing through the generator. While it was not possible to make measurements within the generator section itself, the hydrodynamics in this downstream test section indicate the necessary level of generator operation for mussel control. Due to the high level of mixing at the measurement locations no flow structures were visible from the PIV images.

Images were captured at various locations from the generator to determine how far downstream the turbulence was sustainable. Figure 2, which is a plot of the average L_k values within a profile image, shows that any additional turbulence created by the fitting dissipates before reaching 5 pipe diameters downstream where measurements nearly match those of regular pipe flow. However, significant drops of L_k at 1 and 2 diameters downstream (Table 2) indicate that the generator significantly affects the turbulence levels for a small distance downstream before it is dissipated. Future demonstration testing at a field site with live quagga mussels will show whether or not mussel veligers are actually affected by the turbulence.
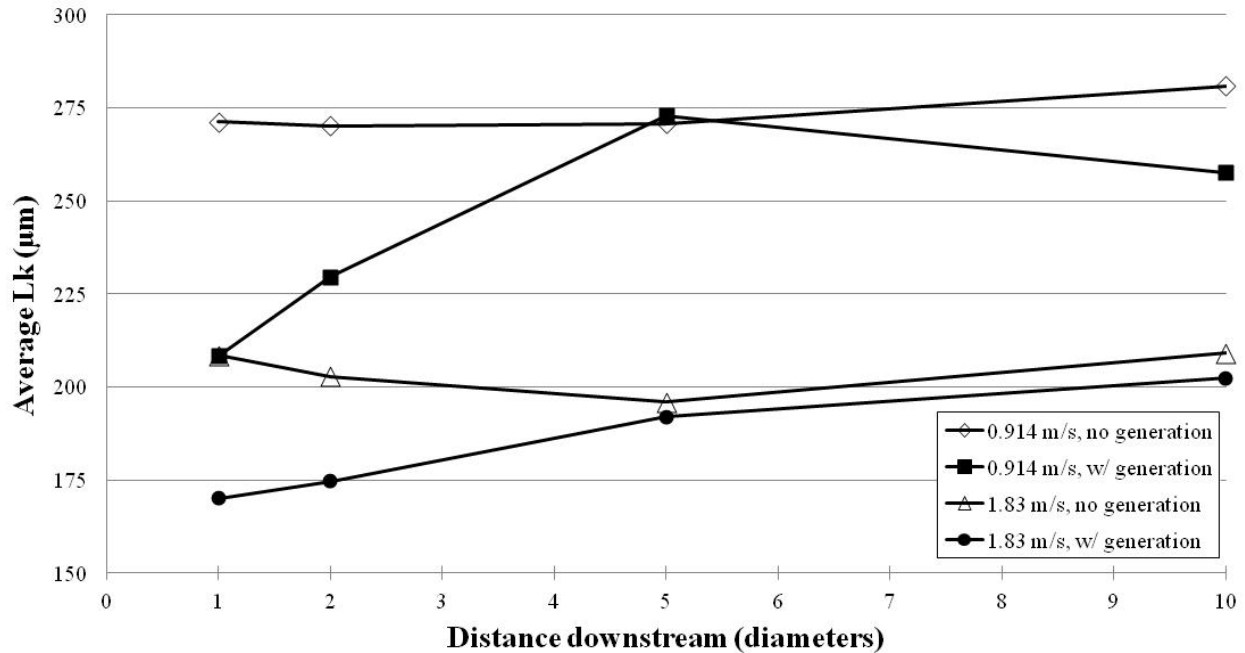
Figure 6 – Average L_k values throughout the pipe profile image at various distances downstream of the turbulence generator.

Spectral analysis is helpful in identifying which turbulent scales contain the most energy. A spectral comparison of velocity data show if there is a significant increase in turbulence energy caused by the generator, particularly at higher wave numbers near the Kolmogorov scale. Figures 3 and 4 show the energy spectrum of spatial velocity data taken vertically through the pipe section at 1 diameter downstream of the generator. E(k_1) represents the mean energy at a particular wavenumber (k_1) which corresponds to eddy size scale. The energy cascade slopes shown in Figures 3 and 4 as well as Table 2 represent data near the higher end of the spectrum as the increase in energy near the Kolmogorov scale was of particular interest.

For U=0.914 m/s, the amount of energy was significantly increased by the generator for the entire spectrum (Fig. 3). The slope was flattened due to generated turbulence particularly near the higher end of the wave number spectrum indicating that significantly more energy was added to the smaller turbulent scales (more than 1 order of magnitude as shown in Table 2). This increase in energy near the Kolmogorov scale will hopefully have an impact on mussel veligers.
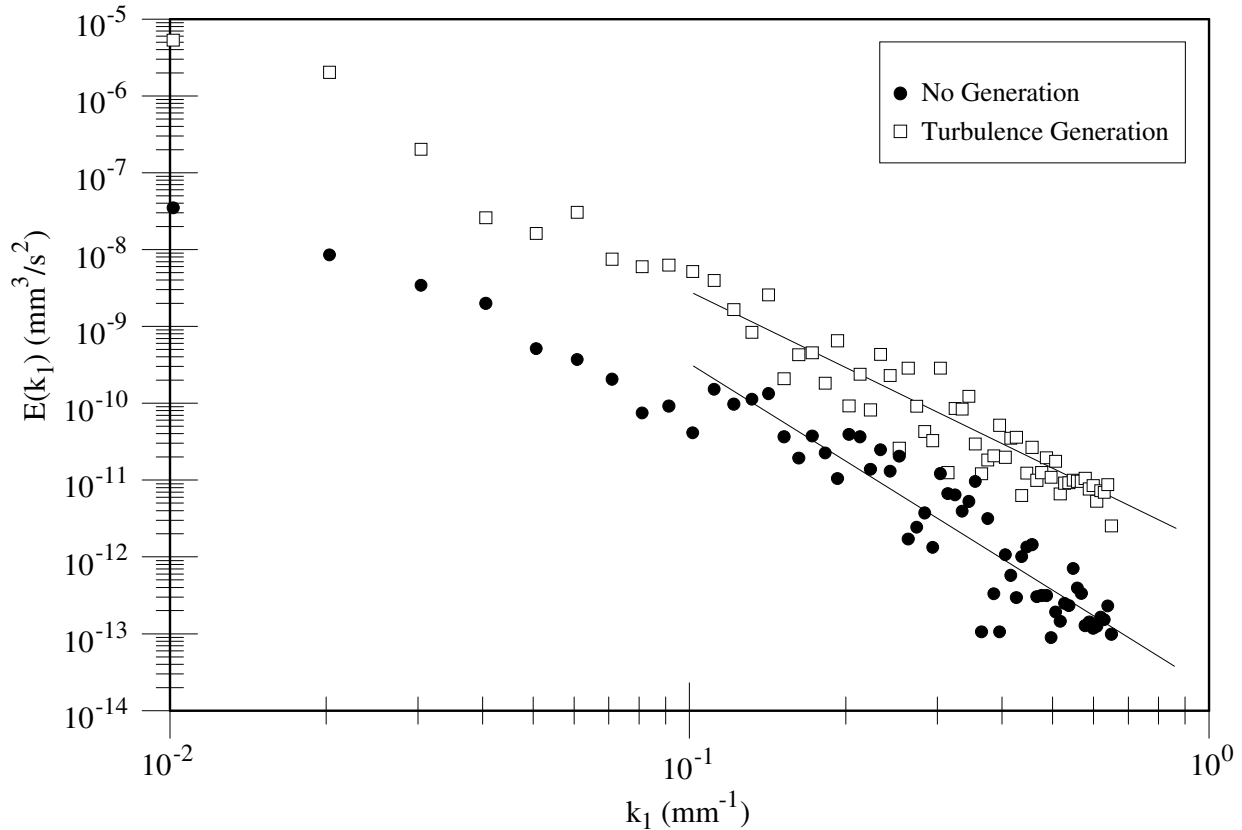
Figure 7 – Spatial energy spectrum of u_1 for U=0.914 m/s, 1 diameter downstream of generator.

Trends for U=1.83 m/s (Fig. 4) were similar but the effect was less significant than that for the lower pipe velocity. This is likely due to the greater natural turbulence of a higher Reynolds number flow. For this pipe velocity additional turbulent energy from the generator was a smaller percentage of the total flow energy as the level of generator operation was the same for both pipe flows. Still, there was a significant increase in energy at the highest wave number and the slope was flattened slightly (Table 2).

Scatter in the spectral data is likely due to differences in spatial velocities along the cross-section of the pipe. This location was chosen because it was the nearest possible cross-section to the generator that could be captured with the PIV and most closely represented turbulence levels within the generator. Also, spatial data were used rather than time series data due to the low frequency of the PIV system. Dense and thoroughly mixed seeding throughout the flow field made it possible to obtain accurate estimates of velocity and L_k values using PIV (PETERS and REDONDO 1997).
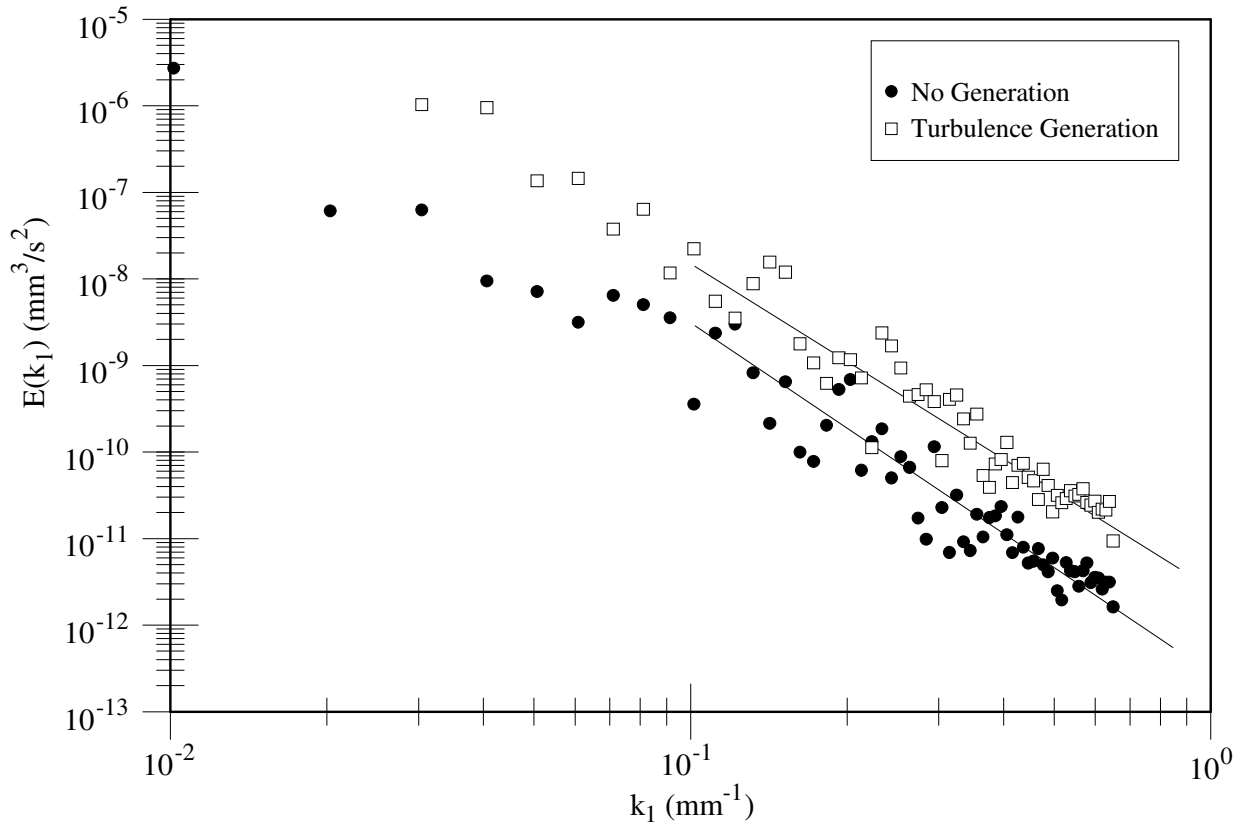
Figure 8 – Spatial energy spectrum of u_1 for U=1.83 m/s, 1 diameter downstream of generator.

Table 3 – Summary of results from figures 2 – 4.

U	% Decrease in Avg L_k		Cascade Slope		Energy increase at L_k (max k_1)
m/s	*at 1 dia. downstream*	*at 2 dia. downstream*	*Turbulence Generation*	*No Generation*	*orders of magnitude*
0.914	23.2%	15.1%	-4.82	-6.39	1.41
1.83	18.4%	13.9%	-2.32	-4.47	0.76

CONCLUSIONS

To determine if turbulence can be used as an invasive mussel control in piping systems, PIV measurements were made to quantify turbulence parameters in pressurized pipe flow. Data with and without generated turbulence were compared and showed that generated turbulence in the downstream pipe was sustained for about 2 diameters downstream. Within this range energy added from the generator drove the Kolmogorov length down to scales likely to impact invasive mussel species (near 200 μm). At 1 pipe diameter downstream, the energy spectrum showed that energy near the Kolmogorov scale was significantly increased for both pipe flows. The results of

added energy and decreased eddy size, particularly at the Kolmogorov scale, will hopefully have a meaningful impact on invasive mussel species within piping systems.

NOTATION

U = mean pipe velocity (m/s)
u_I = stream wise velocity vector (m/s)
L_k = Kolmogorov length scale (μm)
v = kinematic viscosity (m^2/s)
D = energy dissipation rate (m^2/s^3)
Re = Reynolds number of pipe flow (-)
k_I = wavenumber, corresponds to eddy size (mm^{-1})
$E(k_I)$ = spatial energy spectra, corresponds to mean energy at wavenumber (mm^3/s^2)

ACKNOWLEDGEMENTS

REFERENCES

AMEC EARTH and ENVIRONMENTAL. (2009). *Zebra/Quagga Mussel Veliger Transport Model: Tarryall Reservoir to Cheesman Reservoir.* Denver, CO.

DORON, P., BERTUCCIOLI, L., KATZ, J., & OSBORN, T. R. (2000). Turbulence Characteristics and Dissipation Estimates in the Coastal Ocean Bottom Boundary Layer from PIV Data. *Journal of Physical Oceanography* , Vol 31, 2108-2134.

FOUCAT, J., CARLIER, J., and STANISLAS, M. (2004). PIV optimization for the study of turbulent flow using spectral analysis. *Meas. Sci. Technol.*, 15, 1046-1058.

GRUE, J., LIU, P. L.-F., and PEDERSEN, G. K. (2004). PIV and Water Waves. *Advances in Coastal and Ocean Engineering* (p. 73). Hackensack, NJ: World Scientific.

PETERS, F., and MARRASE, C. (2000). Effects of turbulence on plankton: an overview of experimental evidence and some theoretical considerations. *Marine Ecology Progress Series* , Vol. 205, 291-306.

PETERS, F., and REDONDO, J. M. (1997). Turbulence Generation and measurement: application to studies on plankton. *Scientia Marina* , 61, 205-228.

RECLAMATION. (2009, March). *Quagga and Zebra Mussels Fact Sheet*. Retrieved June 2011, from Quagga and Zebra Mussels: http://www.usbr.gov/mussels/history/factsheets/general.html

REHMANN, C. R., STOECKEL, J. A., and SCHNEIDER, D. W. (2003). Effect of turbulence on

the mortality of zebra mussel veligers. *Can. J. Zool.* , 81, 1063-1069.

SAARENRINNE, P., PIIRTO, M., and ELORANTA, H. (2001). Experiences of turbulence measurement with PIV. *Meas. Sci. Technol.*, 12, 1904-1910.

TENNEKES, H., and LUMLEY, J. L. (1972). *A First Course in Turbulence.* Cambridge: The Massachusetts Institute of Technology.

THE EFFECT OF BOULDER SPACING ON FLOW PATTERNS AROUND BOULDERS UNDER PARTIAL SUBMERGENCE

Iordanis MOUSTAKIDIS

IIHR - Hydroscience & Engineering, University of Iowa, USA, iordanis-moustakidis@uiowa.edu

Athanasios (Thanos) PAPANICOLAOU

IIHR - Hydroscience & Engineering, University of Iowa, USA, apapanic@engineering.uiowa.edu

Achilleas TSAKIRIS

IIHR - Hydroscience & Engineering, University of Iowa, USA, achilleasgeorgios-tsakiris@uiowa.edu

ABSTRACT: This study focuses on documenting the influence of boulder spacing on flow patterns within an array of boulders in mountain streams. Boulder arrays modify the flow structures in their vicinity, which in turn regulate the depositional patterns. However, a critical literature review reveals that the effects of boulder spacing on flow have been overlooked. Herein, we hypothesize that the developing flow structures around boulders are controlled by the boulder spacing. The objective of this study is to map the surface flow structures around partially submerged boulders for two different boulder spacing scenarios: (1) $\lambda/d_c = 6$ and (2) $\lambda/d_c = 10$ (where λ denotes the spacing between the boulders and d_c is the boulder diameter). For each scenario, the flow structures are mapped using an IR camera. The IR camera records the motion of ice-cube tracers, which is subsequently analyzed with the Large Scale Image Velocimetry (LSIV) software. The result is a surface velocity field produced by a sequence of successive frames. The flow experiments show that when $\lambda/d_c = 6$, the shear layers emanating from the upstream boulders extend all the way to the downstream boulders, whereas when $\lambda/d_c = 10$, the flow reattaches prior to reaching the downstream boulders.

Keywords: mountain streams, relative submergence, boulder spacing, IR camera.

INTRODUCTION

In many restoration projects, it is a widely spread practice to install arrays of boulders (rocks) into the stream body to minimize the effects of upstream hydraulic structures (e.g. dams, weirs) and restore degraded ecosystems (SHAMLOO et al. 2001). Installation of boulders is a useful tool in engineering practice that can be used to replicate the natural environment, improve fish habitats and support ecosystem diversity by creating in-stream regions that provide feeding and spawning resources to the fish populations (NOWELL and JUMARS 1984, KATOPODIS 1996).

Despite their easy and cost-effective installation, the design of arrays of boulders for restoration purposes involves significant empiricism as the hydraulics around the rocks remains poorly understood. A key parameter governing the hydraulics and sediment transport processes within the boulder array is the relative submergence. Relative submergence is defined as the ratio of the flow depth (H) to the boulder (rock) characteristic diameter (d_c), H/d_c. Mountain streams are characterized by shallow flows due to the limited hydrologic inputs during most of the year. At these shallow flows, the boulders remain partially submerged, thus operating under the Low Relative Submergence ($H/d_c < 1$) regime.

In flow-boulder interactions within an array of boulders, there also exist interactions between neighboring boulders, which are intimately associated with the spacing, λ, between the boulders (MORRIS, 1955; HASSAN and REID, 1990). However, little research has been conducted on these boulder-to-boulder interactions, especially under the Low Relative Submergence (LRS) regime. In this study, it is hypothesized that the boulder spacing affects the flow structures developing around rocks under the LRS regime.

For shallow flows in steep mountainous streams, where the flow depth is typically smaller than the diameter of the boulders ($H/d_c < 1$), the flow patterns around the boulders can be reflected on the water surface (SHAMLOO et al., 2001; PAPANICOLAOU and KRAMER, 2005). This study investigates the surface flow patterns around boulders in a qualitative and quantitative manner by taking advantage of a relatively new technique, the InfraRed Large Scale Image Velocimetry or IR–LSIV. The basic principle behind the IR–LSIV is that the temperature convective velocities are equal to the fluid surface velocities for fluids such as water, which are typically characterized by low thermal diffusivity (HESTRONI et al., 2001). An IR camera can visualize the surface flow patterns by detecting thermal structures developing on the water surface. To enhance the thermal structures on the water velocity, water is seeded with a temperature tracer, i.e., ice cubes or hot water, which differs in temperature from the ambient water. Analysis of the videos showing the water surface thermal structures via the LSIV technique (FUJITA et al., 1997) can yield quantitative information about the water surface patterns. Because the IR–LSIV is a very recent technique (HESTRONI et al., 2001; JACKSON et al., 2009), a sensitivity analysis was conducted to determine the optimal number of (video) frames to be analyzed, as well as the optimal value of the searching radius, that produce consistent results.

The overreaching objective of this study is to investigate the influence of boulder spacing on the developing flow structures around a rock within an array under the LRS regime. The specific objectives of this research can be summarized as (1) qualitative assessment of the flow interaction between neighboring rocks, (2) sensitivity analysis for the IR-LSIV method, and (3) preliminary estimates of the velocity field around a representative group of boulders, utilizing the

IR-LSIV technique for two different packing densities: 2 and 1%.

METHODOLOGY

A number of flume experiments were designed and conducted in order to address the study objectives. Two experimental scenarios, under the LRS regime, were considered and investigated: (1) $\lambda/d_c = 6$ and (2) $\lambda/d_c = 10$ (Figure 1), where λ is the spacing between neighboring boulders and d_c is characteristic diameter of the boulders ($d_c = 55$ mm), corresponding to a 2 and 1% packing density (MORRIS, 1955; BYRD et al., 2000; and YAGER et al., 2007), respectively. During each experimental run, the bed slope and the flow depth were kept constant at 0.0159 and 0.044 m, respectively. The flow conditions used in this experimental study (Table 1) were selected to match the conditions from a previous study (Papanicolaou and Kramer 2005).

Table 1 – Experimental flow conditions

(1)	(2)	(3)	(4)	(5)	(6)	(7)	(8)
Run	H/d_c	H (m)	Q (m^3/s)	S (m/m)	U_{bulk} (m/s)	Fr	Re
1	0.8	0.044	0.0207	0.0159	0.5170	0.7956	7.02E+04
2	0.8	0.044	0.0250	0.0159	0.6244	0.9609	8.48E+04

Experimental setup

This laboratory flume study is conducted at IIHR-Hydroscience and Engineering facilities in the University of Iowa. For the purposes of this research a 21-meter-long, 91-cm-wide, 53-cm-deep experimental flume with an adjustable slope (up to 15%) was used. The side walls of the flume were built with acrylic glass, allowing a side view of the developing flow structures. The boulder section was 5.2 m in length and located 10.9 m from the upstream edge of the flume. An array of 48 and 22 uniform-size boulders was placed atop a flat, immobile, porous, uniform roughness bed, representing the 2 and 1% packing densities, respectively (Figure 1). The bed was comprised of well-packed, colorless glass beads with characteristic diameter $d_b = 19.1$ mm. During all experiments, uniform flow conditions were preserved by placing a set of metal bars, along the flume transverse direction, at the flume exit section, one on top of the other.

The surface flow structures developing around boulders were recorded via an IR camera. The videos created was loaded to the LSIV software, where the surface velocity fields were constructed. The LSIV software makes use of thermal tracers to estimate the flow velocity vectors. In this study, ice cubes were first used as tracers, but the results were not at all satisfactory (Figure 2). Therefore, hot water droplets were finally employed. The hot water

tracers were feeding 0.50 m upstream of the test section. The IR camera was placed on a metal frame above the test section, and the videos were recorded at a rate of 30 frames per second for a total duration of approximately

35 seconds. The Final Cut Pro software was then used to convert the videos into sequences of images. These images were loaded to the LSIV software, which analyzes the successive images to produce the surface velocity field vectors.
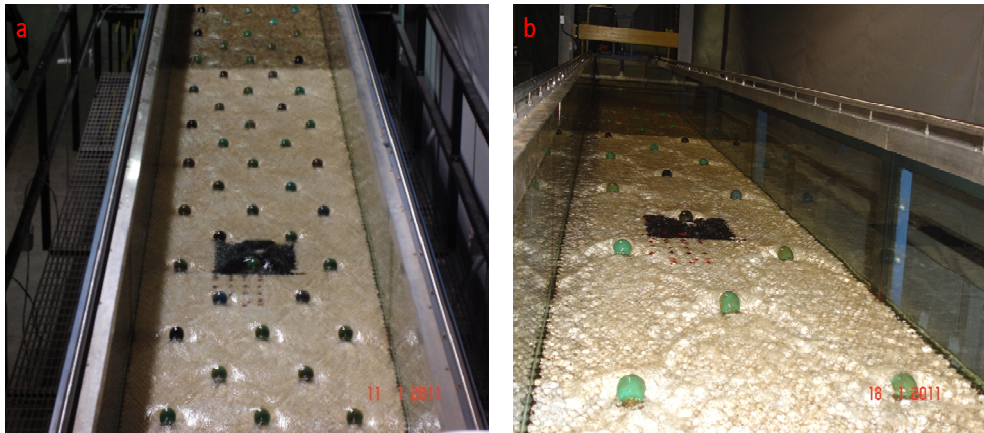
Figure 1 – Experimental setup for (a) $\lambda/d_c = 6$ and (b) $\lambda/d_c = 10$
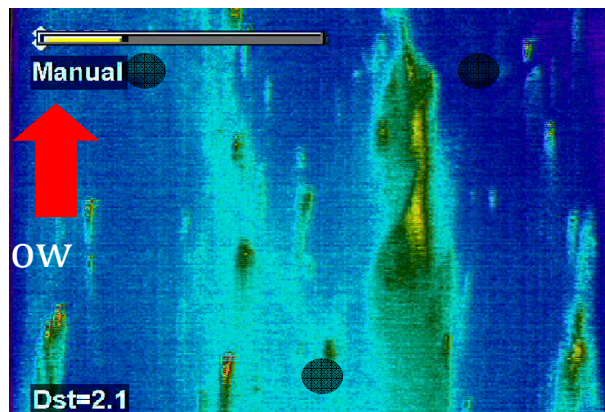
Figure 2 – Flow patterns captured with the IR camera, using ice cubes as tracers

A sensitivity analysis was performed to estimate the optimal number of frames and the searching radius value that introduce the minimum numerical error to the LSIV method in computing the bulk velocity (U_{bulk}) compared to the true bulk velocity. A different number of frames were analyzed (e.g., 50, 100, 250, 500, and 800 frames) and search radius values (e.g.,

20, 25, 30, 35 and 40 pixels) were considered in two runs, one without boulders present, corresponding to two bulk velocities (U_{bulk1} = 0.451 m/s and U_{bulk2} = 0.595 m/s), and one with boulders. These bulk velocities were selected for the sensitivity analysis because they were of comparable magnitude with the ones considered for the experimental runs (U_{bulk} = 0.51 m/s and U_{bulk} = 0.62 m/s). The optimal number of frames and search radius used in this study were the ones that gave the minimum error compared to the bulk velocity measured from the flume flow meter (MAGFLO® MAG 3100 Electromagnetic digital flow meter, accurate to within 0.25% of the flow) and the flume dimensions (Jackson et al., 2009).

RESULTS

The flow structures developing around a group of representative boulders for λ/d_c = 6 and λ/d_c = 10 are presented in Figure 3a and 3b, respectively. For λ/d_c = 6, the different colors in Figure 3a represent different water temperatures. The blue and the violet colors indicate cooler water regions, while the brighter colors, cyan, green, yellow and red, represent regions with progressively hotter water. The boulders in the flow field are denoted by solid black circles. Hot water (white and red colors) was seeded right upstream of the rocks and mixed with the cooler water in the flume while it was advected downstream. The shear layers forming at the downstream side of the boulders are indicated with the cyan color. Because the shear layers consist of high momentum fluid, the seeded hot water was advected downstream faster, hence the higher water temperature corresponds to the cyan color. Figure 3a shows that for λ/d_c = 6, the shear layers forming around the upstream boulders, illustrated as regions with cyan color, extend to the downstream boulders and interfere with the surface flow structures around the downstream boulders. In the wake region of the central upstream boulder, the fluid is characterized with purple color, which denotes cooler and thus decelerated water. Because of the recirculation region forming downstream of the boulder and the shear layers that form around the boulder, the seeded hot water does not mix with the cooler ambient water in the boulder wake region.
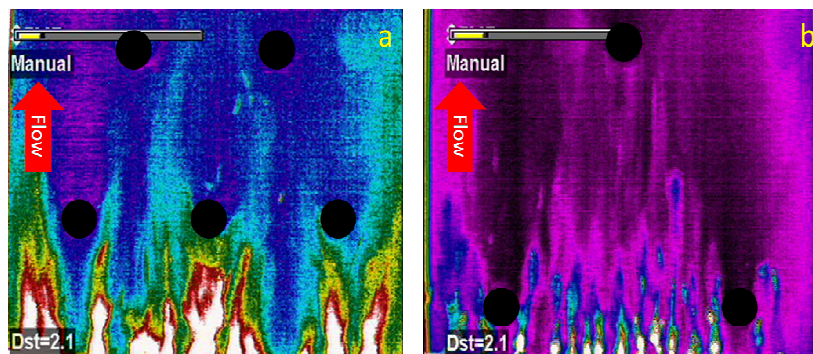
Figure 3 – IR camera depiction of the developing flow patterns for (a) λ/d_c = 6 and (b) λ/d_c = 10

Figure 3b shows a snapshot of the surface water temperature when the rock spacing is $\lambda/d_c = 10$. In Figure 3b, the black and deep purple colors indicate cooler water regions, while the lighter purple, blue, cyan, green, yellow and white colors represent regions with progressively hotter water. Shear layers developed at the wake region of the boulders, forming an inner, low momentum and outer, high momentum regions. The water region forming behind the boulders is characterized by cooler, decelerated water. As can be observed from Figure 3b, the effects of the shear layers emanating from the boulders upstream did not interfere with the flow structures developing around the downstream rocks due to the fact that the shear layers reattached with the main flow far upstream of the downstream rocks. Moreover, the water flowing between the two upstream boulders was not affected by the presence of the developing shear layers. Therefore, for the case of $\lambda/d_c = 10$, no interference between neighboring boulders was observed, and thus the packing density corresponding to this experimental scenario (1%) created an isolated roughness regime, where the wake developed by one boulder had no effect on its neighboring boulders.

The qualitative results of Figure 3 are also quantitatively investigated via the LSIV technique. First, a sensitivity analysis was performed to estimate the optimal number of frames, as well as the value of the searching radius required for the LSIV technique. In Figure 4 the sensitivity analysis curves are presented. Figure 4a shows that when the analysis is based on more than 500 frames, the error in the bulk velocity estimation is less than 10% for both $U_{bulk} = 0.451$ m/s and $U_{bulk} = 0.595$ m/s. Moreover, Figure 4a and 4b show that for both $U_{bulk} = 0.451$ m/s and $U_{bulk} = 0.595$ m/s the error in the U_{bulk} estimation reduces to approximately 5%, when the searching radius is greater than 25 pixels. The results in Figure 4 show overall that 25 pixels and 500 frames are the optimal values for the searching radius and the number of frames, respectively, which are then used to carry out the LSIV analysis.
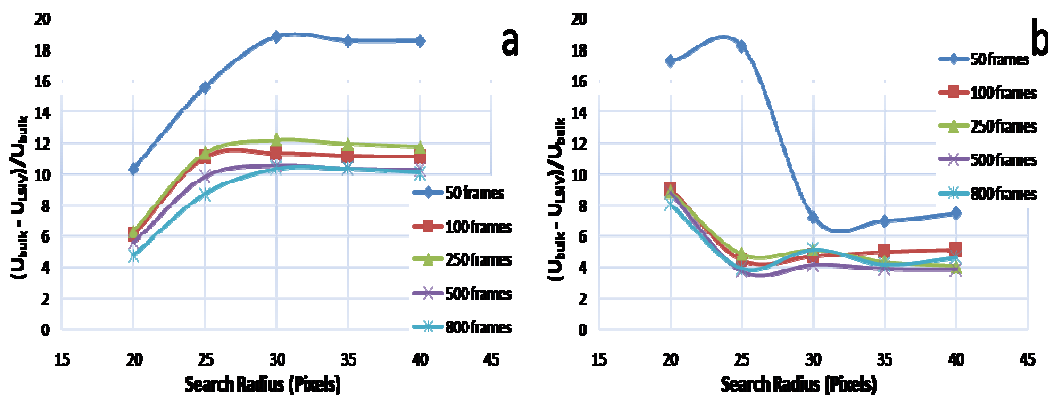
Figure 4 – LSIV sensitivity analysis for estimating the optimal number of frames and the value of the search radius for (a) $U_{bulk} = 0.451$ m/s and (b) $U_{bulk} = 0.595$ m/s

The surface velocity fields corresponding to $\lambda/d_c = 6$ and $\lambda/d_c = 10$, were obtain via the LSIV technique around a representative group of rocks and are presented in Figures 5a and 5b, respectively. Figure 5a reveals that for $\lambda/d_c = 6$, a wake region with decelerated fluid formed immediately downstream of the rocks. This region was characterized by small surface velocities and was separated from the rest of the flow field by the arms of the forming shear layer. Figure 5a captures both the stream wise interactions between upstream and downstream boulders and the transverse interference between boulders located at the same row. The green, yellow and orange colors represent progressively higher velocities, occurring almost at the center of the outer regions, where the effects from the wake regions are minimal.

In Figure 5b, which represents the surface velocity field for $\lambda/d_c = 10$, the effects of the forming shear layers are localized, since the shear layers occupy a limited area of the flow field in the wake region of the rocks. The shear layers reattach with the main flow far upstream of the downstream boulders. Thus, the effects of the shear layers to the downstream boulders and to the boulders being at the same row are negligible. The blue color denotes very small surface velocities that occur in the inner region, the cyan color separates the inner and the outer regions, while the rest of the flow field is characterized by higher surface velocities, represented by the green, yellow, orange and red colors.
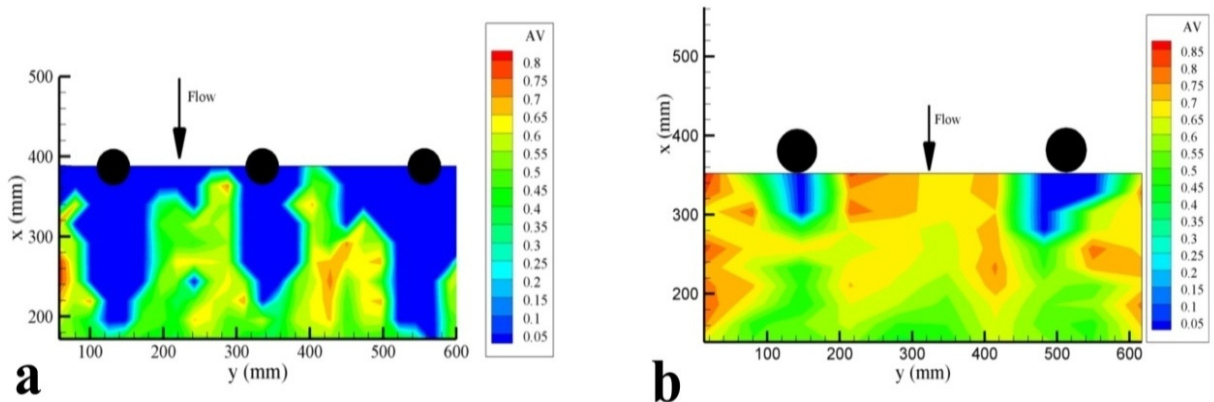
Figure 5 – Surface velocity field constructed via the LSIV technique

CONCLUSIONS

The overreaching objective of this experimental study was to map the surface flow structures around partially submerged boulders, for two different spacing arrangements: $\lambda/d_c = 6$ and $\lambda/d_c = 10$. The objectives of this study were accomplished by using an IR camera to record the surface

flow structures and the LSIV technique to build the corresponding surface velocity field. Prior to the LSIV method, a sensitivity analysis was conducted in order to estimate the optimal number of frames and the value of the searching radius that introduce the minimum numerical error to the LSIV technique.

The observed surface flow patterns via the IR camera were also quantitatively investigated by constructing the corresponding surface velocity fields. Both the qualitative and quantitative results suggest that for $\lambda/d_c = 6$, interference between neighboring rocks occurs. More specifically, the shear layers emanating from the upstream boulders extend to the downstream boulders and affect the surface flow structures developing around the downstream boulders. According to these findings, for a packing density of 2%, the presence of the upstream rocks might still affect the surface flow patterns around the downstream rocks. This raises an interesting question of whether a spacing between neighboring boulders of $\lambda/d_c = 6$ indeed produces an isolated roughness regime for the boulders (MORRIS, 1955). In the isolated roughness regime, the individual boulders do not affect the flow field of the immediately downstream boulders.

For the second experimental scenario, where $\lambda/d_c = 10$, the shear layers emanating from the upstream boulders reattached with the main flow prior to the downstream boulders, and thus, no interference between neighboring boulders was observed. These qualitative results were also quantitatively reconfirmed via the surface velocity field produced by the LSIV method, where the effects of the upstream emanating shear layers were negligible to the downstream boulders.

In summary, for the Low Relative Submergence (LRS) regime, the spacing arrangement of the boulders in the stream affects the developing flow patterns around neighboring boulders. These interesting findings warrant future research, which will focus on the investigation of the parameters that control the depositional patterns for the Low Relative Submergence (LRS) regime and the improvement of the IR camera and LSIV technique.

REFERENCES

BYRD, T.C., FUTBISH, D.J., and WARBURTON, J. (2000). "Estimating depth-averaged velocities in rough channels." *Earth Surface Processes and Landforms*, 25(2), pp 167-173.

FUJITA, I., MUSTE, M., and KRUGER, A. (1997). "Large-scale PIV for flow analysis in hydraulic applications." *Journal of Hydraulic Research*, 36(3), pp. 397-414.

HASSAN, M.A., and REID, I. (1990). "The influence of microform bed roughness elements on flow and sediment transport in gravel bed rivers." *Earth Surface Processes and Landforms,* Vol. 15(8), pp. 739-750.

HESTRONI, G., MOSYAK, A., and SEGAL, Z. (2001). "Non-uniform temperature distribution in

electronic devices cooled by flow in parallel channels." *IEEE Trans. Comp. Packaging Technol*. 24(1) pp. 16–23.

JACKSON, E., ADMIRAAL, D., ALEXANDER, D., STANSBURY, J., GUO, J., RUNDKUIST, D., and DRAIN, M. (2009). "Thermal Imaging for Discharge and Velocity Measurements in Open Channels." *Presented in the 33rd International Association of Hydraulic Research Symposium*, IAHR, Vancouver, Canada, August 9-14.

KATOPODIS, C. (1996). "Ecohydraulics: Challenges and Opprtunities with Fish and Fish Habitat." *Ecohydraulics 2000, Second International Symposium on Habitat Hydraulics*, Quebec, Canada, Vol. B, pp. 555-578.

MORRIS, H.M. (1955). "Flow in Rough Conditions." *Transactions of the American Society of Civil Engineering*, 120, pp. 373-398.

NOWELL, A.R.M., and JUMARS, P.A. (1984). "Flow environments of aquatic benthos." *Annual Review of Ecology and Systematics*, Vol. 15, pp. 303-328.

PAPANICOLAOU, A.N., and KRAMER, C.M. (2005). "The role of relative submergence on cluster microtopography and bedload predictions in mountain streams." *In Gary Parker and Marcelo H. Garcia (eds.), River, Coastal and Estuarine Morpholodynamics; Procedings International Symposium*, Urbana, IL, 4-7 October 2005, Philadelphia: Taylor and Francis.

SHAMLOO, H., RAJARATNAM, N., and KATOPODIS, C. (2001). "Hydraulics of simple habitat structures." *Journal of Hydraulics Research*, 39(4), pp. 351-366.

YAGER, E.M., KIRCHNER, J.W., and DIETRICH, W.E. (2007). "Calculating bed load transport in steep boulder channels." *Water Resources Research*, 43, W07418. doi: 10.1029/2006WR005432.

HAZARDS AT LOW-HEAD DAMS

Riley J. OLSEN

Civil and Env. Engineering, Utah State University, USA, riley.j.olsen@gmail.com

Michael C. JOHNSON

Civil and Env. Engineering, Utah State University, USA, michael.johnson@usu.edu

ABSTRACT: Low-head dams are small structures that are built for many purposes, the most common being to impound small amounts of water for various uses. At certain flow conditions, a dangerous countercurrent, known as a roller, can form downstream of a low-head dam. This current possesses an upstream directed surface velocity that can effectively trap debris, as well as unsuspecting humans, at the downstream side of the dam. It is this current that is responsible for the deaths of many individuals that have ventured too close to these structures over the years. It is the objective of this study to identify a relationship between easily observable parameters and the roller strength that can be used as a classification system. This will be done primarily through the use of computational fluid dynamics software to simulate various flow conditions. The results of these numerical models will then be compared, and a relationship will be identified. This study is currently underway, and therefore conclusive results are not available at this time. Although, comparison of the numerical results to physical model results have been used to verify that the flow conditions being produced by the software accurately represent the physical flow conditions.

Keywords: low-head dam, drowning machine.

INTRODUCTION

Low-head dams have been constructed historically to serve a wide variety of purposes. Some are meant to impound small volumes of water to be used for irrigation and cooling of power plants, supply water to municipalities and industry, and simply to provide for recreational activities. Others are in place to house and protect utility lines at river crossings. Some are built to enhance water quality downstream through the entrainment of air into the water. They can take many different forms, with the most common being the flat-topped and the ogee crested weir.

As water flows over a low-head dam or drop structure in a mildly sloped channel, the

flow regime smoothly transitions from subcritical to supercritical. As it continues past the dam, the flow must eventually return to subcritical flow at a distance downstream depending on the slope of the channel and the tailwater conditions. A transition from supercritical to subcritical flow is not a smooth one as it is when going in the opposite direction. Instead, a hydraulic jump is formed where the transition takes place, with the purpose of dissipating the excess energy possessed by the high velocity supercritical flow.

When flow conditions at a low-head dam cause the hydraulic jump to be submerged, a strong current can be formed at the downstream face of the dam that features a characteristic upstream directed surface velocity. This current, which is commonly referred to as a "hydraulic" by recreational water users or "roller" by the engineering community, can often catch debris and hold it near the face of the dam for long periods of time. Occasionally, an unsuspecting person can get too close to one of these structures and find themselves incapable of escaping the relentless current, often struggling to the point of exhaustion and ultimately drowning before being rescued.

Several studies have been performed on the subject of low-head dams, primarily focusing on the dangerous hydraulic conditions and possible remediation techniques that have been proposed. Some of the more significant studies include those performed by LEUTHEUSSER (1988), LEUTHEUSSER and BIRK (1991), HOTCHKISS and COMSTOCK (1992), and LEUTHEUSSER and FAN (2001). These studies have done an excellent job of identifying the dangerous flow patterns created at low-head dams and suggesting possible solutions to the problem, although it seems little has been done when it comes to classifying the hazards present based on easily obtainable parameters.

In their study, LEUTHEUSSER and FAN (2001) utilize a submergence factor (S) of the hydraulic jump to identify key transition points in the formation of the roller. This submergence factor, as presented in Eq (1), requires the depth of the subcritical sequent depth of the optimum hydraulic jump (Y_2), which can be difficult to determine. Y_4 in Eq. (1) is the downstream tailwater depth.

$$S = \frac{Y_4 - Y_2}{Y_2} \tag{1}$$

This study aims to identify a relationship between easily observable and measurable parameters that will allow low-head dams to be classified according to the danger encountered

by the public. This classification system would help recreational water users and dam owners alike assess hazards and act appropriately in terms of safety and liability.

RESEARCH OBJECTIVES AND METHODOLOGY

This study, which is currently underway at the Utah Water Research Laboratory (UWRL) in Logan, Utah, will use the computational fluid dynamics (CFD) software Flow-3D™ to numerically model flow over low-head dams at various flow conditions. Two dam shapes are being examined as a part of this research: the flat topped weir and the ogee crested weir. Dam heights (P) being tested are 0.61 m, 1.52 m, and 3.05 m, with varying upstream and downstream water depths.

The setup of the numerical models in Flow-3D™ will be identical besides the upstream water depth (h_u) and downstream water depth (h_d). Simulations are being run in series, with a single series consisting of a particular dam size and h_u held constant, while h_d is increased incrementally in each simulation. Once a series of simulations has been completed, a new series is set up using a different value of h_u.

The boundary conditions of the computational domain used will model actual flow conditions at a low-head dam as closely as possible, and will be kept the same for each simulation. The mesh boundaries will be set as follows:

- Upstream boundary (X_{min}): Specified pressure boundary with a stagnation pressure set to zero and specified fluid height
- Downstream boundary (X_{max}): Specified pressure boundary with a stagnation pressure set to zero and specified fluid height
- Bottom boundary (Z_{min}): Wall boundary (no slip)
- Top boundary (Z_{max}): Symmetry boundary (no influence on model due to open channel)
- Side boundaries (Y_{min} and Y_{max}): Wall boundaries (no slip)

Once a numerical simulation has been completed, the flow rate, minimum surface velocity in the direction of flow (negative being upstream directed), water surface elevations at a distance of $2P$ upstream and $3P$ downstream from the upstream face of the dam, and Froude Numbers at these same locations are extracted from the results. A distance of $2P$ is used for the upstream

water depth measurement location to avoid the effects of drawdown as water flows over the dam. A distance of 3P will not be used as the downstream measuring location to avoid turbulence from the hydraulic jump and the associated error. These distances will be used as the standard for this classification system. A three-dimensional animation of the simulations will also be created from the CFD results. This animation will show each cell of the computational domain represented by color based on the magnitude of the x-velocities. A definition sketch of the numerical model setup and physical model setup of a flat topped weir simulation is shown in Figure 1.
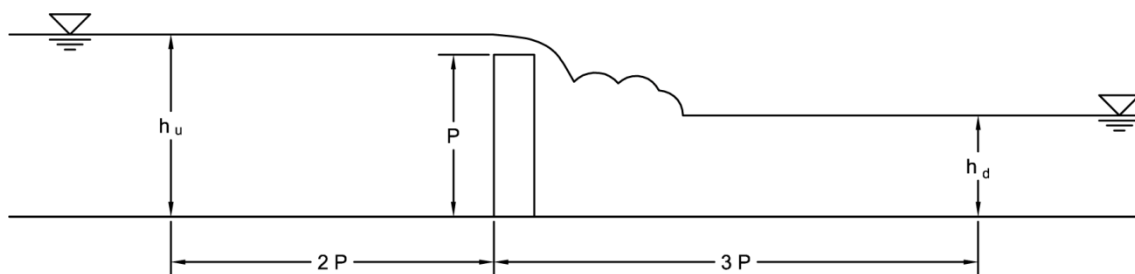
Figure1 – Numerical model setup

In order to verify the accuracy of the numerical results obtained through the CFD program, physical models of several of the simulations will be built and tested at the UWRL, utilizing a gravity fed rectangular laboratory flume (1.83 m x 9.14 m x 1.22 m deep). The physical models will be set up so that the water depths at the specified distances upstream and downstream of the dam match those at the same distances in the corresponding CFD models as closely as possible. Once these water surface elevations are achieved, a flow meter will be used to measure the flow rate. This flow rate, as well as photos and video of the physical flow, will be compared to the numerically obtained flow rates and the CFD animations to verify that the physical process is being accurately reproduced by the CFD setup.

In addition to the verification of the CFD program, the physical model will also be used to test the roller's ability to trap a scaled human model. The human model was cut out of a sheet of high-density polyethylene (HDPE) and modelled to weigh exactly 85.3 kg at a one-fifth scale (0.68 kg model scale). In order to achieve this weight, material was cut out of the chest of the human shaped model. In order for the model to float in the upright position such as a human wearing a life jacket, bolts were attached to the ankles of the model and polystyrene foam filled the hollowed chest cavity. These modifications yielded a test subject that floated upright in the

water with everything below the shoulders being submerged.

RESULTS AND DISCUSSION

Because this study is still underway, data is still being collected and results are not being disclosed at this time. Although there is still much work to do in this study, several pairs of numerical and physical models used to verify the CFD setup accuracy have been completed. The results of these tests are shown in Table 1. Included are the flow rate, Q, upstream water depth, h_u, and downstream water depth, h_d, of both the numerical and physical models tested. Also included are the corresponding percent differences between these parameters.

Table 1 – Comparison of CFD results to physical model data

		Q (m³/s)	h_u (m)	h_d (m)
Comparison 1	CFD	0.064	0.686	0.305
	Physical Model	0.062	0.686	0.290
	% Difference	**3.7%**	**0**	**5.3%**
Comparison 2	CFD	0.064	0.686	0.387
	Physical Model	0.062	0.686	0.381
	% Difference	**3.7%**	**0**	**1.6%**
Comparison 3	CFD	0.303	0.805	0.677
	Physical Model	0.295	0.808	0.649
	% Difference	**2.9%**	**0.4%**	**4.2%**

As can be seen from the data in Table 1, the largest percentage difference in flow rates between a pair of simulations was 3.7% in both comparison 1 and 2. The average percent differences are as follows: 3.4% in flow rates, 0.13% in h_u, and 3.7% in h_d. These small discrepancies have been deemed acceptable for this study, and it has therefore been concluded that the CFD program and setup being used is accurately replicating physical flow conditions at low-head dams. Figures 2 and 3 show a snapshot of the CFD simulation and a photo of the physical model of comparison 2, respectively.
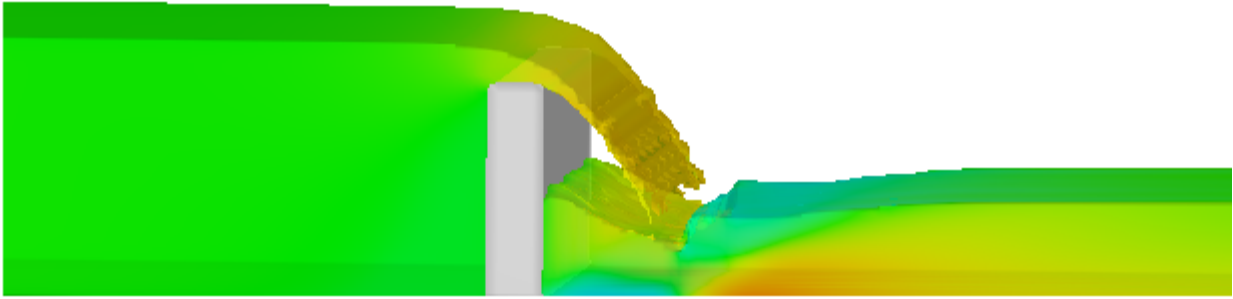
Figure 2 – Animation of CFD model from comparison 2

Figure 3 – Photo of physical model from comparison 2

CONCLUSION

The objective of this research is to increase the understanding of the dangerous hydraulic conditions that can be present at low-head dams at certain flow conditions. It is also hoped that a clear relationship between parameters easily measured and obtained in the field and roller strength can be identified and used as a classification system. This type of system would help recreational water users and dam owners assess dangers and therefore make better decisions in regard to safety and liability.

Because the study is currently in progress and there is still much data to collect and analyze, no conclusions have been made as yet. The data that has been collected and analyzed up to this point shows promising potential for achieving the desired outcomes.

LIST OF SYMBOLS

h_d = Downstream water depth

P = Dam height

Q = Flow rate

S = Submergence factor

Y_2 = Sequent subcritical depth of optimum hydraulic jump

Y_4 = Tailwater depth

REFERENCES

HOTCHKISS, R. H., and COMSTOCK, M. (1992). ''Discussion of 'Drownproofing of low overflow structures,' by H. J. Leutheusser and W. M. Birk.'' *J. Hydr. Eng.*, ASCE, 118(11), 1586-1589.

LEUTHEUSSER, H. J. (1988). ''Dam safety, yes. But what about safety at dams?'' Proc., 1988 Nat. Conf., Hydr. Div., ASCE, Colorado Springs, CO, 1091–1096.

LEUTHEUSSER, H. J., and BIRK, W. M. (1991). ''Drownproofing of low overflow structures.'' J. Hydr. Eng., ASCE, 117(2), 205–213.

LEUTHEUSSER, H. J., and FAN, J. J. (2001). "Backward Flow Velocities of Submerged Hydraulic Jumps." J. Hydr. Eng., ASCE, 127(6), 514-517.

PUMPING SYSTEMS WITH VARIABLE REFERENCE HEAD: THE NON-VISUALIZED PROBLEMS

Boris RODRIGUEZ C.

bcrodrig@bechtel.com

Astrid PÉREZ O.

aperezod@bechtel.com

José Manuel ADRIASOLA V.

jmadrias@bechtel.com

Bechtel Chile Ltda. Santiago, Chile,

ABSTRACT: In several industries, like the mining business, it is very common to observe high head pumping systems, which transport water to more than one discharge point. These discharge points could have, in some cases, variable discharge pressures and, furthermore, could be utilized as water sources (a water reservoir, for example) for other facilities using the same pipes that feed them (flow in double direction). Because of this particular design, the pumping systems can have different Total Dynamic Head (TDH) depending on the water level in the reservoir(s), resulting in a complication for the design and operation of the pumping systems. The objective of this investigation is to understand the operation of pumping systems with variable reference head, visualize the advantages of this type of design, and better understand related operating problems. In this case study, we analysed the design of an existing system that transports water from a river to a 4.2 million m^3 reservoir and then on to a base metal process plant. To address this problem, a steady-state analysis was conducted to determine the TDH and flow discharge per pump for several operation scenarios and different types of problems noted from the calculations performed. The first problem was related to the control system being required to supply pumped water directly to the process plant and to the reservoir at the same time. Another problem was related to the performance of the pumps in all pump stations: a broad range of operation in terms of flow discharge. To avoid this type of problem, a redesign or mitigation measures should be considered, like the use of variable frequency drives for the pump motors or the increase of the water tank volume in pump stations. A redesign of the system was proposed as a result of this investigation.

Keywords: pumping systems, total dynamic head, water pipelines, steady state analysis.

INTRODUCTION

In some mining and industrial projects, rivers are the main water sources near to the process facilities. To take advantage of this resource, the water is pumped from the river to an elevated reservoir (LOCHER et al. 2000). In some cases, industrial projects prefer to use part of the same pipe that supplies river water to the reservoirs as an outlet pipe (bi-directional pipe flow) to convey water from the reservoir to other process plant facilities under gravity flow, for economical purposes.

However, this design can lead to a more complex problem because pumping systems have different Total Dynamic Head (TDH) depending on the water level in the reservoir(s). The water level fluctuations in this specific reservoir can be 30 meters, creating a broad TDH operation range for the pumps. Or, in other cases, the difference of elevation between the river and reservoir can exceed 600 meters with high flow rates (~ 4 000 m³/h), which requires the use of more than one pump station in series, adding additional operational complexities.

These kinds of problems, in general, are not considered in the early stages of engineering since they are operational issues and, at the preliminary phases, it's believed that when fewer elements are considered in the initial design, the possibility of reducing investment costs increase. However, a simple redesign may prevent future difficulties in pump systems for these cases.

This study analysed an actual design, which consists of a pumping system to transport water from a river to a 4.2 million m³ reservoir and a 0.91-m (36-inch) diameter branch pipe to convey water to a base metal process plant. The pumping system must be capable of transporting water from the river to the reservoir and, at the same time, supplying water to the process plant. The system considers three pumping stations in series with a maximum flow rate of 4,200 m³/h. A single 0.91-m pipe connects each pump station. Each pump station operates with four pumps in parallel and considers the use of a water tank. A schematic of the water supply system is presented in Figure 1.

METHODOLOGY

To analyse the system previously described, the energy balance and continuity equations applied to fluids were used. These equations are represented as follows [Eqs. (1) and (2)] (MUNSON et al, 2002),

$$z_1 + \frac{P_1}{\gamma} + \frac{V_1^2}{2g} + TDH = z_2 + \frac{P_2}{\gamma} + \frac{V_2^2}{2g} + \Lambda_{1-2} \tag{1}$$

$$\Lambda_{1-2} = f \frac{L_{1-2}}{D} \frac{V^2}{2g}$$

<div align="right">(2)</div>
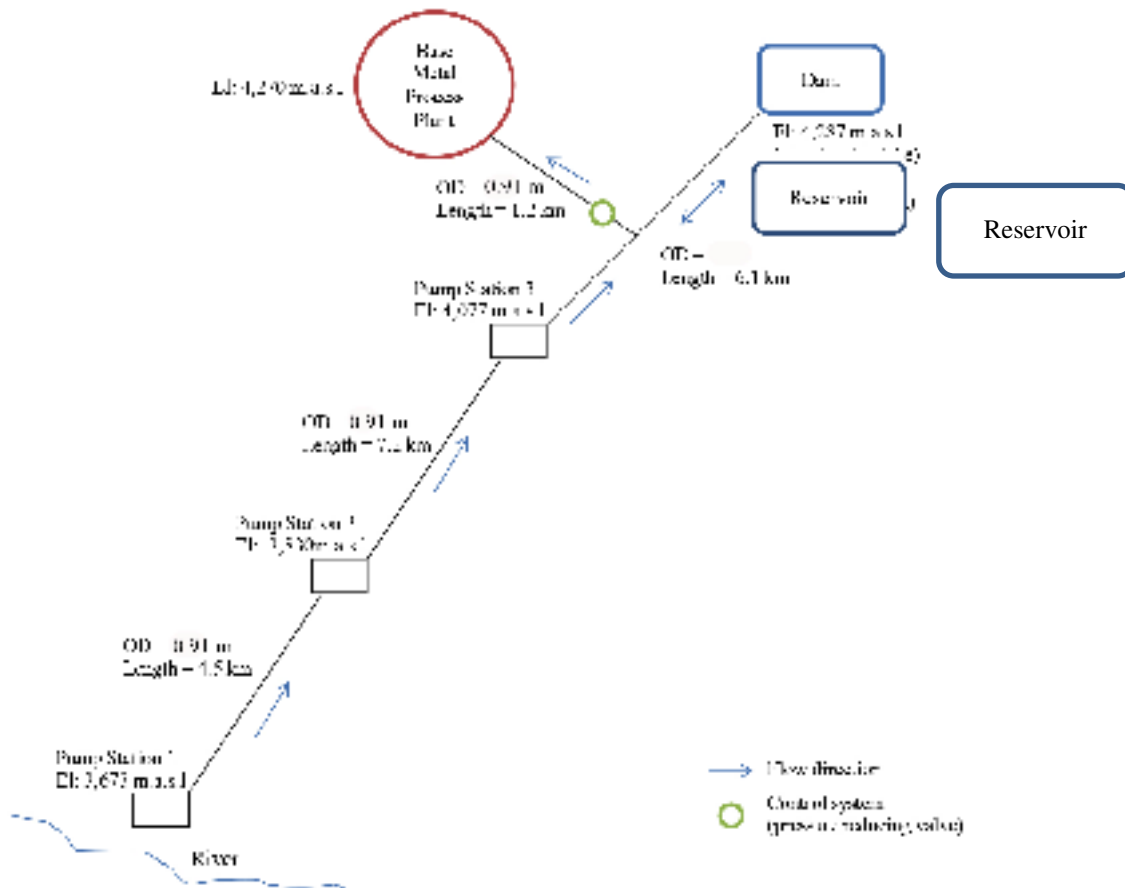
Figure 1 – Schematic representation of pumping system. All the pump stations operate with four pumps in parallel. The first pump station uses vertical pumps and the rest of the pump stations use centrifugal pumps with horizontal axis.

Eq. (1) represents the Bernoulli's equation and Eq. (2) is the Darcy-Weisbach equation for a pressurized water pipeline. In this equation, subscript 1 represent the pump station (initial point in the pipeline) and subscript 2 represent the end point at the pipeline discharge. Subscript 1–2 in Eq. 2 is used to represent the frictional head loss between points 1 and 2 of the pipeline. For a conceptual design, the minor head losses could be assumed as a percentage of the frictional losses. In this case, 5% was assumed. The continuity equation was applied for a pressurized system at the divergent point where the flow from Pumping Station N°3 must be equal to the sum of the divergent flow rates.

The friction factor of the Eq. (2) is obtained from the Colebrook-White equation [Eq. (3)] (MUNSON et al, 2002),

$$\frac{1}{\sqrt{f}} = 1.14 - 2 \cdot \log\left(\frac{k_s}{D} + \frac{9.35}{Re \cdot \sqrt{f}}\right) \tag{3}$$

where, Re represents the Reynolds number, which is computed as follows:

$$Re = \frac{V_1 \cdot D_{1-2}}{\upsilon} \tag{4}$$

By means of the pumps catalogue provided by ITT GOULDS PUMPS (2004) it was possible to obtain the pump curves necessary to convey the flow required for the TDH computed. These pump curves should be compared with Eq. (1) to obtain the operation point of the pumps with the final TDH and flow for one, two, three, and four operating pumps. The results obtained are shown in the next section.

RESULTS AND DISCUSSION

The principal results obtained from the steady-state analysis are the Hydraulic Grade Line (HGL) profiles for the main pipeline, which connect the three pump stations and the operation curve of the entire system. The pipeline HGL from Pump Station N° 3 to the Reservoir (see Figure 1), is presented in Figure 2. These data presented in Table 1 show the difference between the TDH for the full reservoir case and the empty reservoir case. Table 1 also shows the TDH for the Pumping Station N°1, N°2 and N°3.
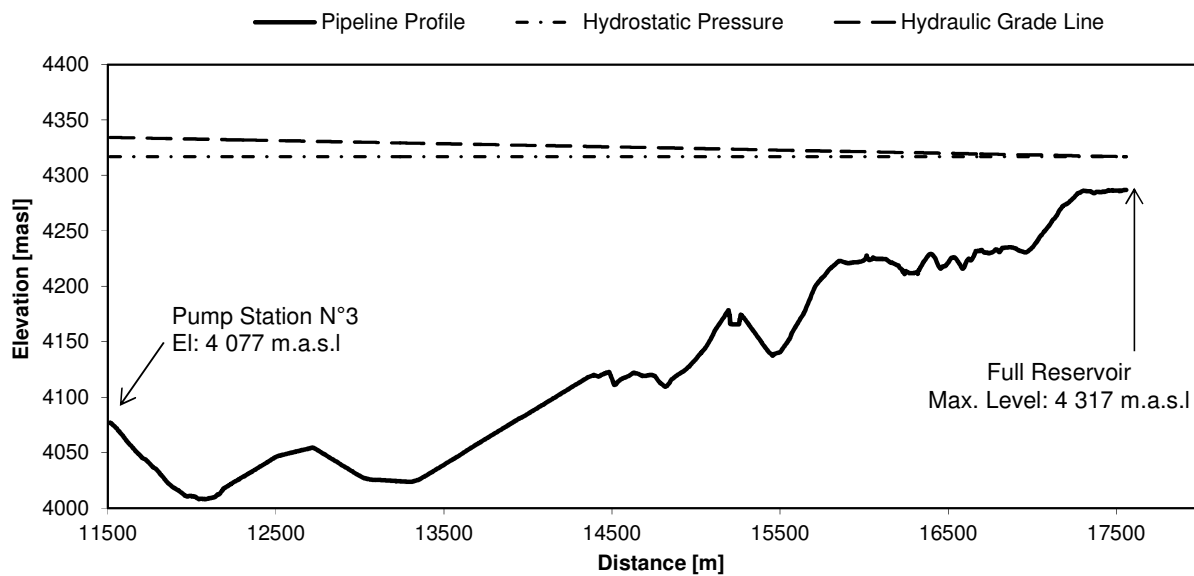
Figure 2 – Hydraulic Grade Line for water pipeline system starting at Pump Station N°3 to the Reservoir. Full-reservoir case.
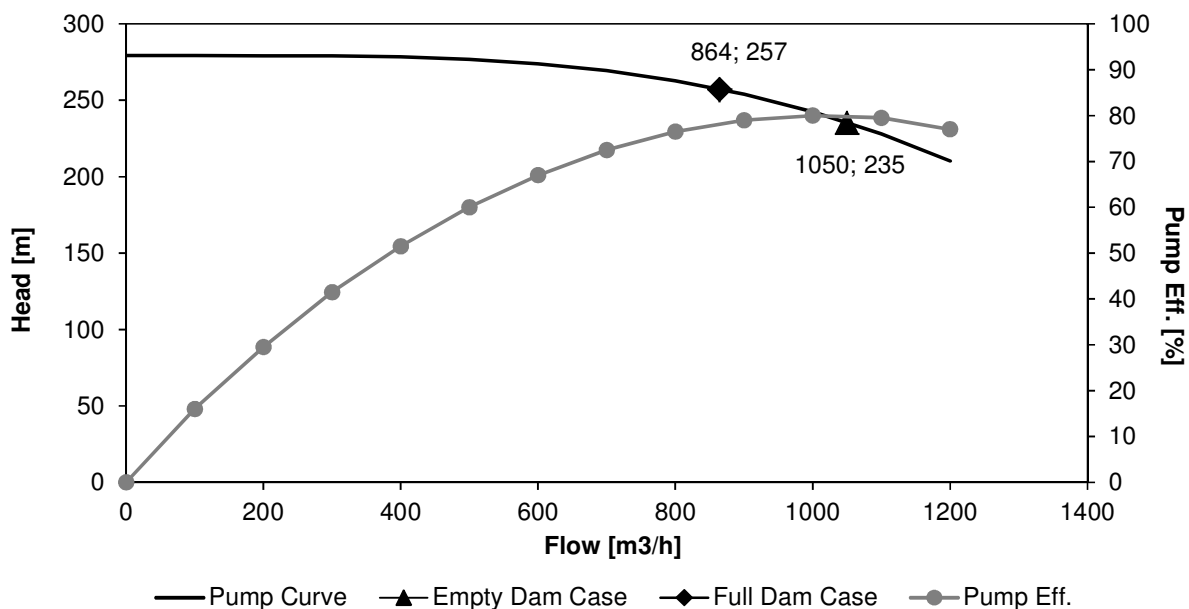
Figure 3 – Operation Points for each pump of the Pumping Station N°3.

Table 1 – Results obtained from steady-state analysis for all pump stations.

Pumping Station	N° of Pumps	Flow per pump [m³/h]	Total Flow [m³/h]	Total Dynamic Head [m]
1	1	1 239	1 239	177
	2	1 195	2 390	181
	3	1 126	3 377	187
	4	1 047	4 188	194
2	1	1618	1 618	268
	2	1444	2 889	277
	3	1239	3 716	287
	4	1051	4 203	293
3 (*)	1	1192	1 192	212
	2	1159	2 318	218
	3	1112	3 336	226
	4	1050	4 199	235
3 (**)	1	1008	1 008	241
	2	975	1 950	245
	3	926	2 778	251
	4	864	3 457	257

(*) Results obtained for the minimum water level in the reservoir (empty reservoir case).

(**) Results obtained for the maximum water level in the reservoir (full reservoir case).

From the results shown in Table 1, a significant difference between the flow per pump for the empty reservoir case and the full reservoir case can be observed. A 185 m³/h average difference

between the two cases (which represents 21% of the per-pump discharge by each pump in the full reservoir case) shows the broad operational range required for the pumps in the third pumping station (see Figure 3). Another observation from the results obtained is the performance of the entire pumping system. In the full reservoir case, the maximum pumped flow will be 3,457 m^3/h if all pumps are working at pump station N°3. For this case, if all pumps are also working in pump stations N°1 and N°2, a non-balanced system will result and Pump Stations N°1 and N°2 will need to shut-down to avoid overflowing in the water tank at Pump Station N°3. Obviously, this will decrease the flow delivered to the processing plant installations. Besides, if the water level diminishes to lower values than Net Positive Suction Head (NPSH) required for the proper functioning of pumps (KARASSIK et al. 2008; WERTH and FRIZZELL 2009; ANSI/HI 1998) in the water tanks at Pump Stations N°1 and N°2, this will carry problems of cavitation that may damage parts of the pumps.

CONCLUSIONS AND FINAL REMARKS

In the present work a complex pumping system has been analysed with a variable reference head. This work showed some problems commonly non-visualized that could lead to operational failures if not taken into account. The non-visualized problems and some solutions for them are:

1. Different Total Dynamic Head, which leads to two different operation points on the pumps' operation curve, with a difference of 21% in the flow pumped.
2. Because of the difference between the flow pumped for the full reservoir case and empty reservoir case, it is necessary to switch-off one pump at Pump Station N°1 and Pump Station N°2. A solution may be to utilize a water level monitoring system in pump station water tanks that turn off pumps when the tank is full and to avoid problems of cavitation problems when the water level is lower than NPSH required.
3. If a non-balanced system is established, an increase of water tanks volume would be necessary to avoid exceeding the overflow level and to keep delivering water required by the base metal process plant.
4. From the above conclusion, a variable frequency driver would be necessary in order to equilibrate the flows between the three pumping stations (KARASSIK et al. 2008).

A redesign could be considered to avoid these problems. A first design recommendation would be to consider an atmospheric discharge to the reservoir from Pump Station N°3. This would avoid the dual operation point in the pump curve and the difference of 21% of pumped flow between the extreme cases analyzed. Furthermore, this would permit a better performance of the three pump stations and help to avoid a non-balanced system with additional elements, such as bigger water tanks or variable frequency drivers for the pumps. Give this redesign, a

second pipe to convey water from the reservoir to the Plant Facilities should be considered, and a hydraulic transient analysis should be carried out to design the final pipe dimensions and hydraulic transient mitigations. Finally, these solutions may increase the project investment costs, so all the alternatives should be economically analyzed.

LIST OF SYMBOLS

z_1 = geometry elevation at the upstream node pipe (m).
z_2 = geometry elevation at the downstream node pipe (m).
P_1 = pressure at the upstream node pipe (Pa).
P_2 = pressure at the downstream node pipe (Pa).
V_1 = flow velocity at the upstream node pipe (m/s).
V_2 = flow velocity at the downstream node pipe (m/s).
γ = specific gravity of the fluid (N/m3).
G = gravity acceleration (m/s2).
F = pipe friction factor (non-dimensional).
L_{1-2} = pipe length between the nodes upstream and downstream (m).
D_{1-2} = pipe diameter between the nodes upstream and downstream (m).
Λ_{1-2} = frictional energy loss (m).
k_s = pipe wall equivalent sand grain roughness (m).
$\square$ = fluid kinematic viscosity (m2/s).
TDH = total dynamic head of the pump (m).

REFERENCES

AMERICAN NATIONAL STANDARD INSTITUTE and HYDRAULIC INSTITUTE (1998) "Pump Intake Design". *ANSI/HI 9.8*, NY, USA.

ITT GOULDS PUMPS (2004) "Pump Selection System". ePrism, Release 1.39.0.0, Goulds Pumps Inc., NY, USA.

KARASSIK, I.J., MESSINA, J.P., COOPER, P., and HEALD, C.C. (2008) "Pump Handbook". *4th Edition, McGraw-Hill,* NY, USA.

LOCHER, F.A., HUNTAMER, J.B. and O'SULLIVAN, J.D. (2000) "Caution: Pressure Surges in Process Industrial Systems May be Fatal". *Proc. 8th International Conference on Pressure Surges 2000*, The Hague, Netherlands.

MUNSON, B.R., YOUNG, D.F. and OKIISHI, T.H. (2002) "Fundamentals of Fluid Mechanics". *4th Edition, John Whiley & Sons, Inc.,* NY, USA.

WERTH, D. and FRIZZELL, C. (2009) "Minimum pump submergence to prevent surface vortex

formation" *Journal of Hydr. Research*, Vol. 47, No. 1, pp. 142-144.

DEALING WITH SEDIMENT TRANSPORT OVER PARTLY NON-ERODIBLE BOTTOMS

François RULOT

Hydraulics in Environmental and Civil Engineering (HECE), University of Liège, Belgium, francois.rulot@ulg.ac.be

Benjamin DEWALS, Pierre ARCHAMBEAU, Michel PIROTTON, Sébastien ERPICUM

HECE, University of Liège, Belgium

ABSTRACT: In depth-averaged flow and morphodynamic models using a finite volume discretization based on explicit time integration, a specific difficulty can arise during a computation: the computed sediment level can become lower than the level of a non-erodible bottom. The original developments presented in this paper enable correction of the non-physical sediment levels. The method, based on iterative limitation of the outward fluxes, is perfectly mass conservative and remains computationally efficient. The resulting model has been validated with several 1D benchmarks leading to configurations with sediment transport over a non-erodible bottom. Two interesting experimental benchmarks are highlighted in this paper to show the efficiency of numerical simulations. In these benchmarks, the computation time has been verified not to increase by more than 15% when using the new method.

Keywords: non-erodible bottoms, numerical simulation, outward fluxes corrections.

INTRODUCTION

For decades, sediment transport has become a major topic of research because man-made structures (dams, weirs, channelization…) affect sediment transport continuity. Thus, sediment transport can have critical consequences for public safety, management of water resources, and sustainability of river systems. In order to deal correctly with these issues, morphological models should be able to simulate the wide range of flow features and sediment characteristics encountered in real-life applications. In this paper, we focus on one of them: modelling sediment transport and morphodynamics in domains including both erodible (alluvial) and non-erodible (non-alluvial) areas. Non-erodible bottoms refer to all areas that may not be set in motion under given hydraulic conditions (i.e. bed rocks, concrete structure, armoured layers, concrete slab...). In the present paper, an original mass-conservative iterative method, both simple and efficient, is introduced for 1D computation. This method, called the Flux Minimization Method (FMM), is inspired by the correction method for the negative water depth in flow computation (DEWALS et al. 2011). Compared to existing methods, FMM provides a good take-off between

computational time and accuracy in mass conservation (RULOT et al. 2011).

The mathematical and numerical model is first described (section 2), detailing the governing equations to which the FMM has been applied. The method is next explicitly described (section 3). In section 4, the numerical model is validated on two experimental benchmarks enabling to a better comprehension of the flow and sediment transport processes.

MATHEMATICAL AND NUMERICAL MODEL

In this section, the derivation of a 1D mathematical model for flow and morphodynamics is first explained. Then, the finite volume numerical technique applied to solve the set of governing equations is detailed.

Depth-averaged hydrodynamic and morphodynamic equations

Following an Eulerian description, depth-averaged 1D equations for flow and bed-load transport can be written in the following vector form:

$$\frac{\partial \mathbf{s}}{\partial t} + \frac{\partial \mathbf{f}_a}{\partial x} = \mathbf{r} \tag{1}$$

with:

$$\mathbf{s} = \begin{bmatrix} h & h\bar{u} & (1-p)z_b \end{bmatrix}^T \tag{2}$$

$$\mathbf{f}_a = \begin{bmatrix} h\bar{u} & h\bar{u}^2 + \dfrac{gh^2}{2} & q_{bx} \end{bmatrix}^T \tag{3}$$

$$\mathbf{r} = \begin{bmatrix} 0 & -g\,h\left(\dfrac{\partial z_b}{\partial x} + J\,\Delta\Sigma\right) & 0 \end{bmatrix}^T \tag{4}$$

Over bars denote depth-averaged quantities. t = time; u = velocity component along the flow direction x; h = water depth; p = sediment porosity; z_b = bed level; g = gravity acceleration; q_{bx} = bed-load unit discharges along x; J = the friction slope and:

$$\Delta\Sigma = \sqrt{1 + \left(\dfrac{\partial z_b}{\partial x}\right)^2} \tag{5}$$

Space and time discretization

The computation domain is discretized by means of a Cartesian grid, having thus the benefits of regular grids in terms of order of accuracy, computation time, and memory requirement.

The space discretization of the divergence form of Eqs. (1)–(4) is performed by means of a finite

volume scheme. Advective fluxes are computed by a Flux Vector Splitting (FVS) method (ERPICUM et al. 2010, DEWALS et al. 2008), which can be formally expressed as follows:

$$\mathbf{f}_a^+ = \begin{bmatrix} h\bar{u} & h\bar{u}^2 & q_{bx} \end{bmatrix}^T \; ; \mathbf{f}_a^- = \begin{bmatrix} 0 & \dfrac{gh^2}{2} & 0 \end{bmatrix}^T \tag{6}$$

where the exponents + and – refer to, respectively, an upstream and a downstream evaluation of the corresponding terms on the finite volume edges. The time integration is performed here by means of a Runge-Kutta algorithm. For stability reasons, the time step is constrained by the Courant–Friedrichs–Levy (CFL) condition.

ORIGINAL METHOD TO HANDLE NON-ERODIBLE BOTTOMS

Exner equation [3rd component in Eq.(1)] provides the evolution of the sediment level as a function of bed-load fluxes, evaluated by means of a transport capacity formula. However, when solving conventionally the Exner equation in the presence of a partly non-erodible bed with explicit time integration, it may happen that the computed values of the bed elevation are found to be below the top of the non-erodible layer. Therefore, additional constraints must be prescribed on the sediment fluxes; to verify everywhere $z_b > z_b^F$ where z_b and z_b^F are the actual and non-erodible bed levels, respectively, while ensuring mass conservation.

Our original approach consists of an iterative procedure in which corrections affect only the cells in which the computed sediment level is below the rigid bottom. To ensure correct mass conservation in the resolution of Exner equation, a three-step procedure was used at each time step:

1. Exner Equation is evaluated (step 1 in Fig. 1).
2. The algorithm checks, among all cells, those in which the current sediment level, as obtained in step 1, is below the fixed bottom level. In those cells, the outflow discharge q_{bi}^{out*} is reduced (step 2 in Fig. 1; dashed arrow) such that the computed bed level becomes strictly equal to the rigid bottom level ($q_{bi}^{out} = q_{bi}^{out*}\alpha$). Regarding Fig. 1, step 1, the parameter α affecting the outward sediment flux in cell I is given by the following formula:

$$\alpha = \frac{\Delta x \left(1 - p\right)\left(z_{bI}^0 - z_{bI}^F\right)}{\Delta t \, q_{bi+1}} + \frac{q_{bi}}{q_{bi+1}} \tag{7}$$

where Δx is the space step and Δt the time step. "*I*" refers to the index of the cell, while

"*i*" refers to the index of the edges.

3. Since these flux corrections may in turn induce other non-physical configuration in neighboring cells, steps 1 and 2 are repeated iteratively. This leads eventually to a configuration in which the levels are all in their physical range, as shown in the final step in Fig. 1. Details on this method are available (RULOT et al. 2011).
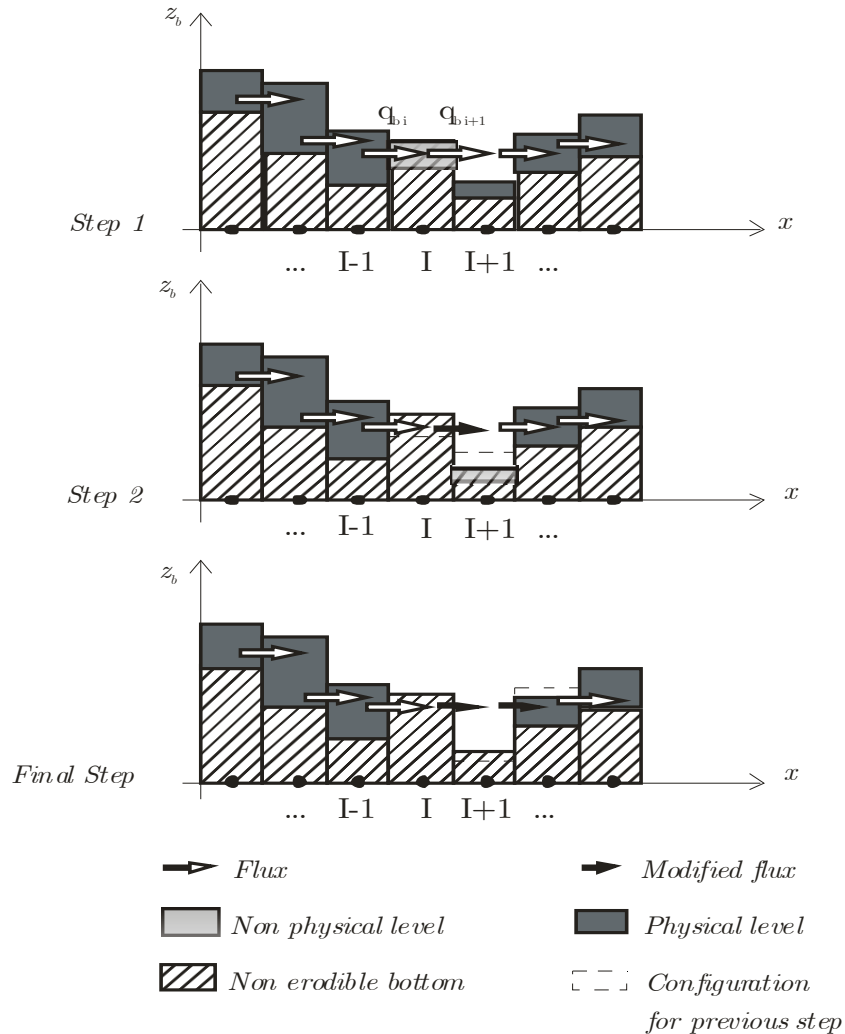
Figure 1 – Three steps procedure

VALIDATION

The cross section-averaged flow model combined with the algorithms of sediment flux correction have been verified and evaluated using several benchmarks leading to configurations with sediment transport over non-erodible bottoms. Comparison with two one-dimensional benchmarks is discussed below: first, the migration of trenches passing over a fixed bump, and then the evolution of the transport of a heap of sediments under simple flow conditions.

Evolution of a trench over a fixed bump

Description

This benchmark considers the evolution of a trench passing over a non-erodible bump (STRUIKSMA 1999). Two experiments were carried out. The length of the straight channel was 11.5 m and its width was 0.2 m. The discharge was 9.2 l/s and the water depth was 0.106 m. A bump was located in the middle of the domain, while an approximately 0.05-m-deep and 2-m-long trench was excavated in the alluvial bed upstream. The grain diameter was equal to 0.45 mm. STRUIKSMA (1999) assumed that the bed-load transport capacity formula is a power function of the water velocity: $q_{bx} = m\,u^5$ where $m = 3.6\cdot10^{-4}$ s^4/m^3 (test n°1) and $m = 4.0\cdot10^{-4}$ s^4/m^3 (test n°2) is a calibration parameter. The upstream sediment transport, including pores, is $q_{b,upstream}$=4.0 l/h (test n°1) and $q_{b,upstream}$=4.4 l/h (test n°2). The bottom Chézy friction coefficient $C_f = 31.8$ m$^{1/2}$/s was used to compute the friction slope. Numerically, the cell size is 0.1 m.

Results

Comparisons between numerical and experimental results are shown in Fig. 2. For both test cases, experimental data are scattered but the overall agreement with numerical predictions is found satisfactory. Looking deeper into the details (Fig. 2), computations over predict erosion depth downstream of the non-erodible bump for both tests. This may result from the simplified transport capacity formula used, accounting neither for an explicit threshold for transport inception nor for gravity-induced sediment transport. Vertical accelerations might also play a part in this region. Results of test n°1 and test n°2 also reveal that the computed sediment level on the bump is under predicted. The deeper sediment layer found experimentally may result from the medium-sized gravels used to build the bump (non-erodible under considered hydraulic conditions) leading to a higher bed roughness, which is not accounted for in the numerical model. The volume conservation error was, for both tests, lower than 10^{-10} m³, which is negligible. CPU time is at most 14% greater using FMM.
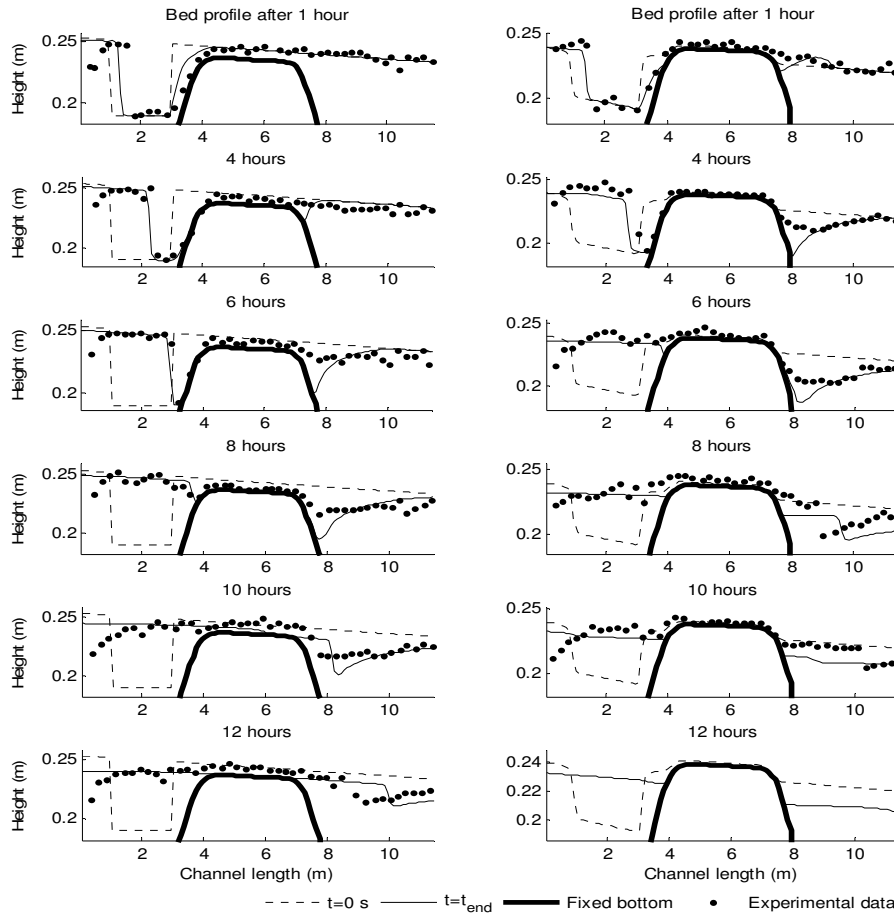
Figure 2 – Time evolution of the longitudinal bed profiles (Test n°1, left and test n°2, right)

Evolution of a heap of sediments

Description

The experimental study discussed in this section was carried out at the engineering hydraulics laboratory of the University of Liège using a rectangular horizontal channel 5.91 m long, 0.75 m high, and 0.15 m wide (CORNIL MOLINO 2011). Two reservoirs were located at the beginning and at the end of the channel to dissipate the energy, avoid boundary effects in the flow and collect sediments downstream. The sediments were plastic particles with a mean diameter of $d_{50} = 2.8$ mm and a density of 1045 kg/m³. The porosity between sediment was calculated to be 0.34. The Strickler friction coefficient (K) was calculated to (JAEGER 1956):

$$K = \frac{21}{d_{90}^{1/6}} = \frac{21}{0.0034^{1/6}} \simeq 54 \ m^{1/3}.s^{-1} \tag{8}$$

The diameter, d_i, accounts for the particle size, of which i % is smaller.

The sensitivity of two parameters was tested: the discharge varying between 5.85 and 7.85 l/s and the weight of sediment heap varying between 1 and 5 kg. The free surface level was set to 0.238 m. The discharge, Q_{eq}-, was equal to 1.8 l/s at time t = 0 second and increased linearly during 60 seconds to reach a constant value of Q_{eq}. A 4-cm cell size was used. The Meyer-Peter Müller bed-load transport formula, in which the dimensionless critical shear stress for inception of motion is $\tau_{cr}* = 0.03$, was solved. A Manning-Strickler formula was used to evaluate the friction slope. The main difference with the previous benchmark is that all parameters are physically-based or empirical.

Results

Comparisons between numerical and experimental results are shown in Fig. 3. Point 'A' is the beginning of the upstream slope of the dune, point 'B' is the end of the downstream slope of the dune, and the highest point of the dune is named the crest. The agreement between experimental data and numerical predictions was found satisfactory. The overall shape of the sediment heap is well reproduced. However, for the upstream face, the observed slope was milder and smoother than the numerical one. This observation is probably due to the vertical component of the velocity [15 % of the horizontal one (CORNIL MOLINO 2011)], which is not reproduced in the numerical model. For the downstream face, the slope was shaped by the gravity induced sediment motion rather than the flow induced sediment motion. Indeed, downstream of the dune crest, there is a recirculation zone leading to negative velocity along x direction. This was computed by activating only gravity induced sediment motion downstream of the sediment heap. The sensitivity tests show that the velocity of the sediment heap is directly linked to the water discharge. The sediment crest height is directly linked to the initial sediment heap height.
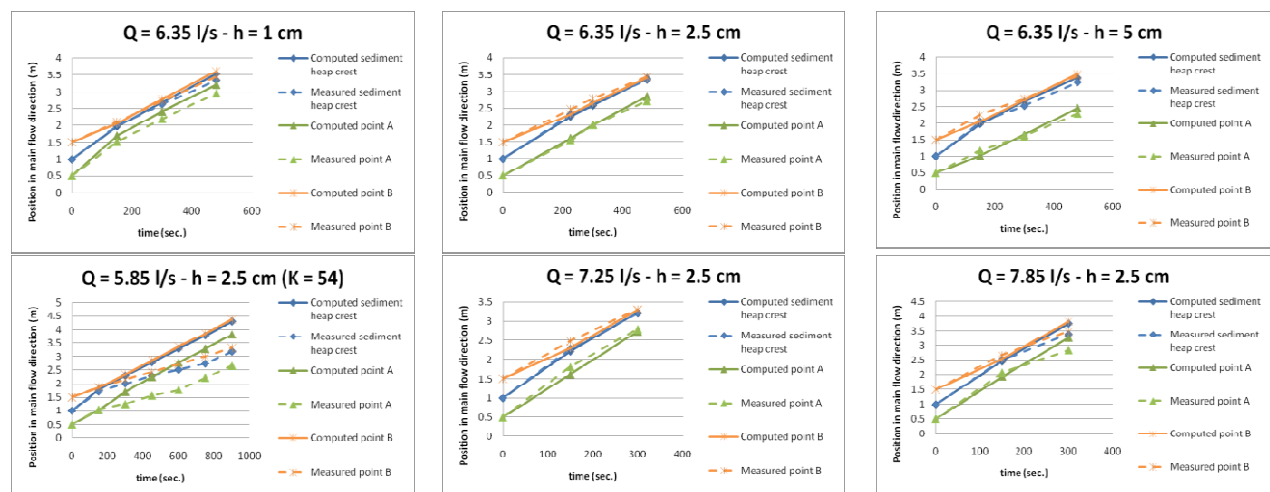
Figure 3 – Time evolution of the location of three points (A, B, crest)

Using the FMM, the sediment volume is conserved at the floating-point accuracy, while there is more than 184% error between initial and final volume when correcting the non-physical levels by simply putting it back at the non-erodible level. CPU time is 8% greater when using FMM.

CONCLUSIONS

Relying on a validated 1D numerical model to describe the flow and bed-load transport, an original algorithm has been developed in order to handle sediment transport on partly non-erodible bottoms. The method consists of limiting the outward fluxes in order to ensure that the sediment level remains higher than the non-erodible level on each cell of the domain. It has proved its efficiency in terms of computational time, as well as for respecting a non-erodible bottom constraint, while enabling verification of the sediment mass conservation close to the floating-point accuracy. Two benchmarks presented in this paper highlight the good agreement between numerical solutions and experimental observations. In addition, the increase in computational time is very limited for each benchmark. In the worst case, the computation time has been verified not to increase by more than 15% compared to the same simulation without a non-erodible bottom.

For further research, an interesting topic will be the corrections of computed sediment concentrations in suspended sediment transport in which the concentration of sediment in water must remain between zero and one.

REFERENCES

CORNIL MOLINO, A. (2011), "Gestion des sédiments : opérations de chasses en géométrie idéalisée", Master Thesis, University of Liège, June 2011, 109 pages.

DEWALS, B., RULOT, F., ERPICUM, S., ARCHAMBEAU, P. and PIROTTON, M. (2011). "Advanced topics in sediment transport modelling: non-alluvial beds and hyperconcentrated flows", INTECH, 30 pages.

DEWALS, B. J., KANTOUSH, S. A., ERPICUM, S., PIROTTON, M. and SCHLEISS, A. J. (2008). "Experimental and numerical analysis of flow instabilities in rectangular shallow basins", Environmental Fluid Mechanics, Vol. 8, No. 1, pp 31-54.

ERPICUM, S., DEWALS, B. J., ARCHAMBEAU, P. and PIROTTON, M. (2010). "Dam-break flow computation based on an efficient flux-vector splitting", Journal of Computational and Applied Mathematics, Vol. 234, No. 7, pp 2143-2151.

JAEGER, C. (1956). "Engineering fluid mechanics", Blackie, 548 pages.

RULOT, F., DEWALS, B. J., ERPICUM, S., ARCHAMBEAU, P. and PIROTTON, M. (2011).

"Modelling sediment transport over partially non erodible bottoms", International Journal for Numerical Methods in Fluids, Published Online: 10.1002/fld.2684.

STRUIKSMA, N. (1999). "Mathematical modelling of bedload transport over non-erodible layers", Proc. IAHR Symposium on River, Coastal and Estuarine Morphodynamics, Genova, Italy, pp 6-10.

MEAN VELOCITY EFFECT IN BIO-FOULED PIPES

Maria Ximena TRUJILLO

Department of Civil and Environmental Engineering, Universidad de los Andes, Colombia,

mx.trujillo92@uniandes.edu.co

Juan SALDARRIAGA

Department of Civil and Environmental Engineering, Universidad de los Andes, Colombia,

jsaldarr@uniandes.edu.co

ABSTRACT: The hydraulic resistance of pipes with biofilm surface coatings can be difficult to predict based on smooth-wall pipe theory. The impacts of biofilm growth in distribution networks and the influence of mean velocity in their development were studied in a recirculation model system at the Hydraulic Laboratory of Universidad de los Andes, using as nutrient a grass specie called "*kikuyu*" (s.p. *Pennicetum clandestine*), which is common in raw water sources of Bogotá, Colombia. Water flowed constantly through the system during 150 days, and biofilm measurements were taken from monitors installed on the pipe's wall. Bio-fouling was observed for various mean velocity flow conditions, although significant differences were observed in biofilms characteristics: thickness and bacterium community. The most important finding was that the friction factor of bio-fouled pipes was incongruent with Moody´s Diagram.

Keywords: pipes, biofilms, Moody Diagram, potable water.

INTRODUCTION

Biofilms are composed of bacteria held in a polymeric matrix. When they are formed on the surface of conduits, frictional flow resistance increases, resulting in major energy losses and reduction of pipeline capacity (PICOLOGLOU et al. 1980), (LAMBERT et al. 2009). Bio-fouling also represents a risk to public health, enhancing the formation of potential pathogens inside distribution networks (KNOBELSODORF et al. 1997).

The objective of the current study was to evaluate the influence of mean velocity flow in biofilms growth. Biofilms have been researched at the Universidad de los Andes since 2009 as a result of several biofilm detachment events reported by the local water distribution network operator: *Empresa de Acueducto y Alcantarillado de Bogotá*. A prototype was designed to determine the pipe material's influence over bio-fouling with different carbon sources such as *jaggery* and grass *kikuyu* (s.p. *Pennicetum clandestine)*. The main result of that research showed that distribution networks were vulnerable to biofilm presence and it was impossible to prevent

them (CIACUA 2009). Additionally, it was found that biofilms can lead to chlorine demand, coliform growth, pipe corrosion, and water taste and odor problems (HALLAM et al. 2001).

In 2011, the previous experimental setup was redesigned to evaluate the impact of mean velocity flow. LEHTOLA et al. (2006) experimentally determined that velocity affects the mass transfer of nutrients from fluid to biofilm and the friction factor of bio-fouled pipes. The empirical approach for the current study consisted of growing biofilms at three different velocities: 1.0 m/s, 1.5 m/s, and 3.0 m/s while conditions like nutrients, chloride, water temperature and sunlight remain constant. The potential outcome of this research will be an expression to estimate the friction factor of bio-fouled pipes, where the influence in different hydraulic conditions will be quantified.

METHODOLOGY

The constructed recirculation system is displayed in Figure 1, where three PVC pipes of the same diameter (108 mm) and lengths (7.470 m) were connected to a supply tank and inlet tank. Head losses were measured using a set of piezometers hoses installed in each pipe 2.765 m apart. Moreover, two glass pipes where connected in parallel to the two PVC pipes, which permitted us to see biofilm growth; however, this qualitative approach did not give reliable results.
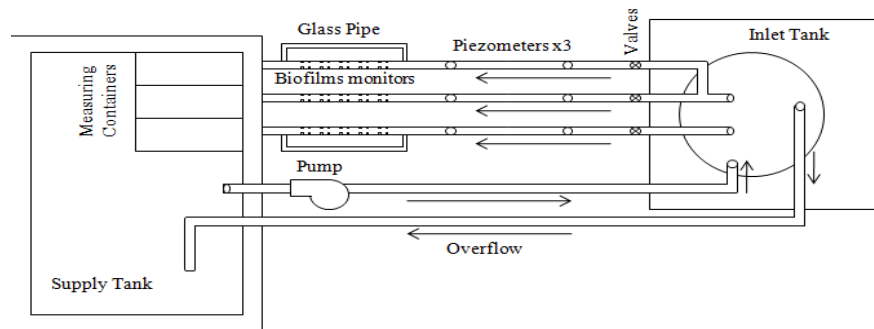
Figure 1 – Experimental diagram

In order to achieve the objective, two procedures were followed. One of the procedures was used to estimate biofilms thickness, and another procedure was utilized to determine friction factor in bio-fouled pipes. Biofilms thickness (E_{prom}) estimation required turning off the pump and measuring the water temperature. Biofilm monitors installed on the pipe's wall were removed and weighed. The mass data was compared with the initial weights (see Figure 2), and the difference was attributed to bio-mass.
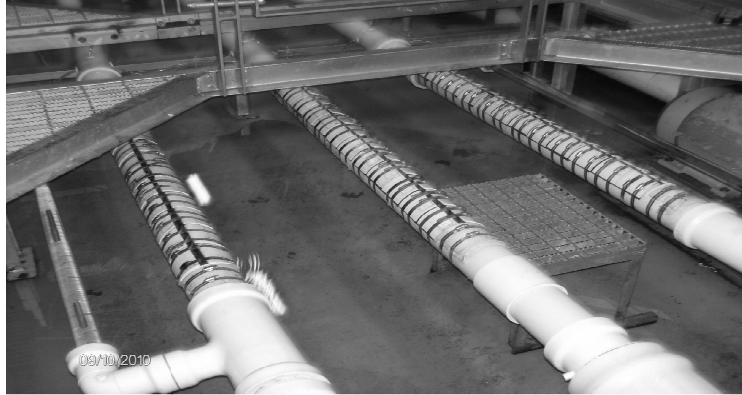
Figure 2 – Picture of biofilms monitors

Determining friction factor in bio-fouled pipes required recording the volumetric flow rates and head loss of each pipe. Two valves out of the three were closed, and the remaining valve was manipulated in order to observe head loss variation. Once data were collected, the valve was closed and another valve was opened so necessary measurements could be taken. The procedure was repeated until data for the three pipes were gathered. When finished, valves were opened, allowing flow in each pipe to be equivalent to the established mean velocity. Measurements were used to calculate friction factor using Darcy-Weisbach's Equation [Eq. (1)].

$$f = h_f \frac{d}{L} \frac{2g}{u^2} \qquad (1)$$

where h_f = head loss (m), f = friction factor (dimensionless), l = length of pipe (m), d = pipe diameter (m), u = mean velocity (m/s) and g = 9.81 (m/s^2). Through Colebrook-White's Equation [Eq. (2)] the estimated friction factor and Reynolds number (Re) were used to determine pipe roughness (k_s).

$$\frac{1}{\sqrt{f}} = -2 \log_{10} \left(\frac{k_s}{3.7d} + \frac{2.51}{\mathrm{Re}\sqrt{f}} \right) \qquad (2)$$

The registered head loss measurements were used to calculate the thickness of laminar viscous sub-layer (δ') using Eq. (3). Where v = cinematic viscosity (m^2/s).

$$\delta' = 11.6 \frac{v}{\sqrt{\frac{d}{4} g \frac{h_f}{L}}} \qquad (3)$$

With the equations above and frequent regular measurements, it was possible to record the friction factor, pipe roughness, and thickness of laminar viscous sub-layer throughout the growth of biofilms.

RESULTS

Frictional Resistance

Figures 3, 4, and 5 show the behavior of friction factors in bio-fouled pipes with u = 1.0 m/s, 1.5 m/s and 3.0 m/s. Lines represent the friction factors for clean pipes and data series for the bio-fouled pipe friction factors were assigned different shapes according to each recirculation day.
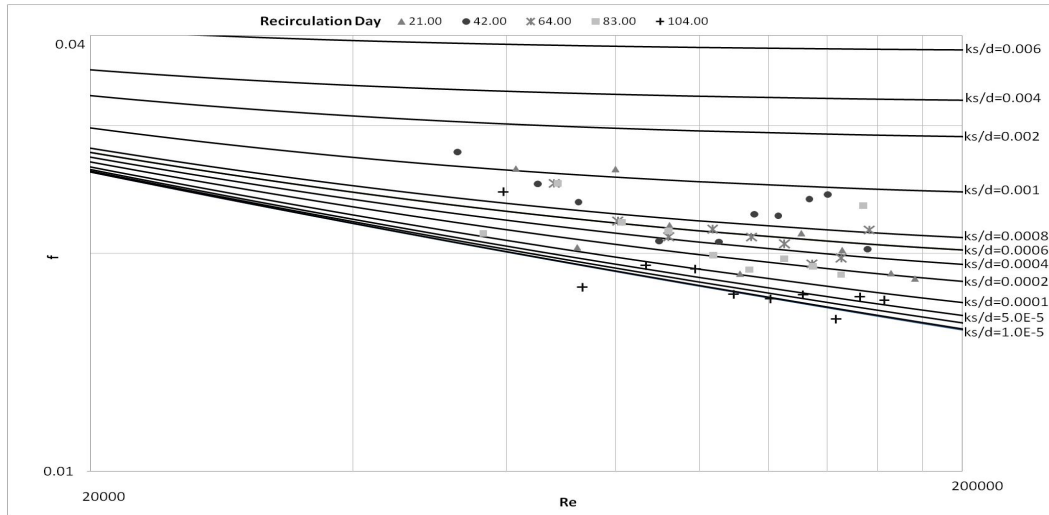
Figure 3 – Moody's Diagram for u= 1.0 m/s.
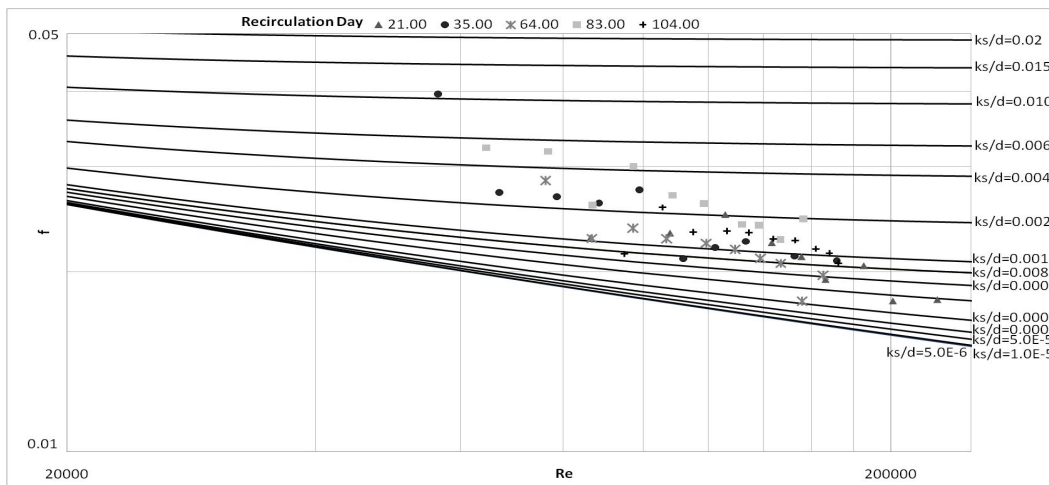
Figure 4 – Moody's Diagram for u= 1.5 m/s.
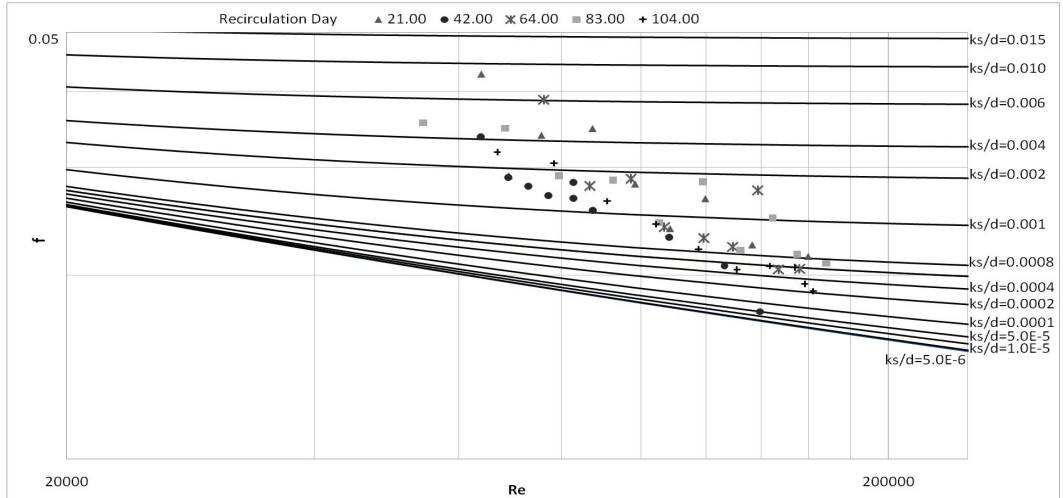
Figure 5 – Moody's Diagram for u= 3.0 m/s.

Biofilm Thickness

Figures 6, 7, and 8 show the evolution of E_{prom}, k_s, and δ' during the recirculation period for bio-fouled pipes with u = 1.0 m/s, 1.5 m/s and 3.0 m/s. These results correspond to a similar Reynolds number, equal to 10,500.
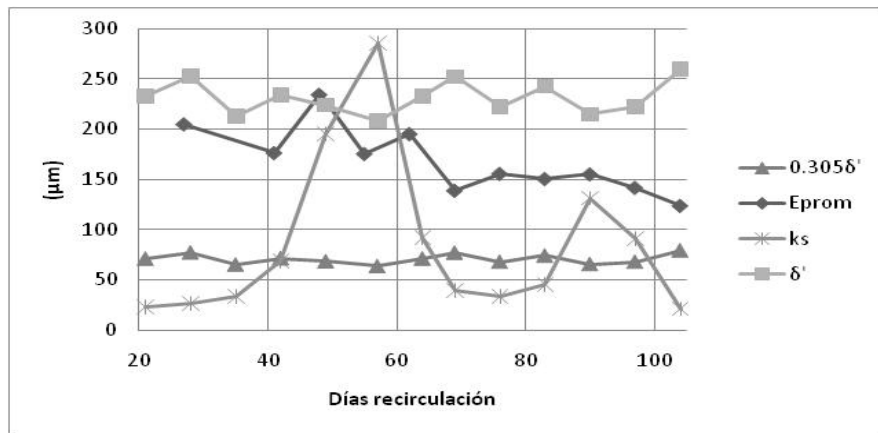
Figure 6 – Comparison between δ', E_{prom}, k_s, y 0.305 δ' for u= 1.0 m/s
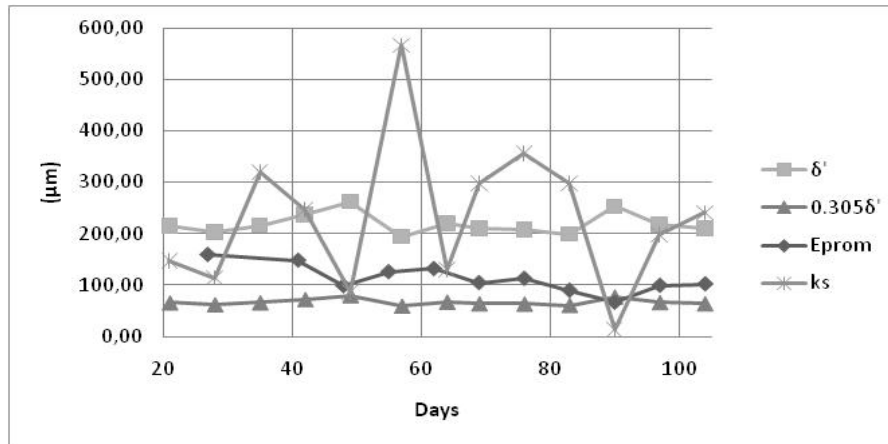
Figure 7 – Comparison between δ', E$_{prom}$, k$_s$, y 0.305 δ' for u= 1.5 m/s
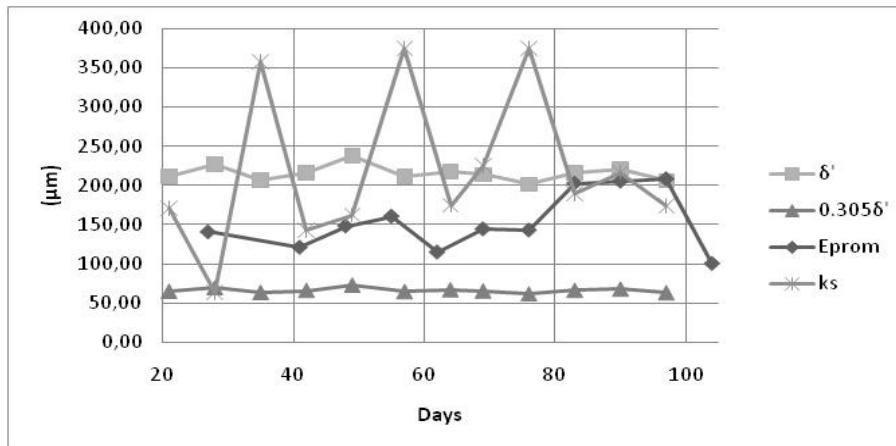
Figure 8 – Comparison between δ', E$_{prom}$, k$_s$, y 0.305 δ' for u= 3.0 m/s

Identification Tests

The 67 day recirculation process permitted us to see the growth of different bacteria species in each pipe. Test results identified *Bacillus pasteuri* in the pipe with u = 1.0 m/s, an aerobic bacteria that is common in soil and is capable of synthesizing calcite in carbon calcite. Identification test found *Staphylococcus capitis* in the pipe with u =1.5 m/s, an aerobic *coccus* that lives in human skin but has been associated with urinary and catheter infections. Research shows *Bacillus subtilis* in pipe u = 3.0 m/s, an aerobic or facultative aerobic bacteria capable of forming spores resistant to disinfectants, water temperature, and radiation.

The second test took into account samples from recirculation day 92. The bacteria community was more uniform; they were all facultative aerobic bacteria that could form spores and eventually became opportunist pathogens. Identified species were: *Bacillus circulan* and *Bacillus licheniformis*.

DISCUSSION

Frictional Resistance

Results yielded a different variation in friction factors with regards to Reynolds number compared clean pipe. In general, friction factors do not follow the Moody´s Diagram trends. A comparison of Figures 3, 4, and 5 show that friction factors in bio-fouled pipes increased with increasing flow velocity. LEHTOLA et al. (2006) also discussed the influence of mean flow velocity flow on friction factor values.

On the other hand, experimental friction factor variation is attributed to biofilms' viscous-elastic properties. This allows them to deform while absorbing or liberating energy (PICOLOGLOU 1980). For example, in Figure 3, during recirculation day 104, some friction factor values are extremely low, while other measurements of the same day are higher.

Biofilm Thickness

When observing sub-layer thickness (δ') and k_s in Figures 6, 7, and 8, it could be determined that the type of flow presented in all pipes is a smooth turbulent flow. A wide oscillation of roughness coefficient was observed in all pipes. In general, comparing roughness of bio-fouled with clean pipes shows a considerable increase of magnitude; clean PVC pipes have a k_s equivalent to 1.5 µm. The shape of k_s reaches a high peak in all pipes around day 60. This is related to available nutrients constantly supplied until that day. Afterwards, biofilms experienced a nutrient restriction period, which was reflected in a k_s decay.

Furthermore, the roughness coefficient of biofilms grown under u =3.0 m/s presented a roughness variation with peaks of similar magnitudes different to those grown under lower velocities. Figure 8 shows that k_s not only started to grow earlier in relation with Figures 6 and 7, but also it was less vulnerable to the nutrient restriction period. Previous results are in accordance to LEHTOLA et al (2001), about the relevance of mean velocity flow in mass transfer from fluid to biofilm.

CONCLUSIONS

Research into the conditions that govern biofilm growth illustrated that even though mean velocities were different, microorganism presence increased friction losses, making the friction factor incongruent with Moody's Diagram. Evidence showed that nutrient availability and velocity flow influence the friction factor of bio-fouled pipes because higher velocities imply major mass transfer of nutrients to biofilms. Also, it was observed that mean velocity flow is a dominant factor in determining roughness magnitude and shape of biofilms.

Identified species are aerobic and facultative aerobic bacteria capable of forming spores

resistant to disinfectants, water temperature and radiation, which are classified as opportunist pathogens that could affect a vulnerable population. Distribution networks are vulnerable to biofilm growth, but an optimal potable water treatment can affect biofilms development since they are sensitive to available nutrients. Traditional smooth-wall pipe friction factor theory cannot be applied to accurately predict flow resistance in bio-fouled pipes. They are limited because biofilms are dynamic living systems.

SYMBOLS

h_f = head loss (m);

f = friction factor (dimensionless);

u = mean velocity flow (m/s);

l = length of pipe (m);

d = pipe diameter (m);

Re = Reynolds Number (dimensionless);

k_s = Roughness coefficient (µm);

k_s/d = relative roughness (dimensionless);

δ' = thickness of laminar viscous sub-layer (µm);

E_{prom} = biofilm width (µm);

ν = kinematic viscosity (m2/s);

REFERENCES

CIACUA, Centro de Investigaciones en Acueducto y Alcantarillado. "Investigación sobre los factores que generan la formación, crecimiento y posterior desprendimiento de biopelículas en las redes matrices de acueducto. Fase I." Bogotá, Colombia, 2009. (In Spanish)

HALLAN, N.B., WEST, J.R., FORSTER, C.F., and SIMMS, J. (2001). "The potential for biofilm growth in water distribution systems." *Water Research,* Great Britain, Elsevier Science Ltd., Vol 35, No. 17, pp.4063-4071.

KNOBELSODORF, J., MUJERIEGO, R. (1997). "Crecimiento bacteriano en las redes de distribución de agua potable: Una revisión bibliográfica". *Ingeniería del Agua.* Barcelona : Universidad Politécnica de Cataluña, Vol. 4, 2. (In spanish)

LAMBERT, M.F, JHON EDUARDS, R.W., HOWIE, S.J., DE GILIO, B.B. and QUINN, S.P. (2009). "The impact of Biofilm Development on Pipe Roughness and Velocity Profile." *World Environmental and Water Resources Congress 2009*, ASCE, pp. 122-134.

LEHTOLA, M.J., LAXANDER, M., MIETTINEN, I.T., HIRVONEN, A., VARTIAINEN, T. and MARTIKAINEN, P.J. (2006). "The effects of changing water flow velocity on the formation of

biofilms and water quality in pilot distribution system consisting of copper or polyethylene pipes."*Water Research,* Elsevier Science Ltd. 40 (2006) pp. 2151-2160.

PICOLOGLOU, B.F., ZELVER, N. and CHARACKLIS, W.G. (1980). "Biofilm growth and hydraulic performance." *Journal of the hydraulic division*, ASCE. Vol 106, No. 5, pp. 733-746.

HEAT EXCHANGER SYSTEM PIPING DESIGN FOR
A TUBE RUPTURE EVENT

Fadi Antoine WAKIM, MSc

Hydraulics and Hydrology Engineer, Bechtel Oil, Gas and Chemicals Inc., USA,

fwakim@bechtel.com

Pinar CAKIR KAVCAR, PhD, PE

Senior Hydraulics and Hydrology Engineer, Bechtel Oil, Gas and Chemicals Inc., USA,

pkavcar@bechtel.com

Mustafa SAMAD, PhD

Senior Hydraulic and Hydrology Engineering Specialist, Bechtel Oil, Gas and Chemicals Inc.,

USA

masamad@bechtel.com

ABSTRACT: Tube-rupture events in shell and tube heat exchangers can result in significantly high surge pressures. Steady state and dynamic methods can be used to assess the impacts of these events on heat exchanger system piping networks. This paper presents the findings of a set of dynamic surge simulations on the impacts of tube-rupture events in a Propane-Feed Gas Heat Exchanger System. Once adjacent piping design is considered, the Joukowsky formulation-based method is not always appropriate to estimate tube-rupture surge impacts. Dynamic simulations need to be conducted to assess the tube-rupture impact on piping systems due to the surge wave amplification as it is transmitted and reflected in the complex pipe network. For blocked-in (no-flow) or isolated systems, properly designed relief mechanisms are required to alleviate the tube-rupture resultant pressure build-up.

Keywords: hydraulic transient, surge, tube-rupture, heat exchanger.

INTRODUCTION

It is not uncommon for the design of shell-tube type heat exchangers to involve high-pressure differentials between the shell and tube sides. Driven by sufficiently high-pressure differences, a tube-rupture event would generate fluid flow from the high-pressure side to the low-pressure side, significantly increasing the pressure sometimes beyond its design pressure. The pressure pulse generated by the tube-rupture will then propagate to the system at wave speeds close to sonic speed. Depending on the system configuration, transmitted and reflected surge pressures could be considerably higher than the initial rupture pressure pulse.

Design considerations vary with the location and proximity of the pressure relieving system. If the relief device is located on the heat-exchanger shell, assuming an instantaneous response, the pressure pulse is not likely to propagate to adjacent piping. If the relieving system is located some distance away from the heat exchanger shell, the pressure pulse travels into the piping network and exposes different equipment and piping to high surge pressures.

A common method used to estimate surge pressures due to a tube-rupture event is based on the Joukowsky equation [Eq. (1)] (WYLIE & STREETER 1993)

$$\Delta H = \frac{a}{g} \Delta V \qquad (1)$$

where ΔH is the change in head in [m], $\square$ is the pressure wave speed in [m/s], ΔV is the change in velocity in the low pressure fluid due to the high-pressure fluid discharge in [m/s], and g is the gravitational acceleration in [m/s^2]. The initial pressure pulse of the tube-rupture is determined by solving the Joukowsky equation and determining the mass flow rate of the incoming high-pressure fluid taking into account the changes in its properties due to interaction with low-pressure fluid.

Eq. (1), also known as the basic water hammer equation, holds in the absence of pressure wave reflections. This key concept makes the use of this equation alone inappropriate for the design of heat exchanger piping systems where surge waves can magnify as they propagate. This is particularly applicable for piping networks involving piping dead ends, reducers, enlargers, and throttled valves. WYLIE & STREETER (1993) note that pressure waves double at piping dead ends due to reflections (WYLIE & STREETER 1993). PARMAKIAN (1963) provides a simplistic approach for estimating reflection and transmission coefficients at junctions in piping systems indicating that the pressure wave can be magnified as it propagates due to pipe cross-sectional flow area changes (PARMAKIAN 1963). The coefficients of transmission and reflection of a surge wave are a function of the ratios of pipe cross-sectional areas to wave speeds at the junction. A reducer would amplify the surge wave upstream, while an enlarger would dampen it. While this approach gives some guidance on the magnitude of pressure waves in the system, it would not address the complexity of the hydraulic response of the system in the event of a tube-rupture.

Recent changes in codes and standards provide limited guidance on how to address pipe network designs for tube-rupture events. The American Petroleum Institute (API) Standard 521 (2007) recommends that dynamic simulations be performed to analyze tube-rupture events when the pressure differential in the heat exchanger is in excess of 70 barg (API 2007).

A one-dimensional liquid-phase model was established to conduct a hydraulic transient analysis to assess the hydraulic response of a piping network to a tube-rupture event in its shell-tube type Propane-Feed Gas heat exchanger where the pressure differential exceeded 70 barg.

Simulation results were used to evaluate the need for surge mitigation. The findings of the analysis were used to provide guidance for designers on tube-rupture mitigation measures.

PROPANE-FEED GAS SYSTEM AND MODEL DESCRIPTIONS

System Description

The heat exchanger in which the tube-rupture was postulated to occur is one of two identical heat exchangers located downstream of a propane source vessel (Figure 1). Liquid flowing out of these heat exchangers is routed to downstream kettle-type heat exchangers and other equipment. Propane discharges into these components via letdown valves. Pipe branches with closed valves create dead ends to the system. Fast closure valves located on both sides of the heat exchangers create isolation points. Two small pressure relief valves are located near the outlets of the heat exchangers for fire protection purposes.
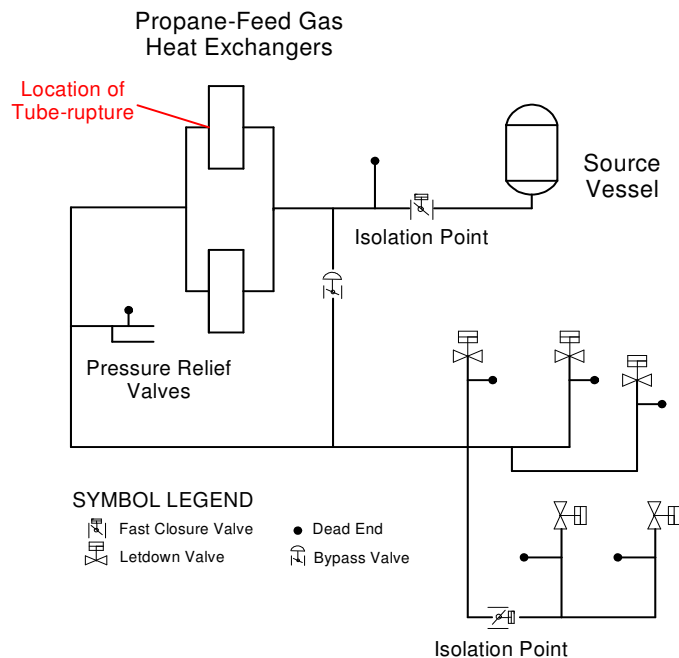
Figure 1 – System Schematic Drawing

Tube-side feed gas is heated by shell-side propane as it goes through the heat exchanger under consideration. The tube-side maximum operating pressure is approximately seven times that of the shell-side. Calculated liquid propane wave speeds for this system vary between 590 m/s and 630 m/s with pipe size and liquid temperature changes.

Methodology and Model Description

An in-house hydraulic transient simulator was used to conduct the analysis. Like many other software of its kind, this simulator is based on the method of characteristics that is used to solve hydraulic surge propagation in piping networks. The model extent was determined based on known boundary conditions. Two operational configurations were considered for the purposes of the analysis: (1) normal operating conditions at design volumetric flow rate and normal system operating pressure, and (2) isolated system conditions with no flow in the lines and where the pair of heat exchangers is completely isolated. Under normal operating conditions, the liquid level in the upstream vessel is maintained at normal level. Propane flow into the downstream kettle-type heat exchangers flashes through the letdown valves. This creates a pressure break in the continuity of the liquid flow stream. The downstream boundaries of the transient model were therefore established at these valves as discharging flows at the elevation of the flashed liquid vapor pressure. Under isolated system conditions, letdown valves and fast closure valves downstream and upstream of the Propane-Feed Gas heat exchangers are closed.

The heat exchanger was modeled using an equivalent pipe diameter preserving the hydraulic properties through the heat exchanger such as pressure drop and the representative design flow velocity. The length of the equivalent pipe corresponds to the total baffled flow path length in the heat exchanger. Pressure relief valves were modeled allowing free discharge. Their operation was considered to follow a pressure-liquid flow relationship derived from the valve characteristics and flow capacities using the orifice discharge relation.

Tube-rupture Description and Modeling

In shell-tube heat exchangers, bundled tubes are welded to the backside of the tube sheet. The rupture is described in API Standard 521 (2007) as a sharp break in one tube at the tube sheet. As the tube breaks, the low pressure side is exposed to high pressures from the tube stub remaining in the tube-sheet and the longer end of the broken tube. Sonic flow conditions develop as the high-pressure fluid flows from both ends of the broken tube into the low-pressure side. The development of the initial pressure pulse is best described by solving Joukowsky's equation (1) and determining the mass flow rate of the high-pressure fluid.

Reported tube-rupture time frames in the literature are in the order of milliseconds. SIMPSON (1971) notes that a theoretical tube-rupture time of 0.6 milliseconds provides an excellent fit to his mathematical model results on rupturing mechanisms. Developments of peak pressures within milliseconds are reported in Institute of Petroleum Guidelines (IP 2000).

The tube-rupture was postulated to occur at the heat exchanger outlet for modeling purposes since it is very close to the tube sheet in the internal arrangement of the heat exchanger under consideration. The rupture was modeled by linearly increasing the pressure outside of an orifice

type air inlet valve, used as an internal boundary condition, with a fixed coefficient of discharge of 0.7 over 1 millisecond. The cross-sectional area of the air inlet valve was considered twice the broken tube area to account for discharge from both ends. The coefficient of discharge of 0.7 was used with the assumption that both halves of the break behave as square edged orifices. A linear variation of the coefficient of discharge over the rupture time frame is a better representation of the physical phenomena itself. Upon careful consideration, test results for both approaches were insignificantly different.

SIMULATION RESULTS

<u>System Response during Normal Operation</u>
A pressure time-history at the location of the tube-rupture is shown in Figure. 2 for a tube-rupture event at the Feed Gas design pressure. Due to the proprietary nature of some of the information, all reported design pressures and resultant surge pressures are relative to the liquid-side system operating pressure at the source vessel. For a tube-rupture at 0.002 seconds, the initial pressure pulse simulated was found to equal 3.4 barg as shown in Figure 2 at 0.003 seconds. This value is close to the estimate from the Joukowsky based approach. The variation of the pressure surge between 0.003 seconds and 0.06 seconds is due to reflected waves from adjacent piping as they come back to the heat exchanger. The unobstructed ends of the system under normal operating conditions provide sufficient relief to alleviate the tube-rupture pressure build-up as shown in Figure 2 with the decreasing pressures after 0.2 seconds.

The overall system response to the tube-rupture event under normal operating conditions indicated that the initial pressure pulse significantly amplified as it was reflected and transmitted in the pipe network (Figure 3). Maximum pressure envelopes are plotted versus cumulative pipe length starting from the source vessel.
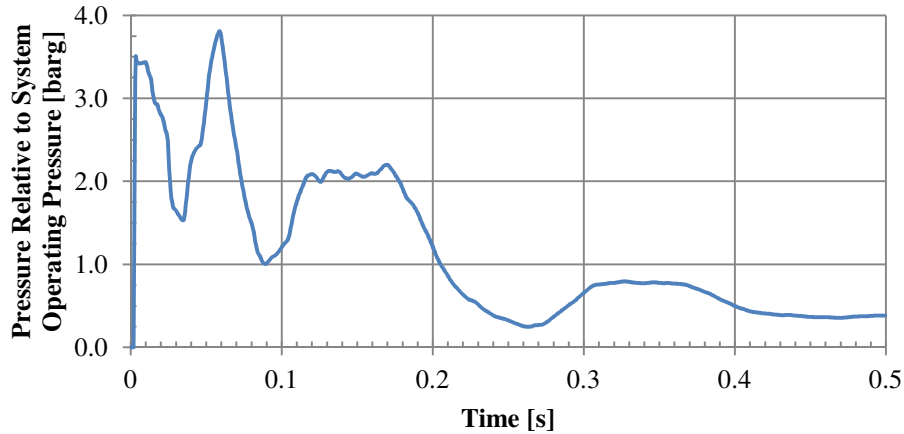
Figure 2 – Tube-rupture Pressure Time-history
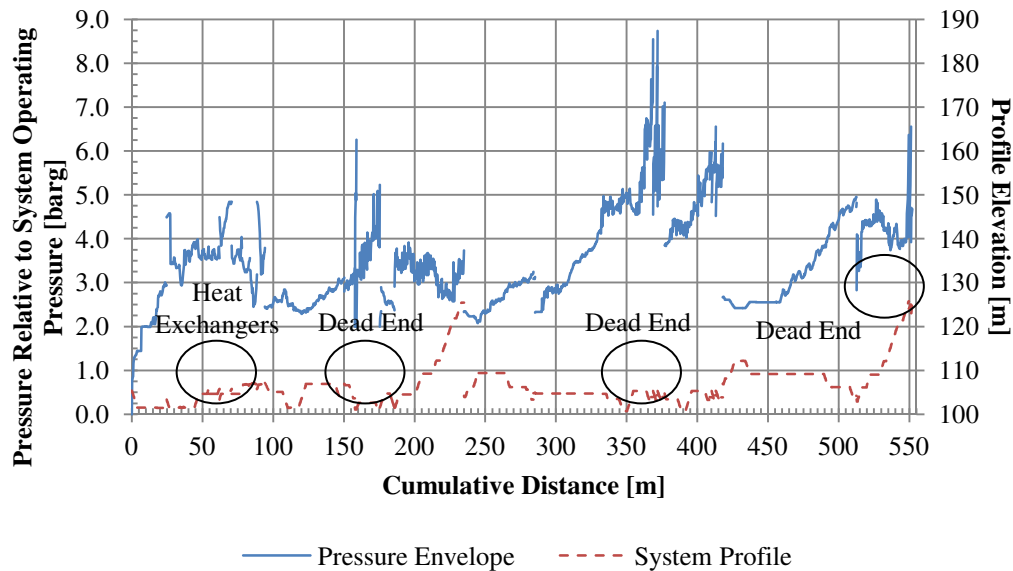
Figure 3 – Normal Operating Conditions Maximum Pressure-Envelope

Simulated pressures were significantly higher than the initial pressure pulse of 3.4 barg. As the surge wave travelled away from the heat exchanger, it was transmitted through several junctions, where it was dampened, and reflected at several dead ends, where it doubled. The maximum surge pressures imposed on the system exceeded by more than two and a half times the initial Joukowsky estimate (Figure 2). The above results highlight the transformation and amplification of the initial tube-rupture pressure pulse as it propagates in the piping network as a result of the superimposition of reflected and transmitted waves.

Isolated System Response

Under isolated system conditions, the absence of a relief point in the isolated portion of the system results in a continuous pressure build-up that equilibrates once the system-wide pressure reaches that of the high-pressure fluid (Figure 4).

In order to mitigate the effects of the tube rupture under isolated conditions, pressure relief is needed to halt the pressure build-up. The response of the analyzed system indicates that the system of small pressure relief valves located near the outlets of the heat exchangers—originally sized for fire protection purposes—does not provide the necessary relief for tube-ruptures. The relief requirements for fire protection are significantly lower than those of tube-rupture.
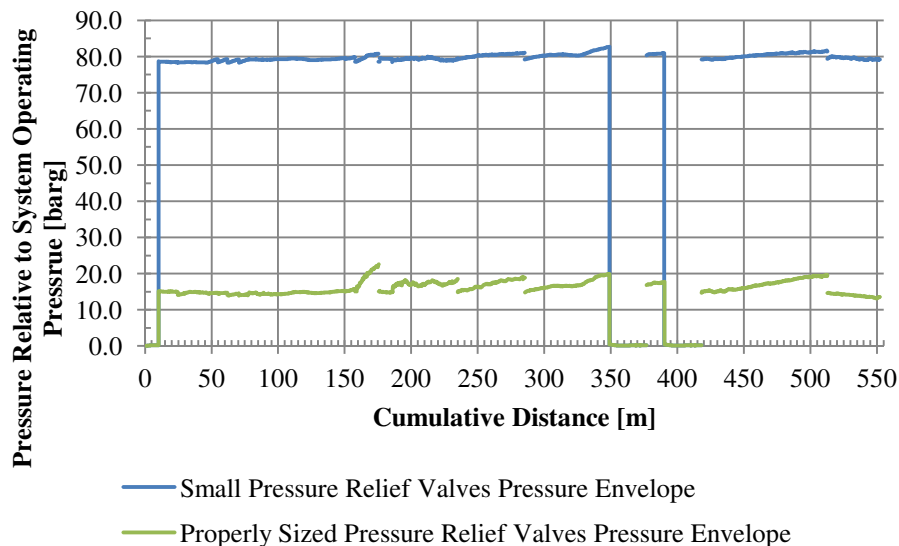
Figure 4 – Isolated Conditions Maximum Pressure-Envelope

Conventional pressure relief valves are spring-loaded devices designed to open at a predetermined pressure and protect a system from excess pressures by relieving liquid, gas, or liquid-gas mixture. When the valve is closed during normal operation, the system pressure acting against its disc is resisted by its spring force. The valve opens as soon as it senses a pressure equal to its set pressure, and it gradually starts relieving pressurized fluid. The opening behavior of the valve depends on its service (liquid vs. gas) and is mainly driven by pressures.

The pressure relief valves were resized to provide the required relief capacity to alleviate the pressure accumulation. The set pressure of the valves was determined to avoid nuisance bursts during normal operation. The relief capacity of the valves was determined from the dynamic simulations for a set pressure 8 barg above the normal system operating pressure. Valves were assumed to be fully open at 110% of their set pressure per API Standard 520 Part I (API 2008). Simulation results indicate that a peak liquid discharge of 1,910 m^3/hr is required to stop the

pressure build-up at acceptable levels. Once the total volume of liquid contained between the heat exchanger and the pressure relief valves is exhausted, gas starts flowing out of the relieving devices. The sizing of the pressure relief valves considered both liquid service and gas service peak discharges. For the system analyzed, the sizing was governed by liquid discharge requirements. This finding is in alignment with API Standard 520 Part I, whereby spring-loaded pressure relief valves designed for liquid relief are recommended for two-phase applications where the fluid being relieved may be liquid, gas, or multi-phase mixture.

CONCLUSIONS

The study described in this paper provides guidance on the design of heat exchanger piping systems for tube rupture events. The method based on the Joukowsky formulation provides a good estimate of tube-rupture resultant surge pressures for the design of heat exchanger shells in unobstructed systems, with a fast responding relieving device located on the shell. If the relieving device is located away from the shell, the transmitted surge wave needs to be evaluated for reflections. However, the Joukowsky based pressure estimate does not account for wave reflections and superimposition in the piping network. Hydraulic transient analyses are therefore required to properly design the piping systems for tube-rupture events.

In isolated systems, properly designed and sized, relief mechanisms are required to alleviate the tube-rupture resultant pressure build-up. The sizing and selection of the devices should consider both liquid service and gas service discharge. Relief devices sized for liquid service are recommended for multi-phase application.

ACKNOWLEDGMENTS

REFERENCES

API (2007). "Pressure-relieving and Depressuring Systems – ANSI/API Standard 521". American Petroleum Institute, Washington D. C., USA.

API (2008). "Sizing, Selection, and Installation of Pressure-relieving Device in Refineries". American Petroleum Institute, Washington D.C., USA.

IP (2000). "Guidelines for the Design and Safe Operation of Shell and Tube Heat Exchangers to

Withstand the Impact of Tube Failure". Institute of Petroleum, Colchester, UK.

PARMAKIAN, J. (1963). "Waterhammer Analysis". *Dover Publication*, New York, USA, 157 pages.

SIMPSON (1971). "High Pressure Gas-Filled Tubing Rupture in Liquid-Filled Heat Exchangers". *Safety in Design and Operation of Venting Systems Symposium*, American Institute of Engineers, California, USA.

WYLIE, E. B., STREETER, V. L. (1993). "Fluid Transients in Systems." *Prentice Hall*, New Jersey, USA, 463 pages.

ROUNDTABLE SESSIONS

International Junior Researcher and Engineer Workshop on Hydraulic Structures
17 - 20 June 2012, Logan, Utah, USA

SESSIONS 1 | REPORT

SESSION 1

TECHNICAL SESSION PRESENTATION

Chairman: Adam Witt

Rapporteur: Fadi Wakim

Advocatus diaboli: Nathan Christensen

Speakers: Bryan Heiner – Maria Trujillo

ROUND TABLE DISCUSSION

Moderator: Boris Rodriguez

Rapporteur: Fadi Wakim

Session Chairman: Adam Witt

Session Speakers: Bryan Heiner – Maria Trujillo

External Expert: Robert Janssen

Other Conference Participants

Title: Water Level Sensors: What Works?

Author(s): Bryan Heiner, Thomas Gill

Speaker(s): Bryan Heiner

Brief description of author(s) approach:

The author presented his research on the effectiveness of various water level measurement devices when used in extreme temperature environments. The main focus of the talk was on the types of devices investigated (pressure transducers, ultrasonic downlocker, potentiometer, bubbler sensor…) and the methodology of the experimental setup, and device calibration, to test the sensitivity of the devices measurement accuracies to outside temperatures. Since the research was still at its early stages at the time of the presentation, potential data collection and device field maintenance issues were identified.

The ultimate objective of the research is to identify the type of water level measurement devices that is consistently reliable when used in extreme temperature environments.

Questions and answers:

Q: How do you handle surface waves?
A: Measurement are averaged every 2 minutes and logged every 15 minutes.

Q: What's the best overall value approach for all the studied sensors?
A: At this stage of the research, devices that do not work in extreme environments have been identified. No recommendations could still be made on what devices work well.

Q: Would static calibrations be the most appropriate in dynamic environments?
A: Static calibrations are not necessarily the most appropriate in dynamic settings. There are planes to look more into this.

Q: What is the effect of temperature changes on calibration?
A: Manufacturers claim their devices measurements are adjusted for temperature compensation. Issues were found with temperature changes effects on calibrations.

Q: What is the effect of the reflective surfaces being used on the measurements?
A: Water surfaces will cause some signal diffusion. Signal reflection will not be perfect. In addition, there are issues with the effect of the mass of air between the measurement device and water surface.

Rapporteur's appreciation:

The presenter did a great job at communicating the problem, his research progress so far, and the future steps of his research. The presentation was clear and well delivered. A main point that came up during the roundtable discussions was related to the method of communicating the results of the research. The implications of reporting comparative results from different manufacturers need to be properly considered.

Title: Mean Velocity Effects in Biofouled Pipes

Author(s): Maria Trujillo

Speaker(s): Maria Trujillo

Brief description of author(s) approach:

The author presented her research on changes in mean flow velocities in Biofouled pipes. To assess the change in mean flow velocity due to biofilm growth on pipe perimeters, the author attempted at calculating a Darcy-Weisbach head loss coefficient for biofouled pipes. After describing her experimental setup for friction factor assessments and methodology, the author shared her results which showed friction factor variations for various pipe types and flow velocities. Findings indicate that friction factor patterns were not in alignment with Moody's diagram.

Questions and answers:

Q: Are you surprised that your friction factors did not match well with Moddy's diagram?
A: Yes, because my first expectation was that microfilm growth should not have had that big of an impact on friction factor patterns.

Q: Do you have any design recommendations given the variability of your results?
A: The ultimate goal would be to develop a new equation for biofilm friction factors that would be different from the typical equations currently used in practice.

Q: What was the effect of pipe roughness on biofilm growth?
A: Rougher pipes seemed to have less biofilm growth.

Q: What about hydrodynamic vortices formations due to bottom boundary layers? Any effects?
A: 21-day recirculation results indicate there might be some hydrodynamic impacts.

Q: Any optimum velocities to limit microbial growth?
A: Biofilms are there. Higher velocities result in thinner film formations. Nutrient supply will sustain growth. The detachment of biofilms could cause water hammer events and have implications on recirculation.

Q: Is the thickness of these biofilm layers self-limited? Is there any limit?
A: The thickness of the layers is probably limited by the thickness of laminar viscous sub-layers in the pipes.

Rapporteur's appreciation:

I found this presentation and research very interesting. The author did a very good job at presenting her experimental setup and describing her research and results. Roundtable discussions brought up three points worth highlighting: (1) the hazard associated with the release of these biofilms into water distribution systems, (2) the effect the variation in nutrient supply could have on the results (especially since nutrient supply was interrupted and restarted at separate stages of the experiment), and (3) the origin of Moody's diagram and Nikuradse's concept of equivalent sand roughness and how it was developed.

International Junior Researcher and Engineer Workshop on Hydraulic Structures
17 - 20 June 2012, Logan, UT, USA

SESSION REPORT

TECHNICAL SESSION 2

Chairman: Francois Rulot

Rapporteur: Riley Olsen

Advocatus diabolic: Gonzalo Duro

Speakers: Josh Mortensen, Mohanad Khodier

ROUND TABLE

Moderator: Mitch Dabling

Rapporteur: Riley Olsen

Session Chairman: Francois Rulot

Session Speakers: Josh Mortensen, Mohanad Khodier

External Expert: Bruce Savage

Other Participants:

Title: Measurement of Turbulence in Pressurized Pipe Flow Using PIV

Author(s): Josh Mortensen

Speaker(s): Josh Mortensen

Brief description of author(s) approach:

The main objective of this presentation was to discuss the problem of the invasive muscle species known as zebra and quagga, as well as turbulence effects on these muscles using PIV technology. These muscles are a major problem because they can get into pipe networks and other hydraulic structures and cause biofouling, corrosion, and clogging. A proposed management solution for these muscles involves a "turbulence generator" that can be installed in a pipe. The turbulence generator is anticipated to damage young muscles before they reach full size and are capable of attaching themselves to the surfaces of the hydraulic structure. It was pointed out that the actual turbulence generator used in this study is proprietary, and therefore a detailed description could not be provided. It was also emphasized that because of the slow speed of the camera utilized (7.4 Hz), time spectra could not be used, but rather spatial spectra was used.

Questions and answers:

Q: Does the increased turbulence in the field affect the inflow?
A: No, the addition of flow due to the turbulence generator is minimal. Instead, velocities are increased to create this turbulence. Specific characteristics of the turbulence generator cannot be divulged due to the fact that they are proprietary.

Q: Does the Reynolds Number stay constant between the pipes with the turbulence generator and those without?
A: Reynolds Number was not examined in the models that included the turbulence generator, but it is suspected that the Reynolds Number would increase in the tests with the generator installed.

Q: Did you look at other methods of determining turbulence?
A: Other methods of determining turbulence were not discovered in the literature review performed. The majority of studies found used this method so it was assumed to be acceptable.

Q: What was the frequency of the pictures be taken by the PIV camera?
A: 7.4 Hz.

Q: Was this frequency fast enough for accurate PIV analysis?
A: Had to make sure there were sufficient seeding particles, but it was difficult. This study was based on spatial data rather than time data.

Q: How could it be assumed that targeting only baby muscles would help manage them effectively?
A: The young muscles are not capable of attaching to walls, therefore killing them at this early stage would prevent them from reaching maturity and causing the problems discussed earlier

Rapporteur's appreciation:

I was very interested in this presentation because I have heard quite a bit regarding the invasive quagga and zebra muscles within Utah and Idaho. Most of the information I have seen in the past was from a recreational boating perspective, which emphasizes the transportation of these muscles from one body of water to another by "hitchhiking" on boats. For this reason it was really interesting to see this issue from the engineering and management side and see some work that is actually going on with regards to eliminating these muscles from hydraulic structures.

2nd Presentation

Title: Using PIV System in Fish Passage Through Rehabilitated Culverts

Author(s): Mohanad Khodier, Blake Tullis

Speaker(s): Mohanad Khodier

Brief description of author(s) approach:

This presentation focused primarily on Particle Image Velocimetry (PIV) measurements within rehabilitated culverts. The rehabilitated culverts discussed consisted of a liner that has baffles installed horizontally along the length of the culvert. The purpose of these baffles is to decrease the velocity within the culvert and create slow pools to make passage easier for fish. Through use of the PIV, it was found that a relationship existed between the percentage of fish that successfully passed through the culvert and the shear stress at the tip of the baffles. The max shear stress encountered was effective moved from the walls of the pipe without baffles, to the tips of the baffles for the pipes with baffles installed.

Questions and answers:

Q: What happens when flow rates are small? Does a hydraulic jump form between baffles that effects the fish passage
A: It is really only a question of whether there is enough water for fish to get through the pipe.

Q: What species of fish are being used for this study?
A: Brown trout. The fish that is the main concern regarding fish passage through culverts in Utah is the Bonneville cutthroat trout, but could not get licenses to catch these fish from the state. So instead the brown trout was used because it is a weaker swimmer than the Bonneville cutthroat, and therefore it is assumed that if a brown trout can make it through the culvert a cutthroat would as well. This gives a conservative result.

Q: How is sediment accumulation between the baffles expected to be managed?
A: Possibly through the use of a regular maintenance schedule in which the baffles are cleared of sediment manually

Q: Why was shear stressed used rather than turbulence?
A: Because turbulence gives no indication of fish passage, whereas there is a clearer relationship between shear stress and fish passage.

At the round table, the application of shear stress as an indication of fish passage was discussed in quite detailed questions and suggestions. It was also made clear that only culverts with horizontal baffles were tested in this study, none were examined that featured an incline. Much interest was shown in this topic by participants and future direction of study was discussed.

Rapporteur's appreciation:

This presentation was very interesting to me because I had never considered the problem of fish being able to pass through culverts. Now that it has been discussed, I recognize that it is a very important issue when it comes to biodiversity in our rivers and therefore keeping the river ecosystems and fish population balanced. I am interested to see where this research goes from here, and whether or not a different factor can more accurately relate to fish passage than shear stress.

International Junior Researcher and Engineer Workshop on Hydraulic Structures

6/18/2012, Logan, UT USA

SESSION REPORT

SESSION 3

Chairman: Maria Trujillo

Rapporteur: Bryan Heiner

Advocatus diaboli: Francois Rulot

Speakers: Riley Olsen, Adam Witt

ROUND TABLE

Moderator: Mohanad Khodier

Rapporteur: Bryan Heiner

Session Chairman: Jorge Matos

Session Speakers: Riley Olsen, Adam Witt

External Expert: Greg Paxson, Bruce Savage

Title: Hazard at Low Head Dams

Author(s): Riley Olsen

Speaker(s): Riley Olsen

Brief description of author(s) approach:

This research is to identify risks and set parameters which can be used to characterize and decrease the dangers of low head dams. Low head dams are used for many purposes including water supply, grade control, protect utility lines or enhance water quality downstream. Understanding the hydraulic risks of low head dams can help save lives. Problems: Strong countercurrent d/s of dam (roller); Entrainment of air less dense then water; catch debris; upstream surface velocity.

  The CFD software package Flow3D was used to numerically model flow conditions of 2 dam shapes (Ogee and Flat) with 3 dam heights.   A physical model is being used to verify the numerical model. Good agreement was found between the physical and numerical model with the maximum deviation being 5.3 percent. An HDPE doll was used to model what would happen to a human if there got stuck in a roller.

Questions and answers:

Q: What was v*?
A: It was a dimensionless number used to quantify when a roller occurs based on the minimum surface velocity. v* is a commonly used character in fluid mechanics it may be good to use an alternative character to avoid confusion with other versions of v*. It may be better to use the mean velocity instead of the surface velocity, as it would be more useful to use a field measureable physical parameter such as the average velocity.

Q: How will this be used in the public?
A: Level sensors will be tied to a sign near the dam, which will be used to indicate if hazardous conditions exist.

Q: Various characteristics based on the numerical model setup were discussed including:
  1. Obtaining grid convergence for a low and high head above the weir in addition to the one already obtained. The grid should be fine enough that 6 cells can describe the flow over the weir at any location.
  2. Modeling the smaller flows with more cells would most likely increase the accuracy of the numerical model.
  3. Using the GMO to model the human in Flow3D.
  4. Compare surface velocities between the physical and numerical model
  5. Activate the air entrainment model to try and determine the density of the mixed flow.
A: What do you do if you get caught in one? Get as low as you can and ride it out, move laterally to the bank. Remove life vest.

Bruce Tschantz has done lots of data collection of deaths at these sites (ASDSO paper).

Rapporteur's appreciation:

I reviewed the UWRL's website to see the new projects they were working on and was intrigued by this project. Riley did a great job on his presentation. Having some experience with Flow3D I know it can be difficult to learn the program and get the results you anticipate. The agreement shown in Riley's work is impressive; the best part is with some of the advice given the model can improve.

2nd Presentation

Title: Modeling Oxygen Transfer Efficiency at Low Head Gated Dams

Author(s): Adam Witt

Speaker(s): Adam Witt

Brief description of author(s) approach:

A new predictive model was created that improves the prediction of entrainment efficiency with standard deviations from .6 (old models) to 0.07 (new model). The model was used to create a design standard that showed the control factor of transfer efficiency is the tailwater depth. Head has a noticeable effect on efficiency but not as strong as strong as the static tailwater. The new model is an improvement over previous models because it takes into consideration the interactions between bubbles and the water and was developed based on field collected data.

Questions and answers:

Q: Is oxygen transfer temperature dependent? If so, was all the field data collected at the same temperatures?
A: Yes, all field results were temperature indexed to 20 degrees.

Q: When you measure DO isn't it dependent on depth?
A: Yes, most data was measured at multiple depths and different locations and use the depth averaged DO.

Q: What causes the low DO in the rivers?
A: It is caused the upstream pool of the run of river dam.

Q: Why is industry interested in oxygen transfer and water quality?
A: They are concerned with the aquatic bio downstream that needs DO. They are also interested in maintaining the ecology of the river. The main interest in this project is to meet requirements without taking field measurements.

Q: Is super saturation a problem?
A: Not at low head dams.

Q: Are site geometries important to the oxygen transfer project?
A: Yes, it will change when the jump is formed and when it is swept from the structure. Transfer efficiency is increased when the jump becomes submerged. Can you force sites to submerge? It could be done with baffles but Adam is not sure about the design of them. Can be done by increasing the unit discharge. If you pushed more through one gate by closing others would it increase oxygen transfer? Not sure, that gets complicated because

the distribution of flow is concentrated.

Q: Have you looked at water quality and how it affects the oxygen transfer?
A: It was not considered in the field measurements. It would be interesting to see if water quality was affecting things.

Other things to note:
When you get to an H of zero the DO efficiency will start to decrease.
Try to determine the scale effects with prototype, so scaled models can be used.
Several of the roundtable participants felt that the development of the coefficients needs to be verified somehow.

Rapporteur's appreciation:

Having done some measurements of DO associated with fish trap and haul I understand the complexity of the problem. Adam did a great job thinking outside of the box in developing a new method to estimate the gas transfer downstream of low head dams. Hopefully he is able to obtain more field data to continue to develop his model.

International Junior Researcher and Engineer Workshop on Hydraulic Structures
6/19/2012, Logan, UT USA

SESSION REPORT

SESSION 4

Chairman: Gonzalo Duró

Rapporteur: Mitch Dabling

Advocatus diaboli: Josh Mortensen

Speakers: Boris Rodriguez, Fadi Wakim

ROUND TABLE

Moderator: Nathan Christensen

Rapporteur: Mitch Dabling

Session Chairman: Gonzalo Duró

Session Speakers: Boris Rodriguez, Fadi Wakim

External Expert: Warren Frizell

Title: Pumping Problems with Variable Reference Head: the Non-Visualized Problems

Author(s): Boris Rodriguez, Astrid Pérez, José Adriasola

Speaker(s): Boris Rodriguez

Brief description of author(s) approach:

This research investigates the difficulties of designing pumping systems with multiple discharge points and variable reference head. The example given included a metal processing plant and a reservoir. Designing such a system can be difficult because there are multiple cases that need to be considered (e.g. reservoir empty and full). Different TDH's between the full and empty cases resulted in 21% difference in the flow pumped.

Questions and answers:

Q: If needed can you use 4 pumps in parallel and 4 additional pumps in series?
A: You need to be careful to select a pump that has an operation point on the curve. If you have four pumps in parallel and another 4 in series, you maybe have a not efficient system. It might be better to have 6 pumps in parallel.

Q: Did you consider variable speed drives?
A: We considered it as a possible solution, but it was too expensive. Variable frequency drives with a control valve downstream might not be as efficient because the TDH can increase. It seems counterintuitive to add head loss to a system, but you can increase efficiency that way.

Q: You mentioned there are 36 in. lines, what happens if the pump station shuts down? How do you prevent backflow into the pumps?
A: We have not done a transient analysis, but possibly a check valve. Small check valves in parallel will help alleviate the concerns of the large pipe size.

Q: Can you eliminate a pump station?
A: Sure, but the difference in head is 600m. To have only two pump stations with heads of 300 m can be very complicated. 200 m is much more manageable. The power needed to handle a large flow is very high. Also you would need larger pressure pipe.

Q: Is the system ever empty?
A: About 3 months of the year the river is empty. The dam fills the plant but not the other parts of the lines. Then when water is flowing again you fill from the river up to the reservoir.

Q: Would there be any advantages to series pumps? It seems odd to have a parallel pump system with such high head. What if you have a parallel/series pump system?

A: That could be a possibility. You would need to select different pumps.

Rapporteur's appreciation:

As an undergraduate student it was great to learn more about pump system design. One suggestion that was given for both presenters was to explain a bit about the ideas that they discarded before settling on the design. This would help prevent confusion and "why did you not do this?" questions. I thoroughly enjoyed this presentation.

2nd Presentation

Title: Heat Exchanger System Piping Design for a Tube Rupture Event

Author(s): Fadi Wakim, Pinar Kavcar, Sustafa Samad

Speaker(s): Fadi Wakim

Brief description of author(s) approach:

Some of the most damaging events for a pipe network are hydraulic transients. This presentation focused on hydraulic transients caused by a tube rupture in a Liquid Natural Gas system. A guillotine type failure was used for design as it is the most severe type. The author explained how he safely designed a LNG system and provided details on the differences from a standard water pipe system.

Questions and answers:

Q: One of your solutions was to get larger pressure relief valves. How did you know how big was big enough?
A: We experimented using vendor data until the valve was large enough.

Q: Did you have problem with column separation/cavitation?
A: Yes some of the spikes in the system response graph were due to this

Q: What considerations did you have to take into account with LNG as opposed to water?
A: One big difference is that there are different components in LNG. This caused issues with the rejoining of gas bubbles. Because you have different components in LNG, they separate at different vapor pressures. When you have multiple components, after gas begins to rejoin, you can still have other gasses in the line. When you inject air into a line, the gas bubbles in LNG act in much of the same way.

Q: How do you release gas from the pressure relief valves safely?
A: It goes into a burner.

Q: Have you looked into unsteady devices?
A: There are many devices you can use, but the problem is dealing with the manufacturer. When they need to guarantee that the valve will open in 10-15 milliseconds, they usually don't.

Q: How much do you feel the API standards helped guide your analysis?
A: The API standard simply said there was a problem and I needed to design for it, but it did not give any sort of analysis method.

Q: I'm guessing that you are using heavy enough walled pipe you are not worried about pipe collapse?
A: Correct, the tubes are very small, only one inch, so negative pressures are not a concern.

Q: Are ruptures common?
A: No. maybe one in a thousand years. But the effects are catastrophic. Very low probability, very high risk. Pipes can blow out of place.

Q: To start the simulation, did you start a rupture along the pipe?
A: The worst case scenario is that the pipe breaks as a guillotine. There is literature about how this can begin. Most cracks are not a big concern. There is research that shows there is a crack length to tube diameter ratio that the likelihood of a guillotine crack increases.

Q: Do you have any field data?
A: No. That is the challenging part. To create a standard we need data. No one wants to admit they had a failure. There have been field data collected to validate our software using valve closures etc. Our software was very good.

Rapporteur's appreciation:

Having no background in working with hydraulic transients, I found Fadi's presentation very informative. He explained some of the difficulties of working with LNG in the roundtable, and this could be used to help his presentation become clearer. Also explaining some of the design techniques he discarded and why would be helpful.

International Junior Researcher and Engineer Workshop on Hydraulic Structures
18 - 20 June 2012, Logan, UT

SESSION REPORT

SESSION 5

Chairman: Mohanad Khodier

Rapporteur: Adam Witt

Advocatus diaboli: Maria Trujillo

Speakers: Iordanis Moustakidis, Francois Rulot

ROUND TABLE

Moderator: Fadi Wakim

Rapporteur: Adam Witt

Session Chairman: Mohanad Khodier

Session Speakers: Francois Rulot, Iordanis Moustakidis (had to leave)

External Expert: Brian Crookston

Other Participants: K. Warren Frizell, Boris Rodriguez, Fabian

Title: THE EFFECT OF BOULDER SPACING ON FLOW PATTERNS AROUND BOULDERS UNDER PARTIAL SUBMERGENCE

Author(s): Iordanis Moustakidis, Athanasios Papanicolaou, Achilleas Tsakiris

Speaker(s): Iordanis Moustakidis

Brief description of author(s) approach:

There are many benefits to the use boulders in restoration projects. Boulders create more spawning grounds, resting areas and feeding areas for fish populations. When considering dam removal, boulders can be used to regulate sediment transport. However, there is a big limitation in the current knowledge of boulder use – there are no guidelines on optimal spacing of boulders in streams or how many to put in the river. Additionally, very few studies to date have examined the interaction between boulders and the surrounding flow. Difficulties arise in implementing acoustic instrumentation (high turbulence, boundary reflections, boundary interference, bubble flows increase noise). This study presents the experimental results of a new technique, infrared (IR) thermal camera imaging, in capturing the surface flow structures developing around neighbouring boulders within an array of boulders through temperature differences. The hypothesis of the study is that boulder spacing controls the developing flow structures around partially submerged boulders. The objective of the study is to map the surface flow structures around boulders within an array under low relative submergence regime. Two scenarios are studied – increased roughness regime from close spacing (6d), and from far spacing (10d). The IR camera recorded flow with hot water droplets used as tracers. Results showed the IR camera successfully records motion of water surface temp distribution.

Questions and answers:

Roundtable discussion feedback

Q: How are you planning to find shear stress or scour from surface values?
A: These values need additional hydraulic parameters to accurately estimate.

Q: Your images showed two kinds of motion – advection and heat diffusion. Those two motion patterns are governed by different equations. If he is only on surface determining velocity of flow, how does this compare to sediments and shear stress?
A: It seems like hot water droplets on surface are pretty discrete and don't really mix well. The diffusion of heat is more than just from within fluid because you have action of air above surface as well. Have you considered adding hot water from bottom so there is homogenous flow?

Q: Results were so dependent on being close to injection, might not be true picture of flow dynamics, maybe modifying the flow structure by even a little bit.
A: It would be good to look at time scales over which advection and diffusion take place. Correct estimates of these scales may validate his camera placement.

Q: In context of river restoration or enhancing fish habitat, composite roughness of rocks is different than racquetballs. Velocity profiles may be different.
A: From biology standpoint, may not want uniformly placed boulders. Would be surprised if the biologists said place these in uniform spacing. Bigger picture thought.

Additional Comments:
Maybe put the camera to give a cross-section view. This may give better insight into submergence.

Did well with his presenting. Good presentation skills.

Q&A from original presentation

Q: Where does this end up as far as a contribution? Alternative means to estimating flow roughness as result of boulder at different submergence?
A: We know resistance is connected ot spacing between boulders. Focused on flow patterns in this study, how can we map those patterns. Tried to do something similar, difficult to build velocity field distribution. Test a different camera. Map flow structures, see how that affects depositional patterns.

Q: Plots of momentum, which plane?
A: Surface, time averaged. Video lasted 30 seconds, 30 fps. Not symmetric since there is interference between emanating shear layers form boulders.

Q: How repeatable? Chaotic system, repeat image?
A: Took a lot of videos. Sure they have uniform flow conditions upstream, start taking measurements. At least 15-20 videos they analysed. Videos are pretty similar. Some variation in 6 spacing, suspect that has to do with interference. It is random event, but they put hot water in certain way, everything was repeated identically.

Q: When you varied boulders size, see difference in recirculation region depending on spacing?
A: Haven't tried, uniform boulder size.

Q: Have you tried non-uniform spacing)?
A: No, former studies have shown different spacing is sufficient to create roughness regime.

Q: Results, do you show that shear layers are good at altering bed shear stress? What is influence of spacing on shear stress?

A: Yager paper describes in more detail.

Q: Does this technique capture free surface with air entrainment?
A: Record an outlet in river, able to capture the water that was coming out from the outlet into the river, how that interfered with outlet into river. Can transform when camera is at an angle, yes, they can do that. Used standard 30 fps, not sure if the camera can capture the frequency of surface waves.

Q: Other work in Germany on boulder spacing, measured forces in boulders, observed interference.
A: Glad to hear.

Q: Temperature difference between hot water and flume? How does diffusion of heat not captured by camera versus flow velocity? Reference paper that diffusion is significant, not capturing that but flow pattern.
A: Flume variation was 10-15 degrees. Hot water was 45 Celsius. Camera was placed just upstream from the hot water seeding area.

Q: Does number of optimum frames depend on flow?
A: Has to do with analysis of grid of recording videos. About 900 frames. To avoid analysing all 900 frames, find optimum value of analysing frames. By changing flow, number of frames required to analyse should not change.

Q: Injection of hot water was close to inlet, what is close, will you test the influence of distance on diffusion?
A: If you put too close, you have just a bright color, white on IR camera, all over picture, can't analyse. If you put hot water upstream, won't have any hot water flowing in the camera vision. Need to find spot where it will not affect your measurements. Found it, close to 0.5m was optimal. By changing position, accuracy of velocity field changes. Tried different distances.

Q: Would heated rod element work instead of hot water drops?
A: Read paper on that, I don't recall results. Hard to build that in flume.

Rapporteur's appreciation:

The objective of this paper was to present a new technique for estimating flow structures around boulders in an array. The technique appears to resolve several issues that persist in acoustic measurement devices. However, the accuracy of the technique needs to be explored further and validation of the technique could be more robust. Most of the discussion revolved around the use of hot water droplets as tracers, and more specifically the placement of the droplets within the flow, the diffusion of heat and ways to improve flow visualization using hot water as a tracer. The presentation clearly laid out the results of the experimental research, and significant care was taken to provide concise results,

conclusions and objectives for further research.

Title: DEALING WITH SEDIMENT TRANSPORT OVER PARTLY NON-ERODIBLE BOTTOMS

Author(s): Francois Rulot, Benjamin Dewals, Pierre Archambeau, Michel Pirotton, Sebastien Erpicum

Speaker(s): Francois Rulot

Brief description of author(s) approach:

Presented a numerical method that can handle sediment transport over partly non-erodible bottoms. Non-erodible means bedrock in river or concrete structure in river. Sediment transport is modified by manmade structures, which can lead to critical consequences like scour or sedimentation of reservoir. The current problem is that the cells in the finite volume numerical model can become negative in explicit scheme. Exner equation describes sediment transport for erodible bottoms and can apply to non-erodible bottoms, but a correction is required. He used a 2D horizontal model, finite volume method, with a correction for non-physical results through an iterative process. Two processes were modelled – the evolution of a trench over a fixed bump, and the evolution of a head of sediment on a flat fixed bottom. Each had experimental benchmarks used to validate the model. Sensitivity tests show that the velocity of the sediment heap is directly linked to water discharge; height of crest is directly linked to the initial sediment heap height. Results showed that volume conservation was respected, the matching of numerical results to experimental results was good, and that increased computational time was limited compared to the simple reset method.

Questions and answers:

Roundtable discussion feedback

Q: Have you considered a different sediment transport method other than Meyer Peter-Mueller formula?
A: MPM is universally accepted as reasonable sediment transport method, but shear stress values may be more sensitive to various methods of calculation, which could modify your computational results.

Compute height and length of the dune as it propagates down the channel to validate the model using an additional method.

Notation may be a bit complicated, confusing when going between y and z in 2d.

Q: How can you account more for 2D variations in the flow?
A: Account for wall shear forces? This is a complicated phenomenon, 3D naturally. Flow

at downstream boundary is very three dimensional. Can try to put small corrections in shear stress term, in some way account for angle of attack. May try accounting for momentum equation. Not sure how this will affect computational time.

Q: Not clear why you have to correct the negative volumes. Why does that happen?
A: Exner equation is used for whole domain that can be erodible. Can use the same equation for impacted area. Have to correct because in the equation nothing says there is a non-erodible bottom.

Q: You used dx = 10cm, did you look into smaller ones?
A: Tried using different sizes, came up with results that were not representative of physical results.

Q: Did you see instabilities when the water goes up and down?
A: No.

Q&A from original presentation

Q: What is the size of particles used?
A: In second example, size of particles were 2.8 mm, in first size of particles is not important in numerical method, used power law of water.

Q: What was given numerical scheme?
A: Finite volume technique.

Q: Solution is 2d in horizontal plane, why use power law for velocity?
A: Only in first benchmark used power law, was used in previous study. Gives coefficient for sediment transport based on that. Compared with his results. Power law to compute sediment flux, just to compute sediment fluxes as function of mean velocity, not used in model.

Q: Experiments interface at sediment and water attaches almost immediately to boundary at end of bump. Depth averaged but flow behind bump may be 3d.
A: Yes, vertical velocities play important part downstream. Spatial resolution in that area was dx of 10cm.

Q: Could that be measurement error in moving bedload layer as elevation. In model it says no depth.
A: Yes.

Q: Experimental studies, measurements were taken in central flume. Did you measure in center of flume? Did you notice any influence of walls on shape?
A: Small influence of walls because sediment deposits.

Q: Regarding separation between q bottom and q gravity, does particle fall?

A: Critical slope at which sediment falls; gravity is only contribution at that point.

Rapporteur's appreciation:

The author was able to show reasonable agreement between the new CFD method and experimental results. Much of the discussion focused on the 3D characteristics of the flow, how an accurate model would include these effects, and how difficult it would be to actually implement and calibrate this model. Suggestions were given for smaller modifications that may improve the accuracy of the results. Given the work that has been put in and considering future computational effort, these smaller modifications are likely the most efficient direction for future research.

International Junior Researcher and Engineer Workshop on Hydraulic Structures
18 - 20 June 2012, Logan, UT, USA

SESSION REPORT

SESSION 6

Chairman: Boris Rodriguez

Rapporteur: Josh Mortensen

Advocatus diaboli: Riley Olsen

Speakers: Nathan Christensen, Mitch Dabling, and Gonzalo Duro

ROUND TABLE

Moderator: Bryan Heiner

Rapporteur: Josh Mortensen

Session Chairman: Boris Rodriguez

Session Speakers: Nathan Christensen, Mitch Dabling, and Gonzalo Duro

External Expert: Greg Paxson

Other Participants: Dave Campbell, Blake Tullis, Sebastien Erpicum, Riley Olsen, Robert Janssen

Title: ARCED LABYIRINTH WEIR FLOW CHARACTERISTICS

Author(s): Nathan Christensen and Blake Tullis

Speaker(s): Nathan Christensen

Brief description of author(s) approach:

The main objective of this research was to expand previous research of labyrinth weirs to arced labyrinths. Arced labyrinths are often mentioned and may be more hydraulically efficient due to the cycles being more aligned with the streamlines of the flow. However, not a lot of current information is available. Physical model simulations were used to help calculate the Cd coefficients of arced labyrinths of various geometries and develop an equation that can be used for these types of weirs.

Questions and answers:

Q: Why is there a ^2 in your Cd equation instead of a more traditional ^.5?
A: It showed the best fit to our data

Q: Will you expect problems with cavitation in prototype weirs with non-aerated nappes?
A: Yes, it is a concern, that's why we looked at different sidewall angles.

Q: How did you look at aeration and instabilities?
A: Nappe breakers were investigated, which decreased efficiency within certain ranges but eliminated instabilities of the nappe.

Q: Did you look at project costs in comparisons to efficiency?
A: No work was done w/ costs.

Q: Was velocity head included in measurements?
A: Yes, measurement location taken well upstream where zero velocity could be assumed.

Q: Why do curves trail off for the geometry with an angle of 6 degrees
A: This may be an extrapolation past data established in previous work by Crookston.

Rapporteur's appreciation:

As someone with very little knowledge on labyrinth weirs, it was enlightening to see that information was being added upon and expanded to arced labyrinths in a way that can be widely used. There was much discussion about how the data will be applied and consolidated into a useable equation. We look forward to seeing the published version of this work.

Title: NOTCHED AND STAGED LABYRINTH WEIR HYDRAULICS

Author(s): Mitch Dabling and Brian Crookston

Speaker(s): Mitch Dabling

Brief description of author(s) approach:

The presentation focused on labyrinths that are notched in the apex and sidewalls to match the outflow hydrograph. Again, physical models were used of labyrinth weirs with these characteristics. A standard weir equation was used to calculate Cd values. These values were similar among different configurations of weirs if Ht/P > 0.5.

Results were compared to a common design technique and found that Cd values can be used as a rough conservative estimate for design even though they're very specific to various configurations of notched labyrinths.

Questions and answers:

Q: Is it a realistic assumption to aerate the nappe in the physical model?
A: Yes, assuming that prototype scale nappes are generally aerated naturally, and its more conservative.

Q: Please clarify nomenclature of notched apexes on figures in slides?
A: Clarified

Q: Was data from the high Cd used in the curve fitting?
A: Yes.

Q: Can an existing labyrinth spillway be modified to be a staged weir?
A: Not sure.
R: Brian Crookston added that it would depend on other factors not researched here, including costs, etc.

At the roundtable discussion there was discussion on the sidewall effects from velocities as well as location of the total head measurement. Modifications of existing labyrinths to include notches was also discussed which indicated that modifications would depend on costs and exposing critical elements of the weir.

Rapporteur's appreciation:

Again, I have learned much regarding labyrinth weirs and the many different configurations they can take. The research very interesting and well presented. The roundtable discussions were especially interesting with both researchers and designers around the table. These discussions produced great suggestions on taking results from the laboratory to the field in a way that is more effective and realistic.

3rd Presentation

Title: CFD APPLIED TO THE SIMULATIONS OF A HYDROCOMBINED POWER STATION IN SPILLWAY MODE

Author(s): Gonzalo Duro and Mariano de Dios

Speaker(s): Gonzalo Duro

Brief description of author(s) approach:

The presentation focused on a comparison of CFD modelling to physical model results of a dam spillway with hydropower. Turbulence parameters were investigated as well as dynamic pressures. Dominant pressure frequencies were found along with the Strouhal numbers. It was concluded that there was good comparison between both numeric and physical approaches and that CFD can be used as a cost-effective tool in similar situations.

Questions and answers:

Q: Which Re numbers were used in the simulations?
A: Re was not calculated.

Q: Which turbulent characteristic length was used?
A: Recommendations for similar work on spillways were followed.
R: During the roundtable discussion it was clarified that the use of 7-10 percent of spillway crest height was used for the characteristic length, which is consistent with proper modelling guidelines.

Q: Did you look at conservation of mass between the different mesh blocks?
A: Yes, this was checked at the block connections and it was validated.

Rapporteur's appreciation:

This presentation was a good example of comparing numeric and physical approaches. This is a frequent issue that we face in our hydraulics lab and it was good to see more available information. Calculations of turbulence characteristics and the use of spectral analysis were especially interesting to me because of similar analyses used in my research. This provided further opportunities for discussion and sharing resources during the roundtable discussion and throughout the remainder of the conference.